NOVEL IRON(II) TRIAZOLE-PYRIDINE BASED DINUCLEAR COMPLEXES: SYNTHESIS, CHARACTERIZATION AND MAGNETIC PROPERTIES

by

Huan Guo

A thesis submitted to the Department of Chemistry

In conformity with the requirements for

the degree of Master of Science

Queen's University

Kingston, Ontario, Canada

(September, 2013)

Abstract

The major focus of this thesis involves a new approach to spin-crossover (SCO) in iron(II) dinuclear complexes. In order to acquire SCO properties, a series of novel ligands (**L1M, L2M, L3M, L4M**), together with the corresponding iron(II) and/or nickel(II) complexes were synthesized and characterized. Beyond the successful synthesis and characterization of these ligands, some interesting aspects of their synthesis are discussed.

The reported ligands are methyl-derivatives from ligands previously studied in the group. The methyl group in the position 6 of the pyridine group is introduced to induce steric hindrance in the complexes and decrease the ligand field strength. As a result, the influence of the methyl group may induce SCO in low spin (LS) complexes, or tune the SCO properties (such as transition hysteresis or transition temperature) in complexes with SCO.

Ligands were divided into three different types according to their spacers: a ligand with an aromatic spacer (**L1M**), ligands with aliphatic spacer (**L2M, L3M**) and a ligand with no spacer (**L4M**). The difference between their structures helped us to better understand the coordination chemistry of the corresponding complexes.

The nickel(II) complexes formed provided useful background information on the coordination chemistry of iron(II), such as the crystal field stabilization energy (10Dq) value. An approximation of 10Dq value of iron(II) was calculated based on the 10Dq value of analogous nickel(II) complexes using an empirical rule, to provide a prediction of SCO property.

Acknowledgements

I would like to express my sincere thankfulness to my supervisor, Dr. Anne Petitjean. Not only she supervised and assisted me throughout the past two years in my research, from theories to practice, from analyzing abstract experimental data to guiding me washing beakers and flasks properly, but she also shaped me from an undergraduate with little knowledge in scientific method and critical thinking, to a graduate student who gets prepared in facing new challenges in chemistry research. She also helped me to open my mouth: I changed from talking nothing make sense in chemistry in English to giving a group meeting or oral presentation with limited difficulty. It is a great fortune to work with and learn from such an outstanding chemist.

I want to emphasize the help my supervisory committee had offered; lots of meaningful suggestions were like treasure for my later research. Among them were Dr. Suning Wang, who kindly proof-read my thesis and granted the use of the instrument of her group; and Dr. Donal Macartney who offered some very interesting suggestions in the supervisor committee meeting and taught me the background of supramolecular chemistry in the course; Dr. Jean-Michel Nunzi for his great suggestions about spin crossover.

I would like to express my gratitude to former and current group members: Weiwen Zhao, who was always prepared to give a hand when I needed and provided me with all the living tips in Canada; Dr. Yi Yan, who was an omnipotent “chemistry textbook” and was always ready for looking up; Kristina Stevenson, who suggested tips in reaction and helped me with speaking English; Caitlin Miron, who proof-read my

drafts, despite my poor writing English and piles of errors; and Mona Ashrafkhorasani, who gave me a chance to learn shining ideas and suggestions in both my research and thesis. What's more, they light up my laboratory life with their supportive altitude and the share of happiness.

I want to thank those who helped me in characterizations and instruments: Dr. Fran çoise Sauriol, who helped me with NMR tests and understandings; Dr. Jiaxi Wang, for the help of mass spectrometry; Dr. Muralee Murugesu and Fatemah Habib for the test and data of magnetism; and Laboratoire d'Analyse Élémentaire de l'Université de Montr éal for the EA results.

Special gratitude belongs to Yue Tao, who builds a good life for me and supported me all the way in the pursuing of my master degree. I can't imagine what the life would be if you were not on my side.

All the expressions can't express my deepest love to my dad and mom. I finally learn the life is not like a game when I am far away from home and in a foreign environment; but they are the angels who always give me a stick when I slipped, give me warmth when I feel cold, give me encourage when I feel frustrated and give me love when I feel homesick.

Statement of Originality

I hereby certify that all of the work described within this thesis is the original work of the author, except for (i) Job plots and titrations which were carried out by Dr. Anne Petitjean, and (ii) all the SQUID measurements performed by Fatemah Habib in Prof. Muralee Murugesu's group at the University of Ottawa where the magnetism of the complexes was studied.

Any published (or unpublished) ideas and/or techniques from the work of others are fully acknowledged in accordance with the standard referencing practices.

(Huan Guo)

(August, 2013)

Table of Contents

List of Figures

List of Tables

List of abbreviations and symbols

Abs	Absorbance
Å	Angstrom
B	electron-electron repulsion energy
BM	Bohr magneton (9.274×10^{-24} J $\cdot T^{-1}$)
bpy	2,2'-bipyridine
C	Racal parameter
℃	degree Celsius
c	concentration
CFSE	crystal field stabilization energy
cm	centimeter
calc.	calculated
CuAAC	copper catalyzed azide-alkyne cycloaddition
10Dq	crystal field splitting parameter
d	doublet
dd	doublet of doublet
DCM	dichloromethane
DMF	dimethylformamide
EA	elemental analysis
EI	electron ionization

EtOAc	ethyl acetate
ε	molar absorption coefficient
g	gram
GC-MS	gas chromatography-mass spectrometry
h	hour
HS	high spin
HMBC	Heteronuclear Multiple Bond Correlation
HSQC	Heteronuclear Single Quantum Coherence
Hz	hertz
J	coupling constant
J	joule
K	Kelvin
kJ	kilojoule
L	liter(s)
LIESST	light induced excited spin state trapping
LS	low spin
m	multiplet
M	mole(s) per liter
mg	milligram
mL	milliliter
mmol	millimole
mol	mole

MS	mass spectrometry
nm	nanometer
NMR	nuclear magnetic resonance
phen	1,10-phenanthroline
ppm	part(s) per million
quint.	quintet
s	second(s)
SCO	spin crossover
sh	shoulder (peak)
ST	spin transition
THF	tetrahydrofuran
UV-Vis	ultraviolet-visible spectroscopy
λ	wavelength

Chapter 1

Introduction

Spin-Crossover (SCO) with Iron(II) Complexes

1.1 Magic of Magnetism: Spin-crossover & application.

Transition metal materials have dominated our daily life for thousands of years; most of them are in pure metal form. However, interesting properties of their complexes have prompted researchers to focus on them once again. Spin-crossover (SCO) is one of the most shining facets of this beautiful diamond, as many potential applications are associated with the most advanced research, including magnetic switching, molecular memory and display.[1]

Several octahedral transition metal ions like iron(II) can exist in two different spin states depending on the ligand field strength and crystal field strength. One is the high spin state (HS): when the ligand field (LF) is weak and the pairing energy of the metal is relatively large, electrons prefer to be promoted to the higher level d orbitals rather than pairing in the lower level. The other is the low spin state (LS), which occurs when the pairing energy is smaller than the splitting energy and all the electrons are paired in the lower level first. Different spin states may have different colors and magnetic properties. For example, the typical inorganic iron(II) sulfate hexahydrate $[Fe(H_2O)_6]SO_4$ and potassium ferrocyanide $K_4[Fe(CN)_6]$ complexes display the following electron configurations for their d orbitals in Fig. 1.1.

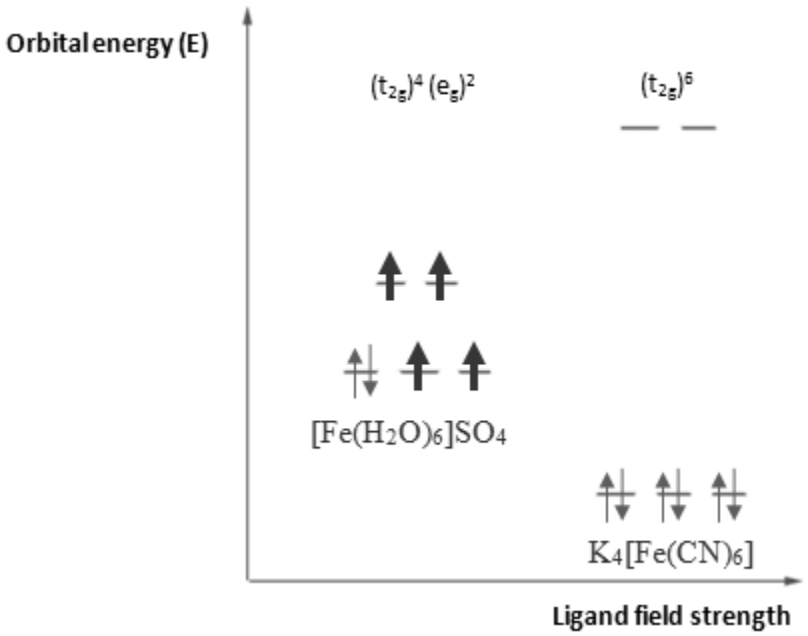

Fig. 1.1 Electronic configuration of $[Fe(H_2O)_6]SO_4$ and $K_4[Fe(CN)_6]$, bold arrows represent four unpaired electrons.

As we know, $[Fe(H_2O)_6]^{2+}$ is light green in solution and $[Fe(CN)_6]^{4-}$ is light yellow. $[Fe(H_2O)_6]^{2+}$ is paramagnetic whereas $[Fe(CN)_6]^{4-}$ is diamagnetic. For some species, ligand field splitting and pairing energy are close enough that the transition from one spin state to another becomes possible. The energy required to initiate this transition between spin states can be provided by external factors such as light, heat, or magnetic field. This phenomenon is known as spin-crossover (SCO) or spin transition. Relationship between spin state and ligand field is depicted in the Fig. 1.2.

The crystal field stabilization energy (CFSE) value, 10Dq, is used to describe the energy difference between the e_g and t_{2g} levels.

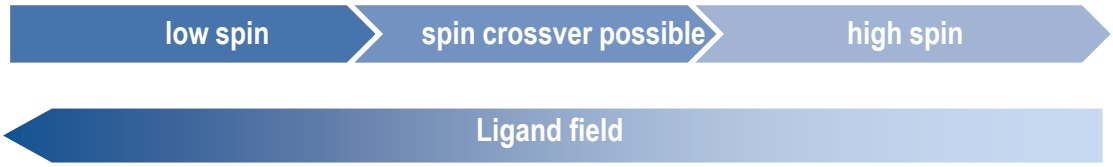

Fig. 1.2 Change of spin state of a metal center as a function of the ligand field.

Spin-crossover was first discovered by Cambi *et al.* in the 1930s during the investigation of an iron(III) complex.[2] In recent years, most research has focused on iron(II) complexes because of the abrupt change in electronic configuration (and magnetic property) between its LS and HS states. Since paramagnetism results from unpaired electrons and diamagnetism from all-paired electrons and colors are affected by the electronic configuration, the change of spin state of iron(II) complexes can be easily detected by both magnetism and UV-VIS methods. Moreover, the abrupt change would be beneficial in potential applications such as magnetic memory.

1.2 Mononuclear, dinuclear and multinuclear SCO complexes.

Mononuclear spin-crossover complexes have been intensely studied in the past several decades. These studies refined fundamental theories in spin crossover and revealed many interesting properties and potential applications.[3]

For instance, the Australian group of H.A. Goodwin *et al*. reported a series of iron(II) complexes based on 1,2,4-triazole-pyridine, illustrating the effect of time, anion, solvent and steric hindrance for mononuclear complexes, example is shown in Fig. 1.3 and Fig. 1.4.[4]

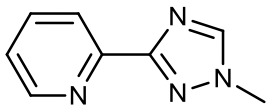

Fig. 1.3 Structure of ligand **L1**.

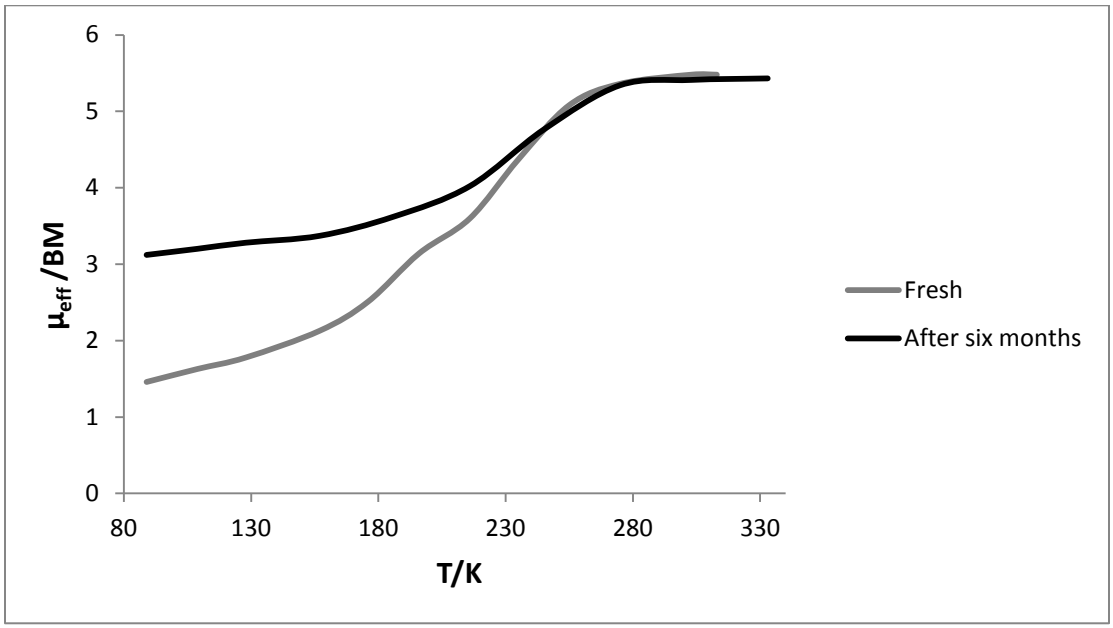

Fig. 1.4 Aging effect, μ_{eff} versus temperature.

The nature of the mononuclear constitution makes it impossible to have more than one spin state change-either from LS to HS or HS to LS, whereas dinuclear and multinuclear complexes may have. As metal centers have individual spin states, either LS or HS, dinuclear complexes can have three spin states: LS-LS, LS-HS, HS-HS and two different spin state transitions. Furthermore, multinuclear systems can have different structural patterns, such as dinuclear helical complexes ("helicates"), polymers and metal-organic frameworks, providing more chances to display interesting properties.

For example, this year C. J. Schneider *et al.* reported 1,2,4-triazole based dinuclear system **1**, as drawn in Fig. 1.5: [5]

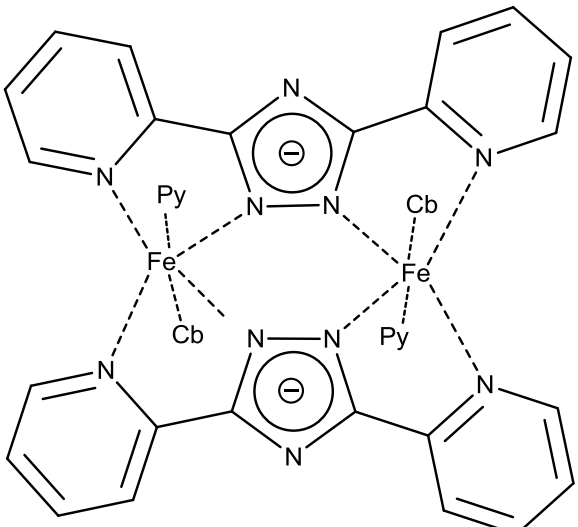

Cb=$NCBH_3$
Py=Pyridine

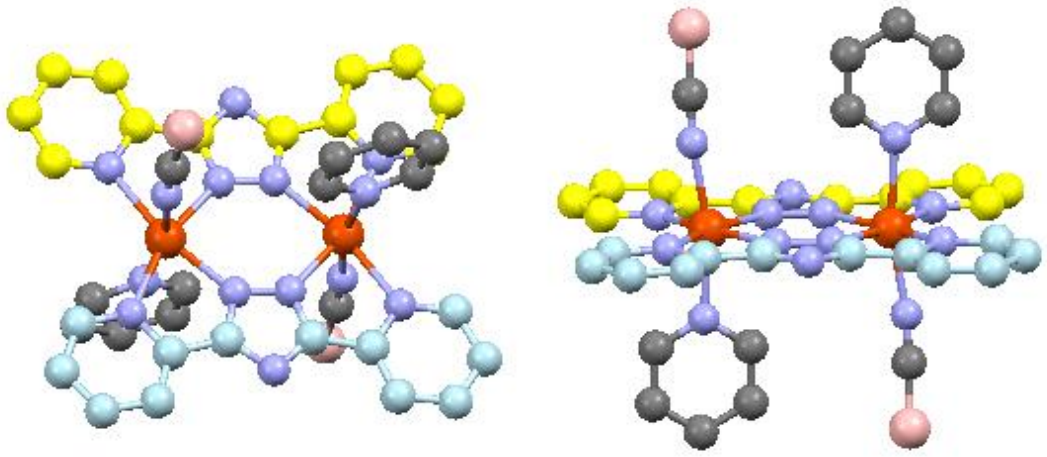

Fig. 1.5 Structure of **1,** based on X-ray study of single crystal. Two 1,2,4-triazole based ligands are on the same plane. H atoms are omitted for clarity.

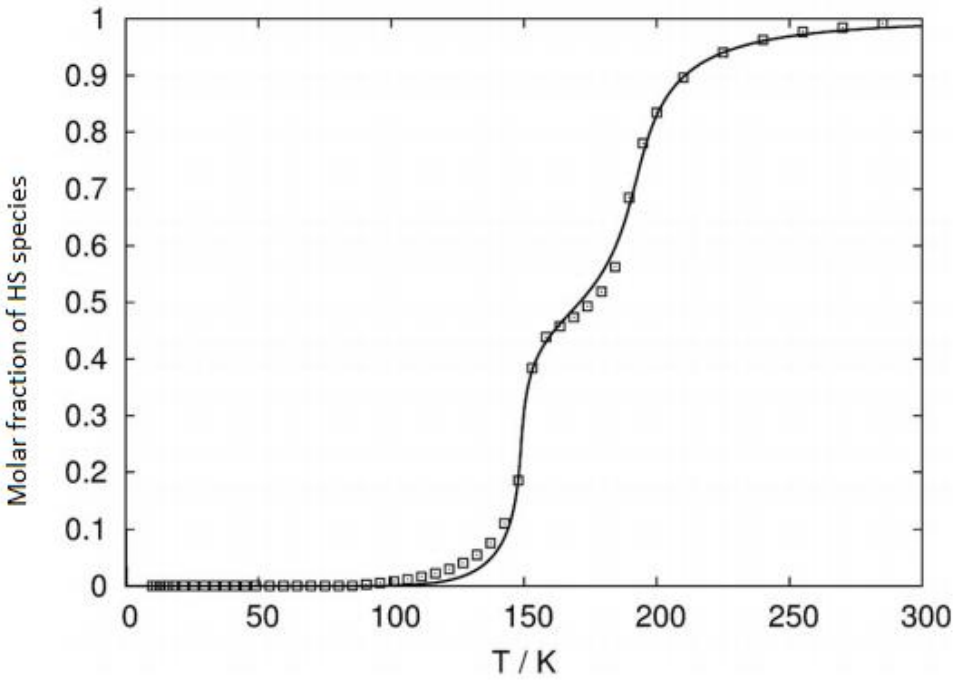

Fig. 1.6 Molar fraction of HS species versus temperature of **1**, the curve is a fitting curve of experimental data (dots). Y axis is mole fraction. This graph is adapted from the original article.[5]

They successfully prepared crystals of **1** both as large irregular crystals for magnetism and large single crystal for X-ray diffraction. The X-ray data suggested that the two 3,5-bis(pyrid-2-yl)-1,2,4-triazole ligands stayed in the same plane. In the magnetism study, they found evidence that the complex displayed a two-step spin transition, from LS-LS to LS-HS and finally to HS-HS (Fig. 1.6).

1.3 Factors influencing spin-crossover

1.3.1 Physical factors.

Heat, light, magnetic field, and pressure can all affect the spin state of complexes. Of these approaches, temperature is one of the most widely used to achieve spin transition. LS species might transition to the HS state by heating, while HS species might switch to the LS state when cooling is applied. The process of heating and cooling samples makes it easier to control and monitor the energy than other methods, therefore thermally induced spin crossover is always the first attempt in research.

Light is another interesting physical factor. It can induce spin crossover both from LS to HS or HS to LS. What's more, this property is common in iron(II) complexes with SCO properties. It is called LIESST (Light Induced Excited Spin State Trapping). However, the complex must have the spin crossover property, and light is used to stimulate the spin transition. An example is shown below (Fig. 1.7).

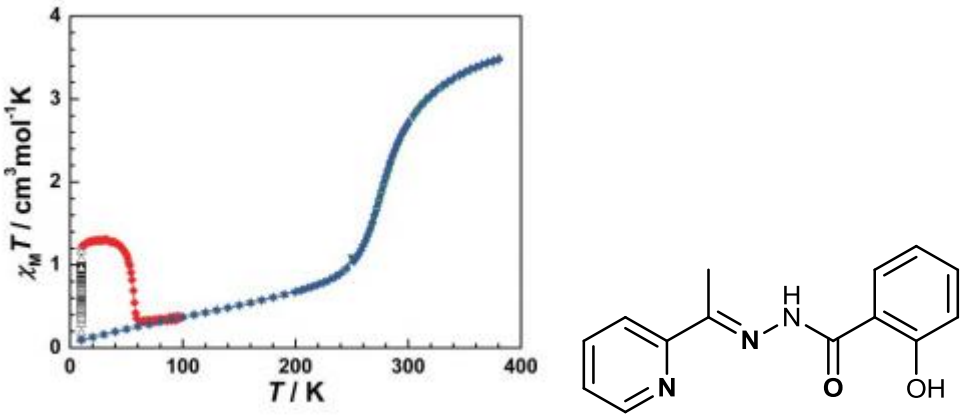

Fig. 1.7 The LIESST effect curve (red dots) and the ST curve (by heating/cooling, blue dots) of $[Fe(\mathbf{L2})_2]^{2+}$. The structure of **L2** is shown on the right. Donor atoms are in bold. The picture is adapted from the paper published by L. Zhang *et al*.[6]

A magnetic field tends to push complexes towards the LS state as it can lower the crystal field. Pressure compresses the crystal of complexes, thus it shortens the bond length between the iron center and donor atom, resulting in stronger ligand field and more LS nature.

However, physical factors usually act as stimuli; a fundamental method of tuning a complex to have spin crossover property should be looked into.

1.3.2 Chemical factors.

1.3.2.1 Solvent and anion effects.

The solvent effect is a valuable method to tune the spin crossover of complexes or adjust their SCO behavior. Water is often used, while other solvents are also popular. In the article published by P. E. Kruger and his collaborators,[7] the same complex with

different solvent molecules showed different spin transition curves, from non-hysteretic (with acetonitrile) to hysteretic (with water). However, the result of solvent and anion effects is quite unpredictable since many examples show reverse effects for different complexes.[8] This may be due to the unpredictable effect on the lattice force. For some anions like Cl^-, the ion itself can act as a ligand and it will compete in coordination, which will certainly affect not only the packing but also the constitution, stoichiometry, and association constant of the complex as well.

In the paper mentioned above, the mononuclear 1,2,4-triazole-pyridine iron(II) complexes reported by H. A. Goodwin's group illustrate the solvent and anion effects (Fig. 1.8, Table 1.1, Fig. 1.9, Fig. 1.10).

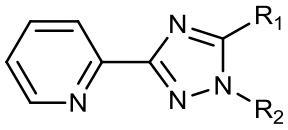

Fig. 1.8 3-Pyridyl-1,2,4-triazole based ligand structure.[4]

Table 1.1. Variations for 3-pyridyl-1,2,4-triazole ligands.

	R_1	R_2
L1	H	Me
L3	Me	Me

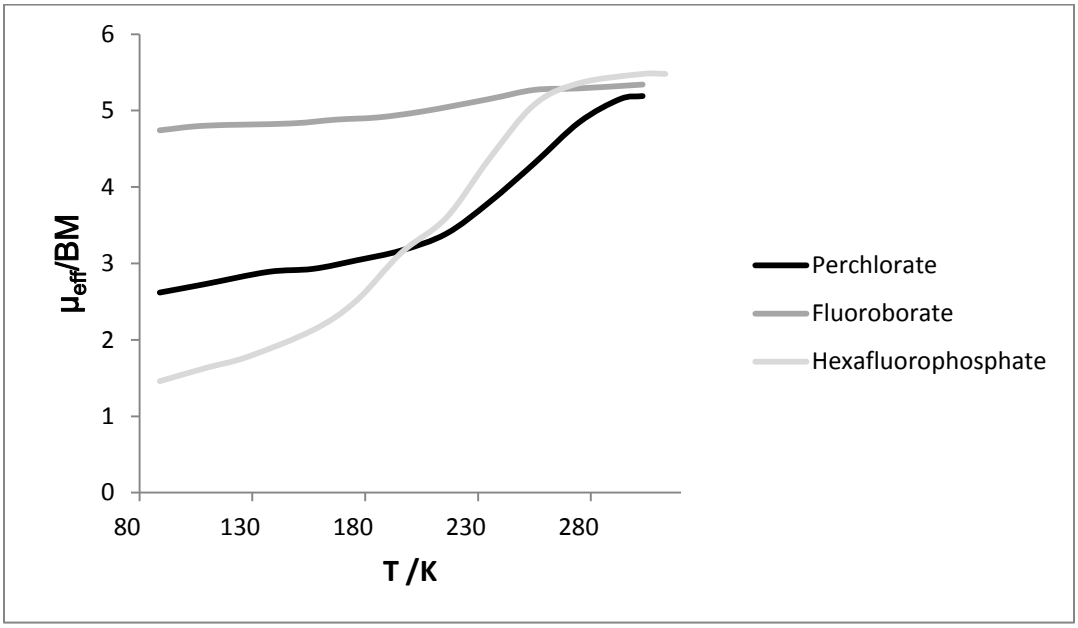

Fig. 1.9 Anion effect of $[Fe(\mathbf{L1})_3]^{2+}$ complex, μ_{eff} versus temperature.

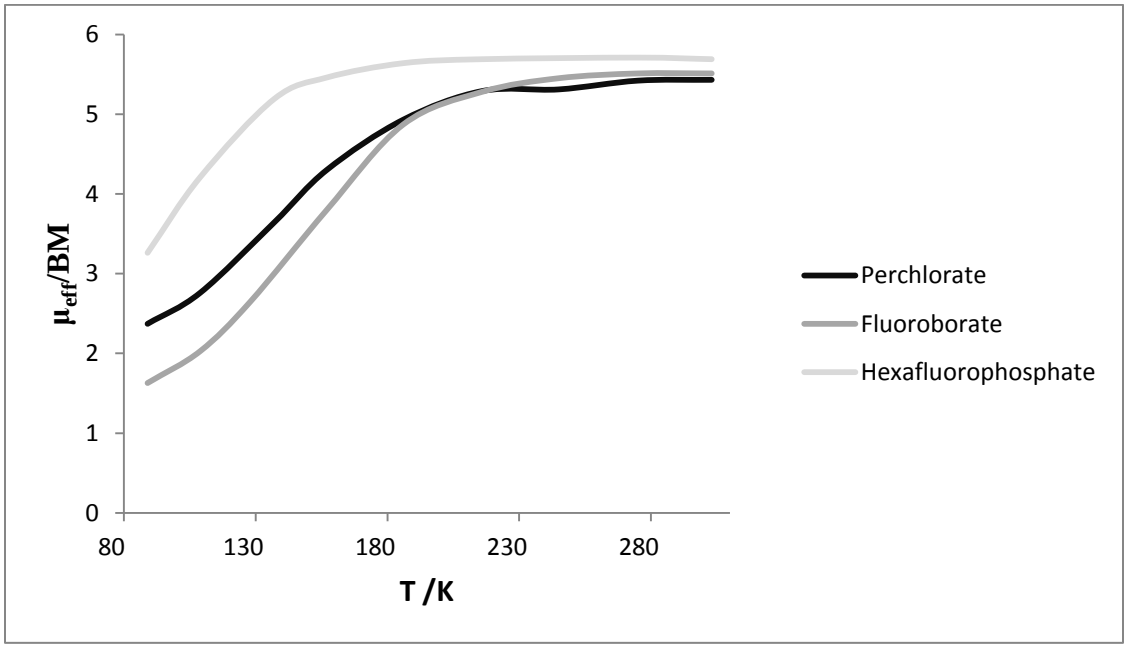

Fig. 1.10 Anion effect of $[Fe(\mathbf{L3})_3]^{2+}$ complex, μ_{eff} versus temperature. Note the difference between $[Fe(\mathbf{L3})_3]^{2+}$ complexes, where the curve for the same anion changed.

From the Fig 1.9, it can be seen that the complex $[Fe(\mathbf{L1})_3](BF_4)_2$ stays in the HS state from 89 K to 303 K, while from Fig 1.10 the complex $[Fe(\mathbf{L3})_3](BF_4)_2$ displays SCO properties. On the one hand with ligand **L1**, based on Fig 1.9, $[Fe(\mathbf{L1})_3](BF_4)_2$ is of a more HS nature than $[Fe(\mathbf{L1})_3](PF_6)_2$. On the other hand, with ligand **L3**, based on Fig 1.10, $[Fe(\mathbf{L3})_3](BF_4)_2$ is of a more LS nature than $[Fe(\mathbf{L3})_3](PF_6)_2$. This suggests that the impact of the counteranion for the two ligands is reversed.

Additional articles support the conclusion that the solvent effect on spin crossover properties is not reliable. In their 1993 article, H.A. Goodwin and his colleagues reported that anhydrous $[Fe(\mathbf{bpp})_3](BF_4)_2$ (**bpp**: 2,6-bis(1H-pyrazol-3-yl)pyridine) stays in the HS state at room temperature, whereas its dihydrate derivative is more LS (in transition between HS and LS) at room temperature. On the other hand, the anhydrous complex of $[Fe(\mathbf{btp})_3]Cl_2$ (**btp**: 2,6-bis(1H-1,2,4-triazol-3-yl)pyridine) is in the LS state at room temperature, and the trihydrate derivative is in the HS state (Fig. 1.11).[6]

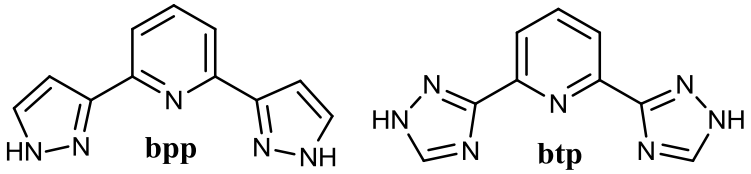

Fig. 1.11 Ligand 2,6-bis(1H-pyrazol-3-yl)pyridine (**bpp**) and 2,6-bis(1H-1,2,4-triazol-3-yl)pyridine (**btp**).

In conclusion, changing anions and solvents to control spin crossover may appear to be a good idea but it is unpredictable and is therefore not a favoured approach for further research.

1.3.2.2 Ligand effect.

As described above, a different ligand contributes to a different ligand field. Because SCO emerges only when the ligand field best suits the metal center (i.e. the splitting energy), changing the nature of the ligand is the key method for research on SCO. The "change" can be a thorough change or just a modification on the original ligand whose corresponding complex only stays in the LS or HS state. Complete changes would surely affect the ligand field, but this is usually not the first strategy that comes to chemists' minds as the SCO property is unknown and unforeseeable if no experience or previous study is available for similar complexes. As a result, many studies have focused on the modifications of known ligands, as illustrated by the literature.[3] The modification can vary in different ways. Electron-rich groups can be introduced to raise the electron density of the donor atom, or a stronger donor can be introduced to increase the ligand field, potentially giving the HS complex new SCO properties. On the other hand, to make LS species more prone to SCO, adding a group just beside the donor atom to introduce steric hindrance and lengthen the distance to the metal centre may be considered as it will impair coordination and lower the ligand field.[9] For example, $[Fe(\mathbf{phen})_3]^{2+}$ (**phen** = 1,10-phenanthroline) stays in LS state at all available temperatures whereas the substituted 2-methyl-1,10-phenanthroline iron complex $[Fe(\mathbf{mphen})_3]^{2+}$ shows spin crossover (Fig. 1.12).[10] This interesting difference inspired researchers to look into their structural difference. The bond lengths between the iron centers and nitrogen donor atoms of both complexes and the structural distortion of $[Fe(\mathbf{mphen})_3]^{2+}$ were compared. SCO was suggested as result from steric hindrance (Table 1.2).[10, 11]

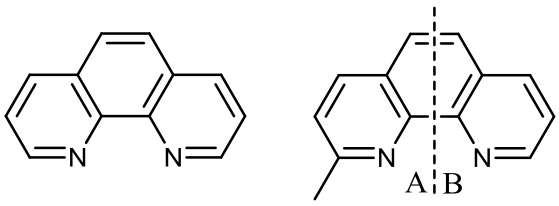

Fig. 1.12 Structure of 1,10-phen and 2-methyl-1,10-phen.

Table 1.2. Average bond length of Fe---N (Å).

	$Fe---N_A$	$Fe---N_B$	Difference
$[Fe(mphen)_3]^{2+[10]}$	2.24	2.16	0.27(A)/ 0.19(B)
$[Fe(phen)_3]^{2+[11]}$	1.97		

This indicates that chemical modifications may tune LS state and lead to potential SCO.

1.4 Methods of SCO analysis.

SCO can be induced by light, pressure, heat and so on as mentioned above, but heat is the most widely used trigger, as it is simple and effective for many complexes.

The most widely used detection methods are SQUID (superconducting quantum interference device) and Mössbauer spectroscopy. In SQUID, the magnetometer actually detects the change of magnetic field down to a very small scale. Since the magnetic field will be influenced by the spin state, spin-crossover can be monitored by SQUID. Although it would not give direct information about the electronic configuration, SQUID is still generally applied. Based on the magnetic moment it provides, an ST curve can be

quickly drawn which is the most obvious and persuasive evidence of SCO.

Mössbauer spectroscopy is one of the best ways to access the electron configuration of an iron center. However, Mössbauer spectroscopy is somewhat limited to iron, as it is the most widely studied among transition metals, and other metal atoms are either non-active or uncommon in Mössbauer spectroscopy. As the change of electronic configuration is the direct evidence of spin crossover, Mössbauer spectroscopy is a powerful tool in physical and theoretical chemistry, although it is less convenient for the acquisition of ST curves (in response to heating-cooling) than SQUID.[3]

1.5 Dinuclear systems of interest- helicates and mesocates.

1.5.1 Helicates- a brief introduction.

Helicates, a term first introduced by Lehn and co-workers to describe polymetallic helical complexes in 1987,[12] are based on the geometric motif "helix" (helix is an abstract geometrical motif; the most common items in daily life resembling a helix are a spring, a spiral staircase and a wire connecting a phone to its receiver). This term describes complexes which contain one or more ligand strands and two or more metal centers forming complexes adopting the shape of a helix (Fig. 1.13). For octahedral transition metals, triple stranded helicates are the most common shapes, although other types like double stranded exist.[13]

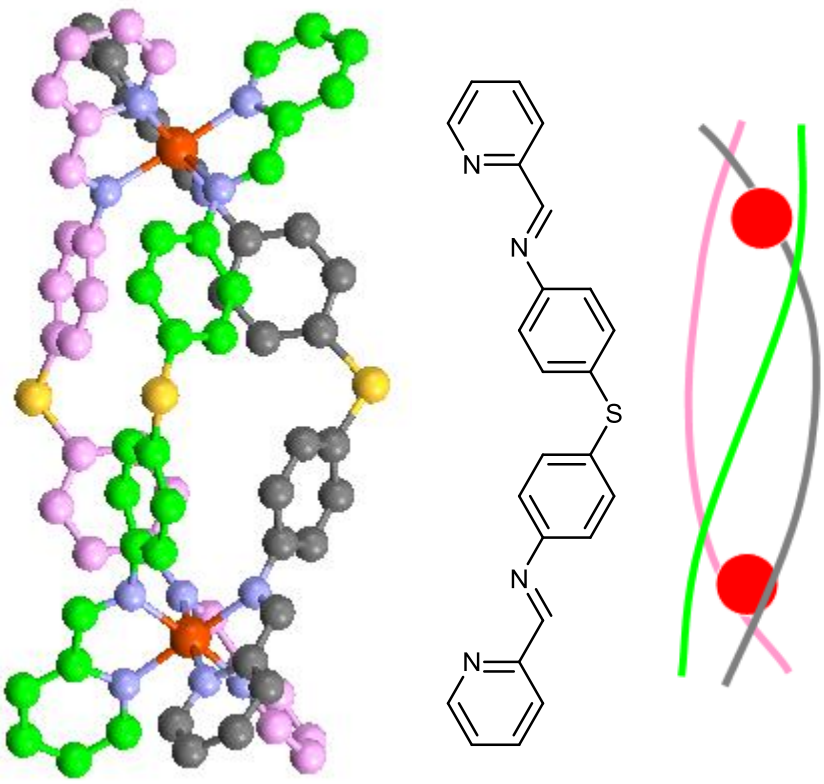

Fig. 1.13 Left: A typical triple stranded helicate **2**, synthesized and characterized by Y. Parajo *et al*.[13] Hydrogen atoms are omitted for clarity. The spheres in the top and bottom centers are Fe(II). Middle: the ligand structure of **2.** Right: Cartoon of the helical ligand strands with metal centers.

Many simple helicates ligands consist of two parts: (i) the coordination centers and (ii) the spacer which connects the coordination centers (Fig. 1.14).

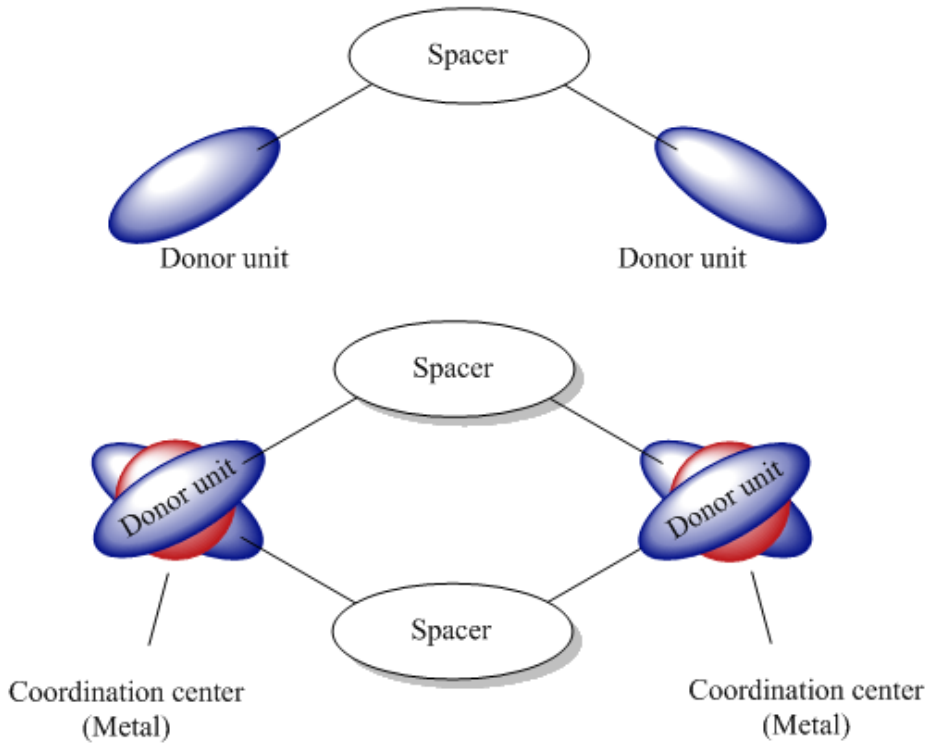

Fig. 1.14 Cartoon of a spacer connecting two donor units. Top: structure of the ligand. Bottom: structure of a double stranded helicate.

Spacers are responsible for some properties such as the size of cavity and the chirality of the helicate.

The chirality of helicates is frequently determined by the preferred geometry of the metal centers. If the metal centers adopt different chiralities, the complex may give a meso structure, or “mesocate”. Only metal centers with the same chirality could form a helicate (Fig. 1.15).

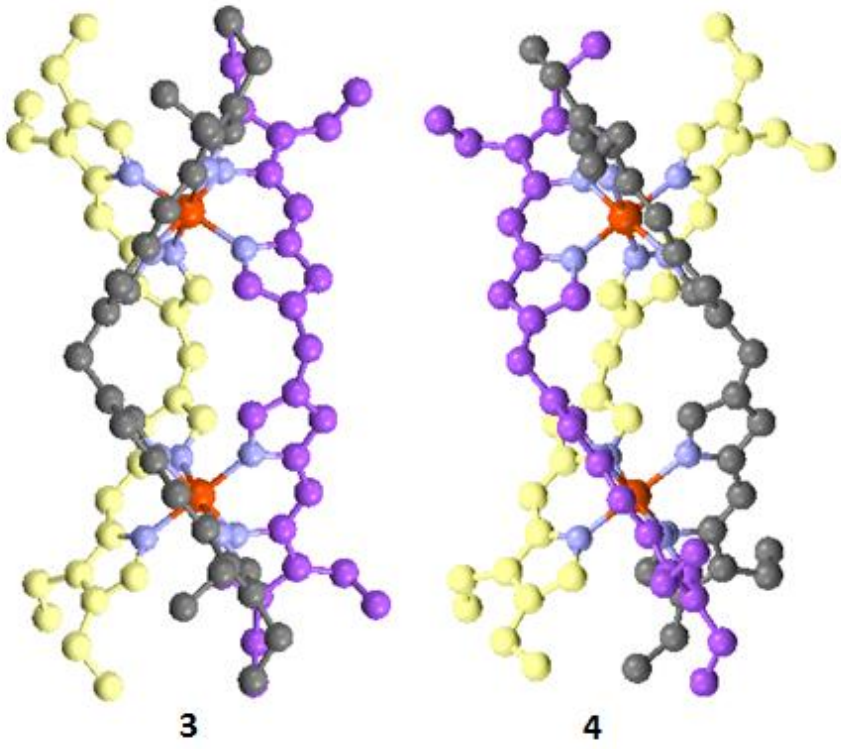

Fig. 1.15 Complexes: helicate and mesocate from the same metal center (cobalt (III)) and ligand, reported by Z. Zhang and D. Dolphin.[18] Structure **3** is in mesocate form, in which two metal ions present different chiralities. Structure **4** is in helicate form; two metal ions have the same chirality. Hydrogen atoms are removed for clarity.

Because of the variety of donors in various ligands and the diversity of metal ions, an explosion in the field of helicates has led to potential applications such as DNA recognition[13, 14] and molecular machines.[15]

1.5.2 Classical bipyridine (bpy) based helicates.

The very first helicates were mostly derived from one typical unit: the 2,2'-

bipyridine unit, or in abbreviation, bipy or bpy. Since the nitrogen on the pyridine ring is a good donor to a series of metal ions, pyridine-pyridine units appear to be convenient ligands to build helicates. Because the coordination is highly dependent on the pyridine, if the structure of the pyridine unit changes, the property of the helicate and the complex stability may change. Various substitution positions on the bpy have been used to prepare helicates, such as 4, 4' bpy, 5, 5' bpy and 6, 6' bpy (Fig. 1.16, Fig. 1.17). [16]

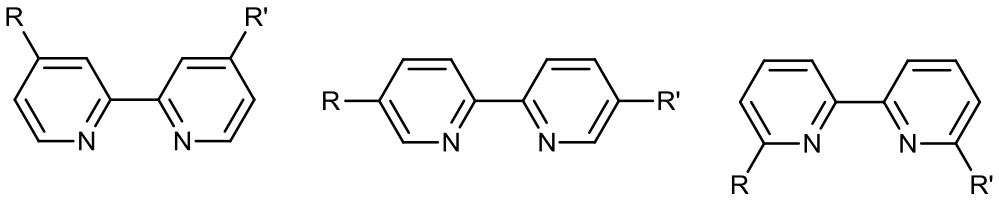

Fig. 1.16 4,4'-, 5,5'- and 6,6'-disubstituted-2,2'-bipyridine units

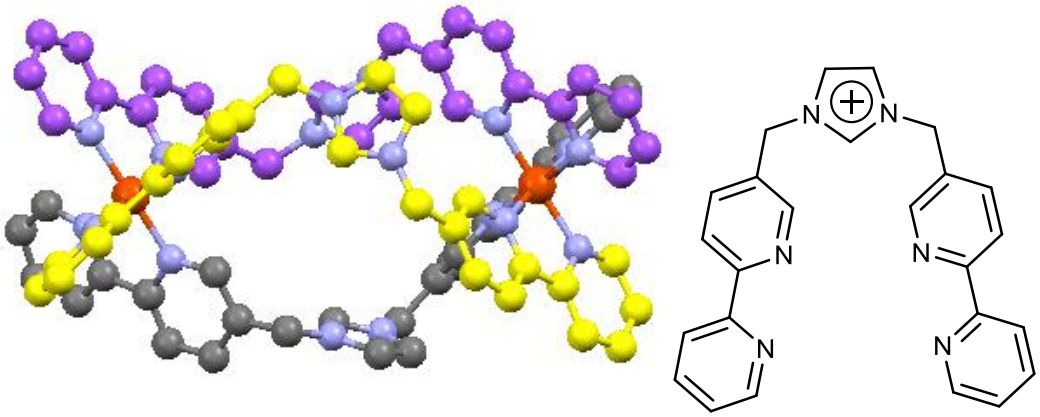

Fig. 1.17 Left: triple stranded 2,2'-bipyridine based iron(II) helicate **5**, bridged by 1,3-imidazole. This complex was reported by F. Cui *et al*.[19] It can switch between mesocate and helicate, depending on the sizes of anion captured in the cavity. Large size tetrahedral anions prefer the mesocate structure, while smaller and monatomic anions lead to a helicate. Right: the structure of the ligand.

The drawbacks of bpy based helicates also come from the pyridine group. The synthesis of this type of ligands is tedious, involving some complicated reactions. Since pyridine is a polar unit, purification can become challenging. Moreover, most of 2,2'-bpy based iron(II) complexes remain in low spin, so this type of ligand is less interesting when investigating spin crossover properties.[3]

1.5.3 Novel helicates: heterocycle based ligands.

Most recently the interest in helicate ligands has moved to a series of five-membered ring heterocycles such as imidazoles, pyrroles, and triazoles.[16] Frequently those units are combined with pyridine units to enhance stability. The most interesting part of this type of ligand is their weak donor nature which provides potential spin-crossover complexes, compared to bpy based helicates.

P. E. Kruger and his collaborators have been focusing on iron(II) complexes with imine-imidazole based ligand for years.[7] In the first reported articles, the spin crossover property of an imine-imidazole based helicate was recorded. The ST curve lacked thermo-hysteresis, and it only had a one-step spin transition, from [HS-HS] to [LS-LS] or *vice versa* (Fig. 1.18, Fig. 1.19, Fig. 1.20). In a further study based on the same species, a two-step spin transition curve was observed as a result of the solvent substitution, from acetonitrile to water (see section on solvent effect above). Aging the sample was also recorded and it appeared that the sample would prefer HS as time went on and dehydration took place. In their third article, they also looked into the mononuclear complex to confirm that the imidazole-imine unit itself was highly valuable as a SCO

complex.

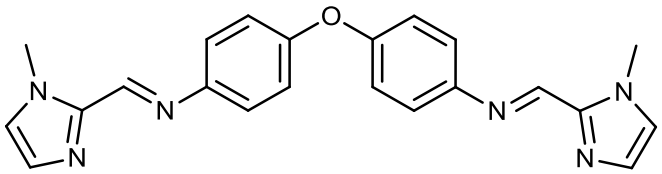

Fig. 1.18 Structure of the ligand **L4**.[7]

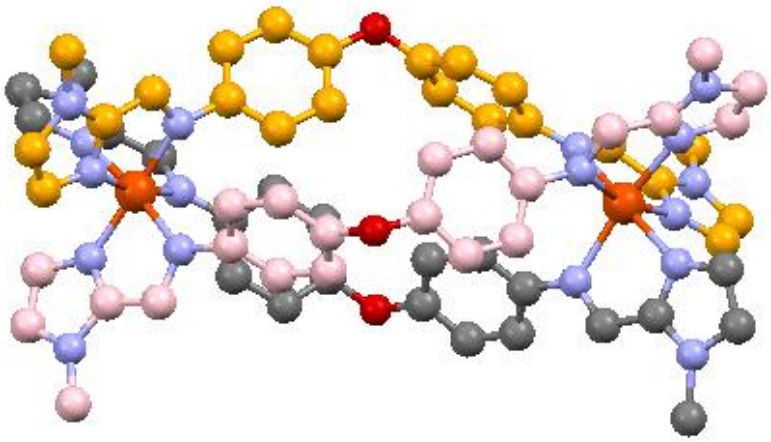

Fig. 1.19 Structure of the complex **6**. All hydrogen atoms are omitted for clarity. Red atoms: oxygen, blue atoms: nitrogen, dark orange spheres: iron(II), all other atoms are carbon.[7]

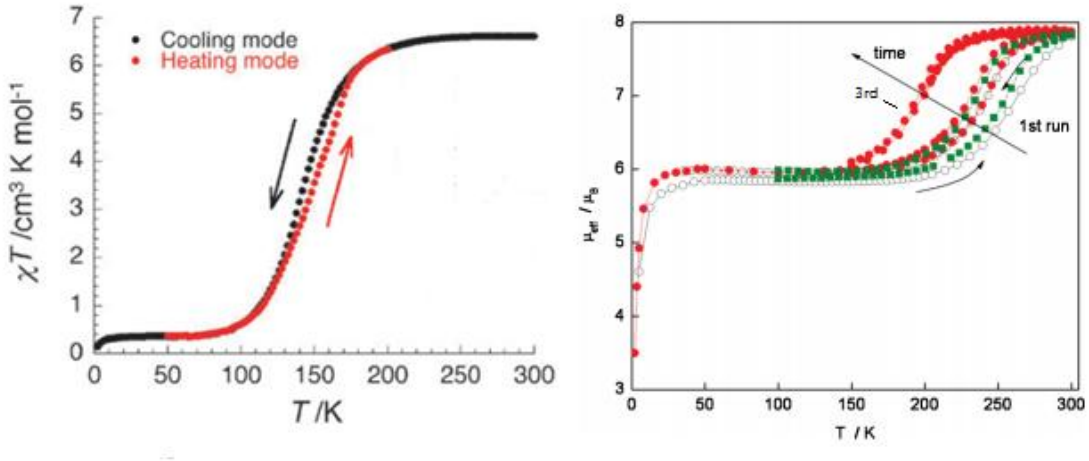

Fig. 1.20 Left: ST curve of the spin crossover helicate **6** developed by D. Pelleteret *et al.*[7] The solvent was acetonitrile. Note that almost no hysteresis can be observed. Right: ST curve of the same helicate **6** but different solvent, which was water. Four sets of different ST curves were depicted; the white dots were the freshest sample and a clear hysteresis could be seen. Aging of the sample showed that the HS state was generally preferred. Green dots were from the rehydrated sample after sitting in the air for weeks. Pictures are adapted from the original article.

1.5.4 Dinuclear complexes with triazole units.

1.5.4.1 Triazole-based iron(II) complexes.

Many ligands can be used in iron(II) complexes, but interestingly one of the most prominent types of ligand is composed of triazole-based ligands. Unlike the pyridine unit, the triazole group needs little to no modifications and can be combined with other types of donor units to acquire spin-crossover properties,[17] which has led to a significant

amount of research in this area.[4, 5] For chemists, the triazole unit is also popular for tuning and adjusting properties related to SCO. Y. Garcia *et al.*[20] prepared iron[(4-(2'-hydroxyethyl)-1,2,4-triazole)] 3-nitrophenylsulphonate trihydrate **7**. This complex appeared to have an extremely large hysteresis of 270 K. When the complex was heated up from 270 K to 400 K the ST curve had an abrupt change at 370 K, while cooling from 400 K, the abrupt change appeared at 100 K. Then they tested heating again starting at 100 K, interestingly, the abrupt transition took place at 115 K. Finally they looked into the change of formula and the large hysteresis resulted from dehydration. The 370 K change is due to the dehydration and the LS trihydrate changed to HS species- dehydrate. Once the anhydrous complex formed the more HS species produced a totally different ST curve with a 15 K-broad hysteresis (Fig. 1.21).

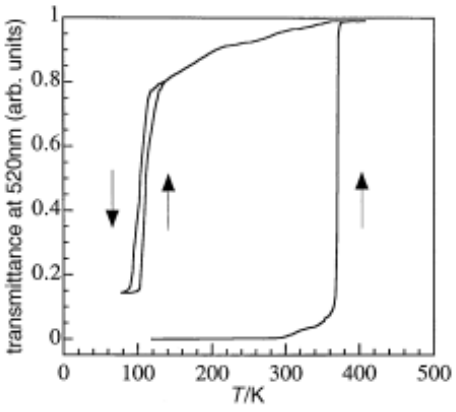

Fig. 1.21 UV-VIS spectrum of the complex **7**. This graph is adapted from original paper.[20]

As described, all triazole based ligands of the complexes shown above are from 1,2,4-triazole based ligands for two reasons:

1. The 1,2,4-triazole is quite popular as it has stronger coordination to iron(II) and the

corresponding complexes are more susceptible to spin-crossover than 1,2,3-triazole.[17]

2. Little progress has been made on 1,2,3-triazole-derived complexes, as reflected by the small number of available iron(II) spin crossover complexes.[17] Therefore research on 1,2,3-triazole has a room for exploration.

In addition, the synthesis of 1,2,4-triazole is not as simple and clean as that of 1,2,3-triazole, because the synthesis of 1,2,3-triazole only involves a "click reaction" (Copper-catalyzed Azide-Alkyne Cycloaddition, CuAAC)[21] under mild conditions (Fig. 1.22).

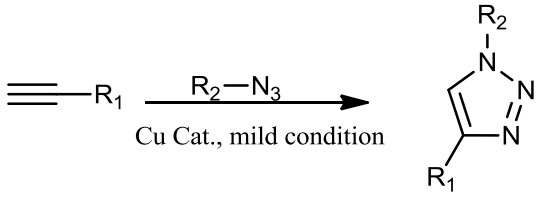

Fig. 1.22 Synthesis of the 1,2,3-triazole unit.[17]

1.5.4.2 Previous studies of 1,2,3-triazole unit based iron(II) complexes.

Several studies focusing on 1,2,3-triazole-based iron(II) complexes have been published and this area is still a virgin land for future adventurers.

Among the little published work, V. Niel *et al*. reported a 1,2,3-triazole based complex with SCO properties, $[Fe(\mathbf{tzpy})_3]^{2+}$ **8** (**tzpy** = 3-(2-pyridinyl)-[1,2,3]triazolo[1,5-a]pyridine), the original triple-ligand complex stays in LS from 2 to 300 K. As neutral molecule and new ligand (NCS^-/$NCSe^-$) was used, the species showed the SCO property (Fig. 1.23).[23]

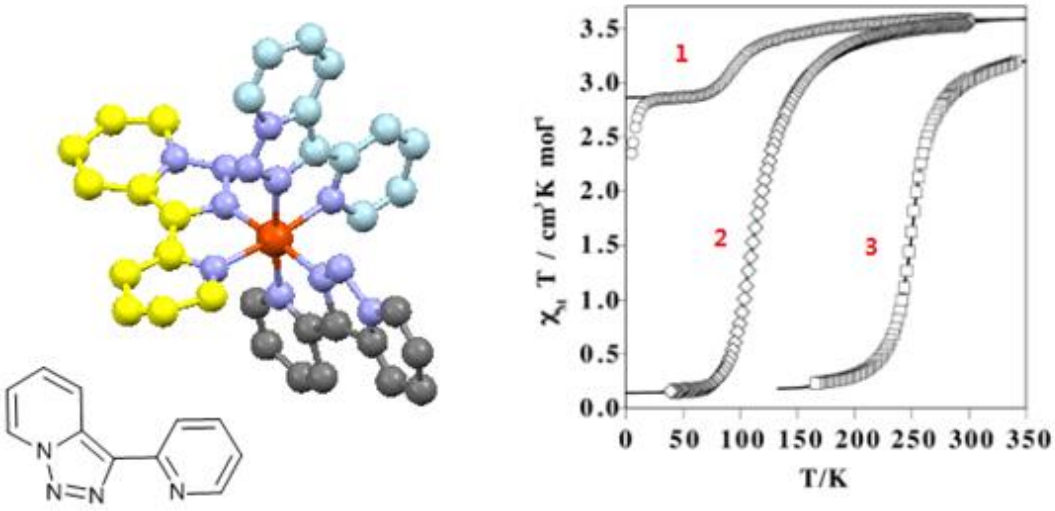

Fig. 1.23 The structure (left) Fe(**tzpy**)$_3$ **8** complexes and ST curve of the [Fe(**tzpy**)$_2$(NCX)$_2$] ·A . In the chart, the difference of three curves comes from different anion and neutral molecule: 1: X=S, A= 2 CH_2Cl_2 2: X=S, A=S, 3: X=Se, A=S. Figure is copied from the original paper.[23]

According to what has been elucidated before, the mononuclear spin crossover species are quite well studied with other ligands and there is little interest to develop them any further. Therefore dinuclear (or even multinuclear) species are considered. However, the scarcity of iron(II) 1,2,3-triazole complexes makes the dinuclear 1,2,3-triazole based iron(II) complexes with SCO properties even harder to find. Hence, since mononuclear complexes derived from the 1,2,3-triazole show spin-crossover potential,[17] dinuclear species are well worth exploring.

1.5.5 "Click Ligands": a simple approach towards helicates.

The name of "click reaction" was first introduced by K. B. Sharpless *et al.* in 2000,

but the original 1,3-dipolar cycloaddition dates back to 1890s. In 1960s Huisgen intensively researched on it.[21] It is also known as “Huisgen cycloaddition”. This type of reaction involves only a simple catalyst and mild conditions, as easy as a “click”. After the introduction by K. B. Sharpless, the application of this reaction has been explosively growing and many areas of research now involve the “click reaction”.[22]

In our research, the click reaction was selected to synthesize the 1,4-disubstituted 1,2,3-triazole groups. A pyridine group was connected to the triazole group to enhance the coordination strength, resulting in a triazole-pyridine unit. Two such units were connected by a spacer to form bifunctional ligands (Fig. 1.24).

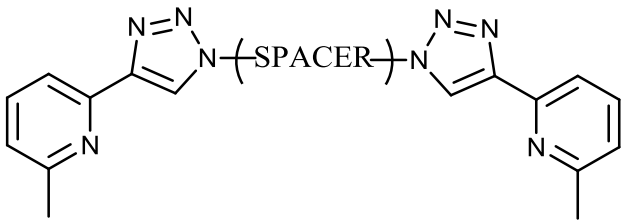

Fig. 1.24 General structure of desired ligands

1.6 Preliminary research on 1,2,3- triazole-pyridine based iron(II) dinuclear complexes.

In our group, the 1,2,3-triazole-pyridine unit was proven to have spin crossover properties in one instance only, with a propyl spacer, in the $[Fe_2(\mathbf{L6})_3](BF_4)_4$ complex (Fig. 1.26).

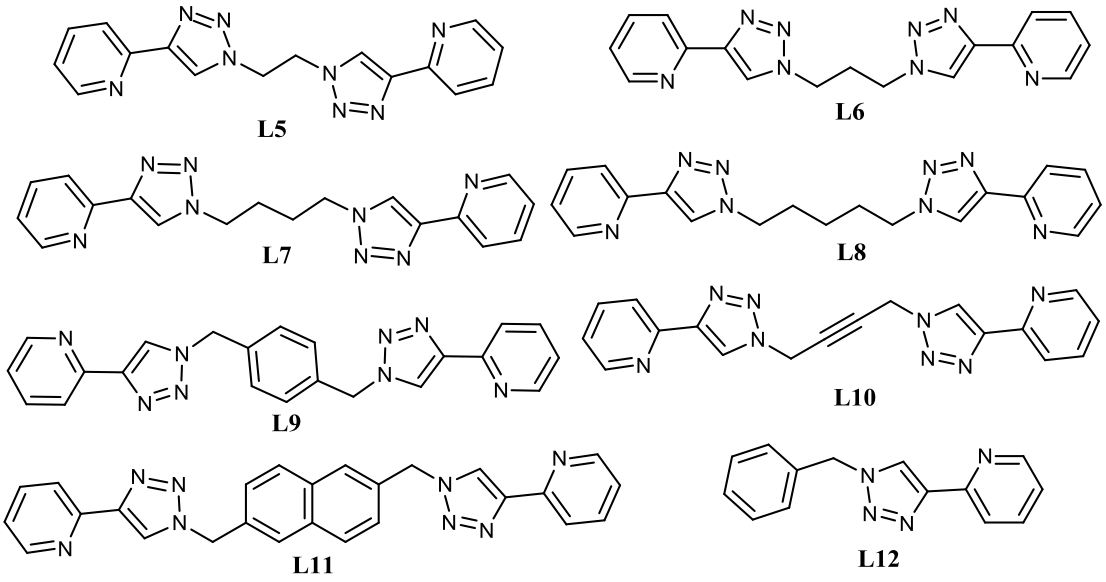

Fig. 1.25 Ligands involved in previous studies in our group.

None of the iron complexes of the other ligands (**L5, L7,** etc.) (Fig. 1.25) showed any spin-crossover.[24] For instance, the iron(II) **L9** complex stays in low spin, even at very high temperature because the LF is too strong. Hence a disturbance should be introduced to decrease the LF and possibly induce SCO.

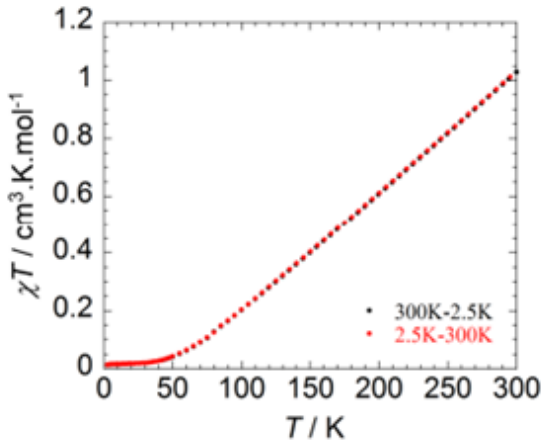

Fig. 1.26 ST curve of the iron(II)-**L6** complex.[24]

1.7 Goal of my research.

Since most complexes from previous studies in our group lack SCO properties, but **L6** gives promising results, research on the modifications on those ligands is undoubtedly worth pursuing. In order to acquire the SCO property, a modification of the current ligands was applied by introducing a methyl group beside the pyridine N atom (6-methylpyrid-2-yl).

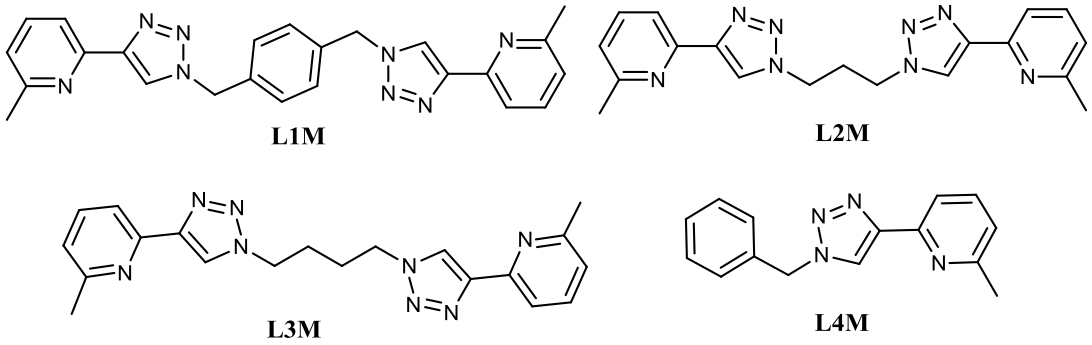

Fig. 1.27 Structures of novel ligands.

A series of modified **L9, L6, L7** ligands (named **L1M/L2M/L3M**) were made (Fig. 1.27). The derived iron(II) complexes were synthesized and characterized, and will be discussed in the following chapters. The nickel(II) complexes were also made to gain some information about the crystal field splitting parameter, 10Dq. Mononuclear complexes (ligand named **L4M**) of iron(II) and nickel(II) were prepared to compare with dinuclear species.

References

1. E. König, *Prog. Inorg. Chem.*, **1987**, *35*, 527-622; P. G. Lacroix, I. Malfant, J.A. Real and V. Rodriguez, *Eur. J. Inorg. Chem.*, **2013**, 615-627; A. Bousseksou, G. Molnár, L. Salmona and W. Nicolazzia, *Chem. Soc. Rev.*, **2011**, *40*, 3313-3335.

2. L. Cambi and L. Szego, *Chem. Ber. Dtsch. Ges* , **1931**, *64*, 2591-2598.

3. P. Gütlich and H.A. Goodwin, *Top. Curr. Chem.*, **2004**, 1-47.

4. K.H. Sugiyarto, D.C. Craig, A.D. Rae and H.A. Goodwin, *Aust. J.Chem.*, **1995**, *48*, 35-54.

5. C. J. Schneider, J. D. Cashion, N. F. Chilton, C. Etrillard, M. Fuentealba, J. A. K. Howard, J.-F. Létard, C. Milsmann, B. Moubaraki, H. A. Sparkes, S. R. Batten and K. S. Murray, *Eur. J. Inorg. Chem.*, **2013**, 850-864.

6. K.H. Sugiyarto, D.C. Craig, A.D. Rae and H.A. Goodwin, *Aust. J. Chem.*, **1993**, *46*, 1269-1290.

7. D. Pelleteret, R. Clerac, C. Mathoniere, E. Harte, W. Schmitt and P. E. Kruger, *Chem. Commun.*, **2009**, 221-223; R. J. Archer, C. S. Hawes, G. N. L. Jameson, V. McKee, B. Moubaraki, N. F. Chilton, K. S. Murray, W. Schmitte and P. E. Kruger, *Dalton Trans.*, **2011**, *40*, 12368-12373; J. R. Thompson, R. J. Archer, C. S. Hawes, A. Ferguson, A Wattiaux, C. Mathonière, R. Clérac and P. E. Kruger, *Dalton Trans.*, **2012**, *41*, 12720-12725.

8. P. Gütlich, Y. Garcia and H. A. Goodwin, *Chem. Soc. Rev.*, **2000**, *29*, 419-427.

9. E. König and K. J. Watson, *Chem. Phys. Lett.*, **1970**, *6*, 457-459.

10. H. A. Goodwin, E. S. Kucharski and A. H. White, *Aust. J. Chem.*, **1983**, *36*, 1115-

1124.

11. A. Zalkin, D. H. Templeton and T. Ueki, *Inorg. Chem.*, **1973**, *12*, 1641-1646.

12. J.-M. Lehn, A. Rigault, J. Siegel, J. Harrowfield, B. Chevrier and D. Moras, *Proc. Natl. Acad. Sci. U.S.A.*, **1987**, *84*, 2565 -2569.

13. Y. Parajo, J. Malina, I. Meistermann, G. J. Clarkson, M. Pascu, A. Rodger, M. J. Hannon and P. Lincoln, *Dalton Trans.*, **2009**, 4868-4874.

14. M. J. Hannon, *Chem. Soc. Rev.*, **2007**, *36*, 280-295.

15. B. L. Feringa, *Nat. Chem.*, **2010**, 429-430; K. Miwa, Y. Furusho and E. Yashima, *Nat. Chem.*, **2010**, 444-449.

16. M. Albrecht, *Chem. Rev.*, **2001**,*101*, 3457-3497.

17. G. Arom á, L. A. Barrios, O. Roubeau and P. Gamez, *Coord. Chem. Rev.*, **2011**, *255*, 485-546.

18. Z. Zhang and D. Dolphin, *Chem. Commun.*, **2009**, 6931-6933.

19. F. Cui, S. Li, C. Jia, J. S. Mathieson, L. Cronin, X. J. Yang, and B. Wu, *Inorg. Chem.*, **2012**, *51*, 179-187.

20.Y. Garcia, P. J. van Koningsbruggen, E. Codjovi, R. Lapouyade, O. Kahn and L. Rabardel, *J. Mater. Chem.*, **1997**, *7*, 857-858.

21. A. Michael , *J. Prakt. Chem.*, **1893**, *48*, 94-95; R. Huisgen, *Proc. Chem. Soc.*, **1961**, 357-369; H.C. Kolb, M. G. Finn and K. B. Sharpless, *Angew. Chem. Int. Ed.*, **2001**, *40*, 2004- 2021.

22. H. C. Kolb and K. B. Sharpless, *Drug Discov. Today*, **2003**, 1128-1137; W. H. Binder and R. Sachsenhofer, *Macromol. Rapid Commun.*, **2007**, *28*, 15-54.

23. V. Niel, A. B. Gaspar, M. C. Muñoz, B. Abarca, R. Ballesteros and J. A. Real, *Inorg. Chem.*, **2003**, *42*, 4782-4788.

24. C. F. C. Melan, N. Wu, K. A. Stevenson, O. Fleischel, H. Guo, F. Habib, N. J. Mosey, M. Murugesu and A. Petitjean, *Inorg. Chem.*, Submitted.

Chapter 2

Novel pyridine-triazole based bifunctional ligands.

2.1 Previous studies of the pyridine-triazole based bifunctional ligands.

The research described in this thesis focuses on the design of novel ligands, which were based on ligands previously studied in the group (**L5- L12**).[1, 3, 6]

The ligands indicated in Fig. 1.25 have been previously studied; some of them formed helicates with iron(II) and nickel(II) while others formed non-helical structures or mixtures of those two forms. Those ligands are precursors of a series of di- or multinuclear complexes in different structures. For example, in 2010 J. Crowley *et al*. reported a series of related bifunctional pyridine-triazole based ligand used in silver(I) coordination, forming interesting polymer structures in the solid state (Fig. 2.1, Fig. 2.2).

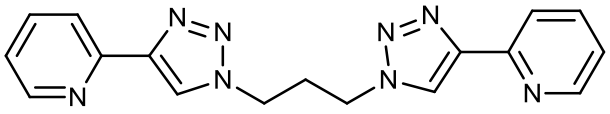

Fig. 2.1 Structure of **L6**.

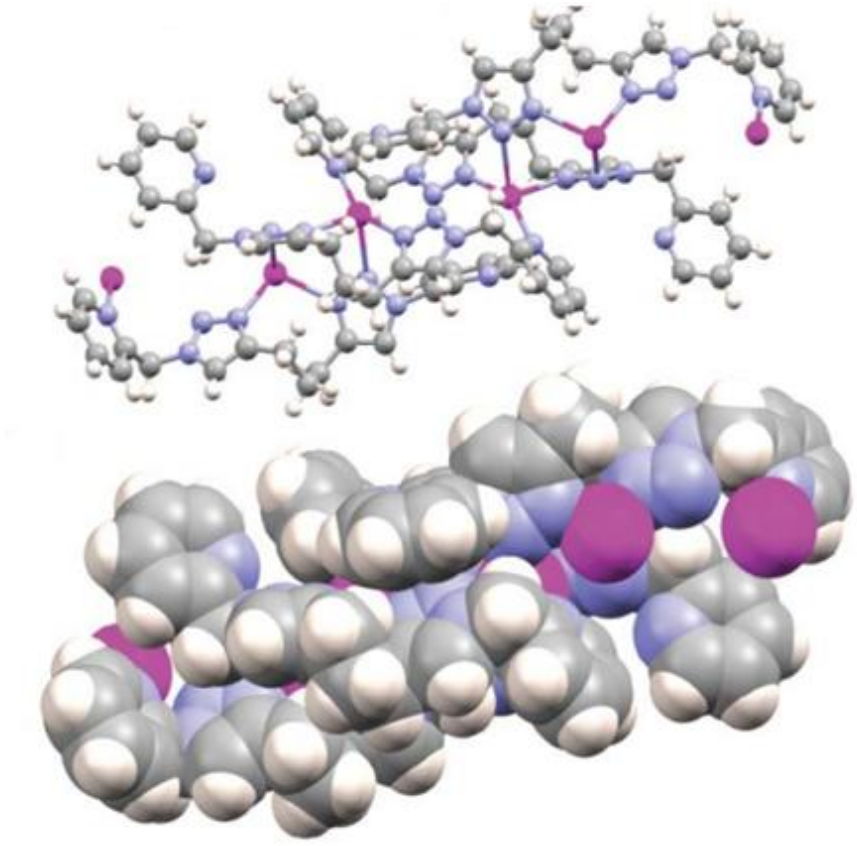

Fig. 2.2 Silver(I) complex with **L6** ligand. The picture was adapted from the original paper.[1]

Interestingly, the same ligand **L6** was synthesized in our group and resulted in dinuclear complexes, or more precisely, mesocates, with both iron(II) and nickel(II). The resulting iron(II) complex has spin crossover property (see Chapter 3). Structure of the two complexes is displayed in Fig. 2.3.

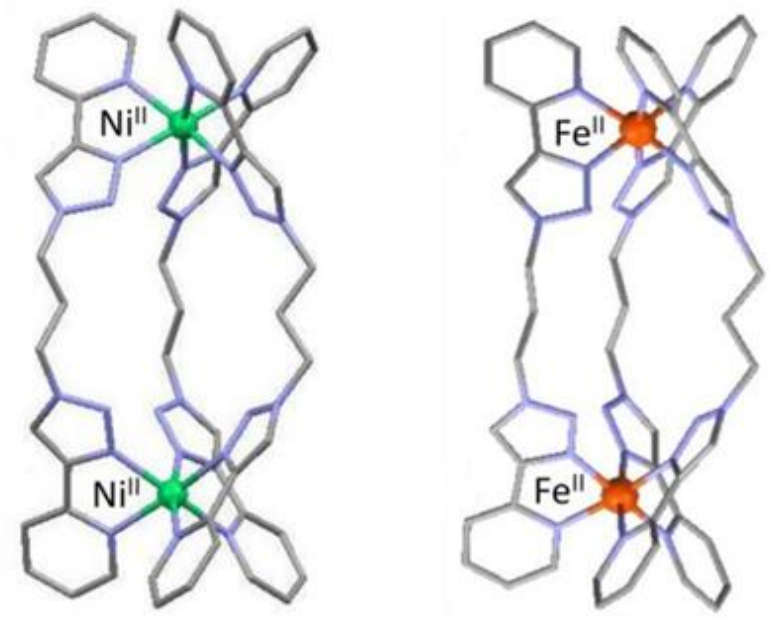

Fig. 2.3 Crystal structures of the iron(II) and nickel(II) mesocate complexes with **L6**.[3]

In order to compare mono- and di-nuclear complexes, a ligand with only one triazole-pyridine unit and a benzyl side chain was prepared (2-(1-benzyl-1H-1,2,3-triazol-4-yl)-6-methylpyridine, **L4M**).

Since **L1M, L2M** and **L3M** ligands have spacers and are analogous to previous ligands that formed helicate and mesocate structures with iron(II) and nickel(II), it was expected that those ligands could also form helicate or mesocate complexes with the two metal ions.

2.2 Design of the synthetic route.

Since the ligands can be divided into two parts (i.e. the coordination unit(s) and the spacer), the synthesis was separated into: 1) the synthesis of coordination unit, and 2)

bridging the coordination unit with the spacer. We first decided to use a commercially available methyl-substituted pyridine, then install an alkyne group, and finally connect the spacer to the methylpyridyl group via a 1,2,3-triazole ring using the CuAAC "click" reaction. Below (Fig. 2.4) is the detailed description of the individual steps in the synthetic sequence.

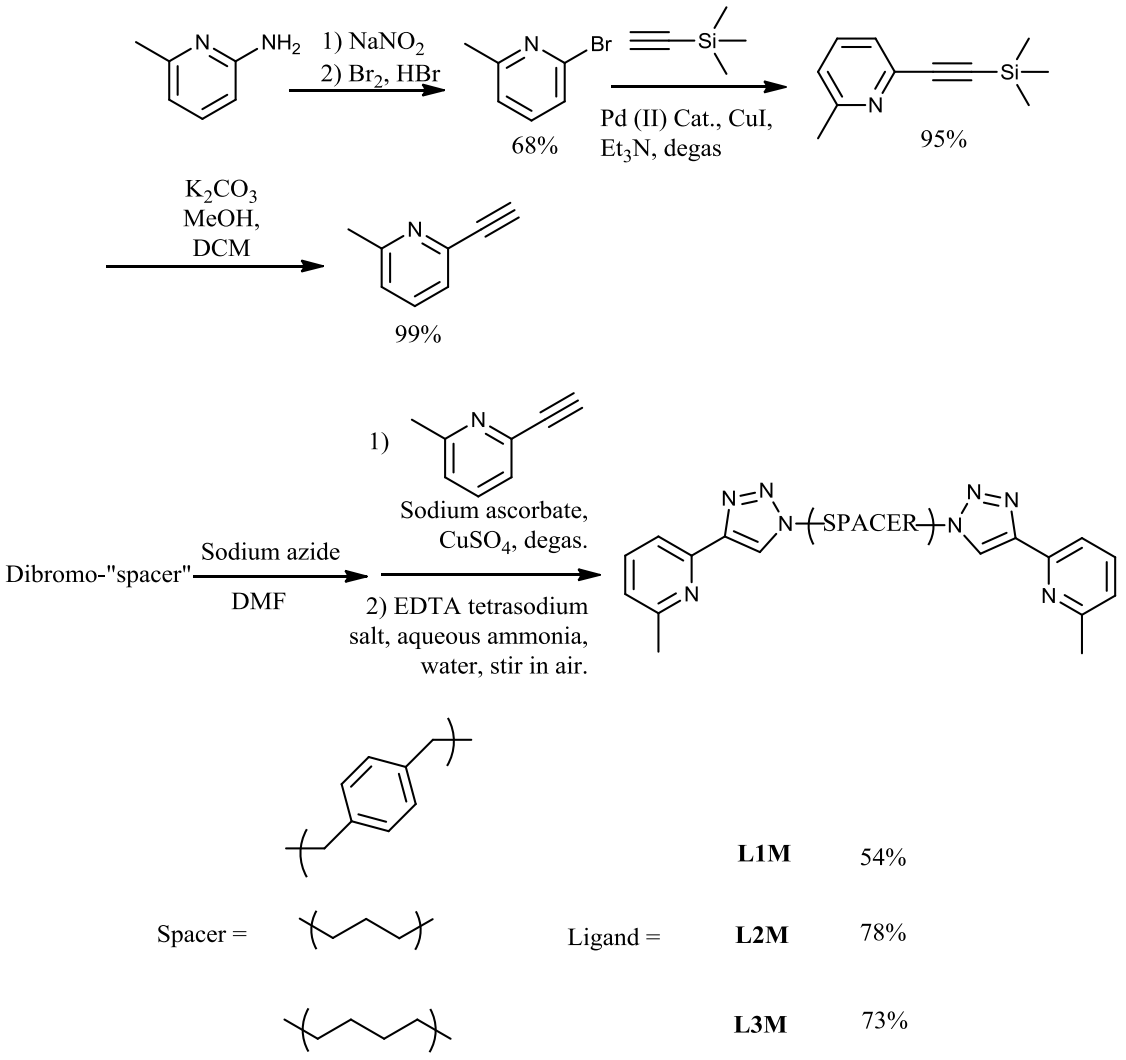

Fig. 2.4 Synthetic scheme of bifunctional ligands.

For **L4M** the synthesis was slightly different. Since it lacks a spacer, the synthesis

only involved one cycloaddition. However, the reaction conditions were identical (Fig. 2.5).

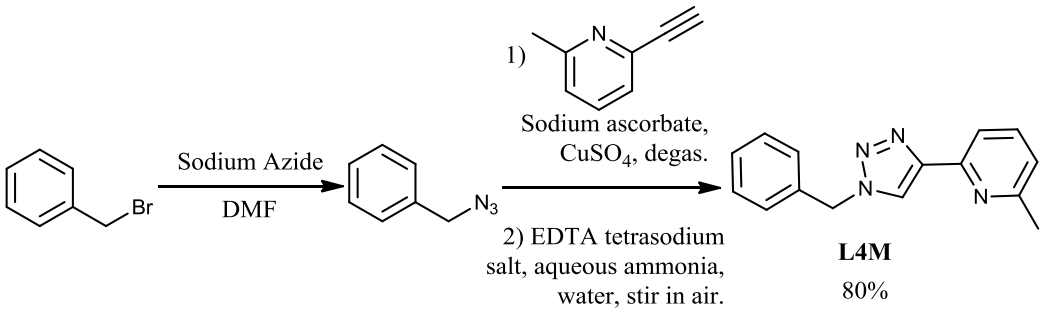

Fig. 2.5 Synthetic scheme of monofunctional ligand **L4M**.

2.3 Details of synthesis.

2.3.1 Substitution of 2-amino-6-methylpyridine.

The aim of this step is to substitute the amino group with bromine. The reaction involves a conversion from an amino group to a diazonium salt, and then addition of sodium hydroxide to decompose the diazonium ion to form the final product 2-bromo-6-methylpyridine. However, the amino group is a known strong activating group (in addition to the methyl group which is weak), thus the reaction needs to be well controlled, or the electrophilic aromatic substitution may take place at the hydrogens beside it (ortho) and opposite to it (para), due to the ortho and para director nature of the amino group. This can be avoided by carrying out the reaction at low temperature. The reaction, however, was not very easy to control, especially in the diazo reaction step and the decomposition step of the diazonium salt. Both of them are exothermic and the reaction

temperature needs to be carefully monitored. The final product, 2-bromo-6-methylpyridine was purified by vacuum fractional distillation. The by-product, which was suspected to be 2,3-dibromo-6-methylpyridine or 2,5-dibromo-6-methylpyridine, was observed in ^{1}H NMR spectrum in other fractions.

2.3.2 Sonogashira coupling.

One of the key difficulties of the overall synthetic sequence comes from the preparation of an alkyne. Traditionally, very complicated elimination reactions from dihaloalkane or vinyl halide are used, and involve a strong base such as sodium amide and high temperature (Fig. 2.6) and therefore can only be applied to some simple and thermo-stable molecules.

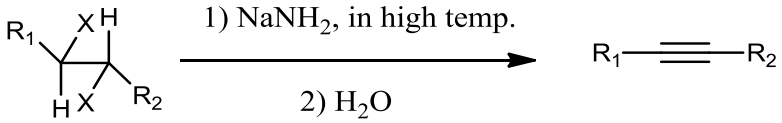

Fig. 2.6 Conventional synthesis of alkynes.

In comparison, we chose to use the Sonogashira coupling (Fig. 2.7), mainly because this method needs only relatively mild conditions and produces relatively high yields and less side product. The method was first described by K. Sonogashira in 1975,[4] who just unveiled a new era for organic synthesis. A significant amount of research based on the method further proved its high efficiency and usefulness.[5]

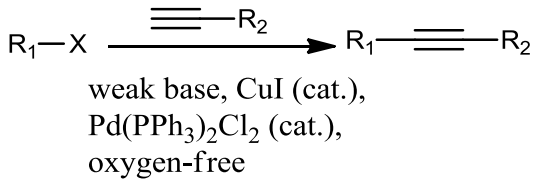

Fig. 2.7 Sonogashira coupling.

The mechanism for co-catalyst homogeneous Sonogashira coupling is still under discussion and some possible clues suggest the generally accepted catalytic cycle that follows (Fig. 2.8).[5]

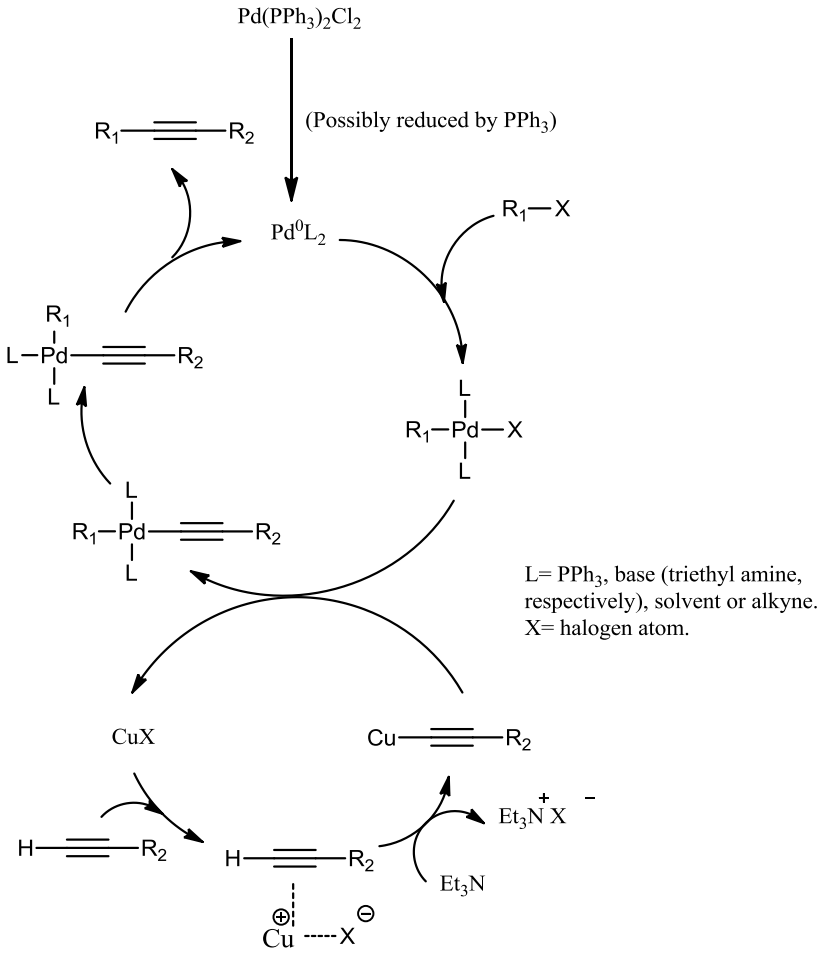

Fig. 2.8 The catalytic cycle of Sonogashira coupling.[5]

The reaction is quite sensitive to oxygen and water. Oxygen is known to yield bis-coupled products, thus lowering the yield of the desired product. What is worse, the presence of oxygen will diminish the amount of $Pd(0)L_2$, which is essential in the catalytic cycle.

The same factors were important in my research. The sequence of addition of reagents and degassing played an interesting role in the final yield. Color of the solution will turn dark (possibly palladium(II) chloride (dark brown in solution) or palladium(0) particles) if some oxygen remains in the reaction flask and oxidizes palladium catalyst, yielding more bis-coupled by-product, as evidenced by GC-MS (see below). Several trials were performed, as charted in Table 2.1.

Table 2.1 Sonogashira coupling (A= trimethylsilylacetylene, B= triethyl amine, C= CuI, D= degassing, S= dried THF Pd = Pd catalyst, Py= 2-bromo-6-methylpyridine).

	Color change in flask	DCM solution in separatory funnel (washed with water)	Final yield
S+A+B+Pd+Py→D→C→D→Reaction	Orange→brown→black	Dark solution with black foam, foam was sticky and hard to remove	59%
S+A+B +Py→D→Pd →D→C→D→Reaction	Orange→brown→black	Dark solution with bubbles.	75%
S+A+B+Py→D→Pd+C →D→Reaction	Yellow→orange→brown	Brownish solution, less bubble than before.	95%

In the very first attempt, the dark solution (which was stirred for more than one week) was sent for a GC-MS and the major side product corresponded to a bis-coupled compound 1,4-bis(6-methylpyridin-2-yl)buta-1,3-diyne and bis(6-methylpyridin-2-yl)acetylene. The formation of the two side products was considered as: 1. When the major product 2-methyl-6-((trimethylsilyl)ethynyl)pyridine formed, the trimethylsilyl group was then removed (because of the water in the air). 2. The ethynyl group then either bis-coupled to form 1,4-bis(6-methylpyridin-2-yl)buta-1,3-diyne or couple with another 2-bromo-6-methyl-pyridine to form bis(6-methylpyridin-2-yl)acetylene. The two species are more polar than major product 2-methyl-6-((trimethylsilyl)ethynyl)pyridine, as two pyridine rings exist in one molecule in those structures. The reaction of 1,4-bis(6-methylpyridin-2-yl)buta-1,3-diyne is known as alkyne homocoupling, but here it is considered as a side reaction and only decreases the yield.

Therefore, the main idea of increasing the yield is to avoid air, make sure to degas before addition of the Pd catalyst, and finish the reaction in a limited time. For the first trial in the chart, the sequence suggested that the Pd catalyst might decompose as soon as it was added, since oxygen might exist in the reagents (THF, base and starting material). In the second attempt, adding the Pd and Cu catalysts separately may have been problematic since air flushed into the flask when the flask was opened for the addition of the copper catalyst, and the exposure to oxygen surely destroyed some of the Pd catalyst. The third trial proved that degassing was effective.

Interestingly, the THF used in the work-up also mattered. If THF from an old bottle was used in the work-up, the solution would immediately turn dark. It was

concluded that the old THF may contain peroxides,[6] which are very strong oxidizers and the product was considered to be oxidized in the presence of the peroxides, together with the Pd catalyst, which explained the color change. An alkyne is not sensitive to weak oxidizers; but strong oxidizer as it is, the peroxide would react with the alkyne, breaking the triple bond and yielding carboxyl species.

2.3.3 Alcoholysis ('de-protection') of the trimethylsilyl group.

Apart from the difficulties in the Sonogashira coupling, the alcoholysis of the trimethylsilyl group only requires potassium carbonate and methanol to produce the methoxide anion in dichloromethane at room temperature. The yield of the reaction was very high (95~99%) and no chromatography was needed. The only important thing to remember is to refrain from using the oil vacuum pump after work-up, since not only the remaining solvent but also the 2-ethynyl-6-methylpyridine product would evaporate under high vacuum.

2.3.4 "Click reaction" and "One-pot" process.

As mentioned above, the "click reaction" provides a simple approach in synthesis. One of the examples mentioned in the article by K. B. Sharpless is the CuAAC reaction (Copper(I)-catalyzed Azide-Alkyne Cycloaddition), which is the reaction applied in my research.[7] The reaction is quite popular because it reveals a new route in heterocycle synthesis. The importance of the reaction is growing in both chemistry and other areas,

such as drug making and biochemistry.

The catalytic cycle is below (Fig. 2.9):

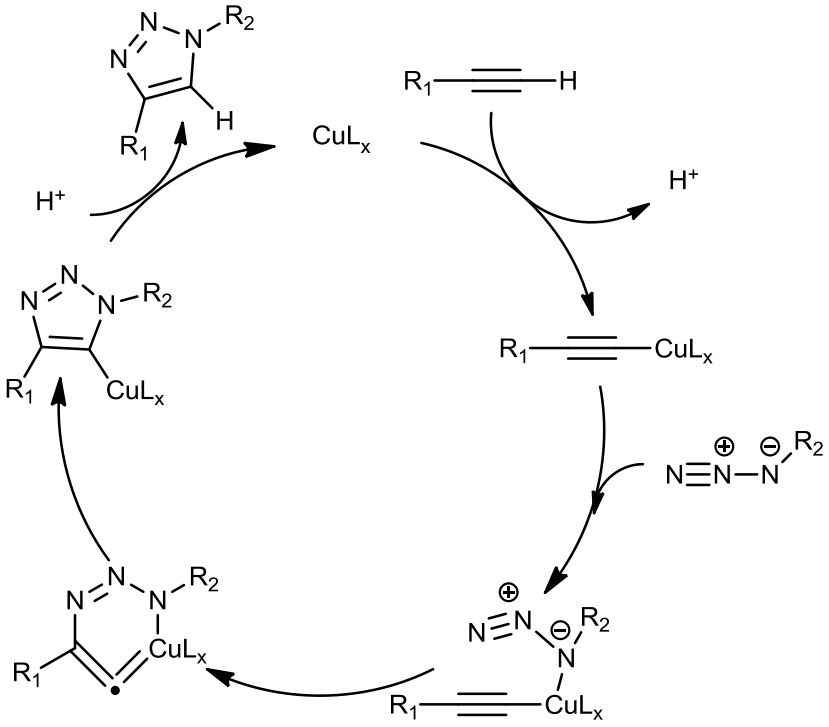

Fig. 2.9 Catalytic cycle of the click reaction.[8]

The final step was adapted from previous studies from our group,[9] and is considered to be a "one-pot, two step" CuAAC click reaction. The reaction starts with a mixture of "spacer" halide (**L1M**: 1,4-bis(bromomethyl)benzene, **L2M**: 1,3-dibromopropane, **L3M**: 1,4-dibromobutane, **L4M**: benzyl bromide) and sodium azide in DMF, where an S_N2 reaction occurs. After several hours, the solution is mixed with 2-ethynyl-6-methylpyridine, copper(II) sulfate, sodium ascorbate, and water, and is degassed. Copper(II) is reduced to copper(I) by ascorbate and tends to coordinate to the triazole N-donor, favouring the production of the triazole group.

In the overall process, the alkyl azide is never separated from the mixture after substitution, and the solution is directly used in the second step ("Click reaction"); that is where the "one-pot" name comes from (Fig. 2.10).

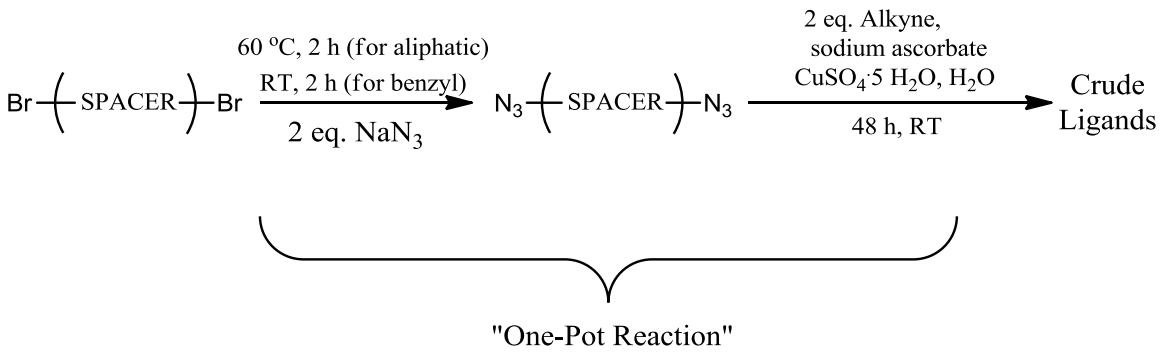

Fig. 2.10 Scheme of One-Pot Reaction

After 24-48 hours, the mixture is transferred to a large beaker with addition of EDTA tetrasodium salt, water, aqueous ammonia and stirred in air. Once oxidation takes place (by oxygen from air), the copper(II) ion is more weakly bound to the triazole-pyridine ligand, and binds to EDTA or ammonia, thus the desired compound is freed, isolated by filtration as a mostly white powder. Finally, column and/or recrystallization are necessary to access the pure ligand.

The reason a one-pot procedure is used is because of the highly explosive nature of the azide. Inorganic azides are quite sensitive to heat and shock, which actually led them to become popular explosives in detonators (lead(II) azide) and safe air bags (sodium azide). At the same time, organic azide compounds are even more dangerous since they provide 'fuel' to the explosion, even in cool conditions.[10] Although aromatic azides are a bit safer, aliphatic azides are thought to be very hazardous due to their poor

stability. Therefore we avoided the separation of the organic azides, and, instead, we carefully prepared the azide in situ and quickly directly used it in next step. This method not only saved time, but was also safer.

Overall, the reaction is quite simple and little effort is needed to get a reasonable yield. This highlights the steps in ligand preparation.

2.4 L1M ligand.

In the very beginning, the **L1M** ligand was considered as the most interesting ligand, as the original **L9** compound only yielded a LS iron(II) complex. The introduction of the methyl group was believed to induce some steric hindrance and may lead to a more HS species or even spin crossover in the iron(II) **L1M** complex. After spending a long time in trials of reaction conditions, successful synthesis and necessary characterization of **L1M** were achieved.

L1M was recrystallized from ethanol giving a yellowish powder. It was then purified by column chromatography after recrystallization, giving a white powder.

Because the flexibility of the ligand was suspected to be an important factor in the complexation, bifunctional ligands with flexible propyl (**L2M**) and butyl (**L3M**) spacers were also prepared.

2.5 L2M, L3M and L4M ligands.

The Click reaction for all bifunctional ligands was carried out using the same

procedure as above, and an excess of alkyne and azide was used to avoid mono-cycloaddition. Once in the **L2M** syntheses, however, only two equivalents of azide were used, and some mono-cycloaddition product was separated as an oil-like liquid, contrary to **L2M** which is a solid. The other alkyl substituent was unknown since the azide group and halide group are undistinguishable by ^{1}H NMR spectroscopy.

The two **L2M** and **L3M** ligands were fully characterized. **L2M** formed very large crystals whereas **L3M** only gave a white powder. The solubility also differed: **L3M** was not very soluble in dichloromethane, acetone and ethyl acetate, but **L2M** had very good solubility in those solvents.

The characterization of **L2M** and **L3M** was simple, because of their highly predictable peaks in proton NMR (see experimental part).

The synthesis of **L4M** was slightly different. The relatively more reactive benzyl bromide (in comparison with aliphatic bromides) only required an equal amount of azide. Since there was no concern with mono-cycloaddition, excess alkyne was not necessary.

2.6 Experimental details.

Materials and Methods: All commercially available compounds were used as received. Deuterated solvents, except for $CDCl_3$ because it may contain acid, were used as received. $CDCl_3$ was pre-treated by passing through a short column of basic alumina (such treated $CDCl_3$ will be signaled below by an asterisk, i.e., '$CDCl_3$*'). ^{1}H NMR spectroscopy and ^{13}C NMR spectroscopy were performed using 300 MHz, 400 MHz and 500 MHz Bruker instruments. Peak listings for all NMR spectra are given in ppm and

referenced against the solvent residual signal. Column chromatography was performed on silica gel with a particle size of 40-63 μm and a pore diameter of 60 Å. GC-MS for crude analysis was carried out on Agilent 6850-5975C MSD GC-MS instrument. Mass spectrometry (MS) was carried out by electron ionization-time of flight (EI-TOF) method on the mass spectrometer of Waters/Micromass GC-TOF system. The EA was carried out by Laboratoire d'Analyse Élémentaire de l'Université de Montréal.

2.6.1 2-Bromo-6-methylpyridine. [11]

To a stirred solution of 2-amino-6-methylpyridine (10 g, 92.5 mmol, 1.0 eq), and 48% hydrobromic acid (50 mL), bromine (13.3 mL, 258 mmol, 2.8 eq) was added dropwise at -8 ℃. The

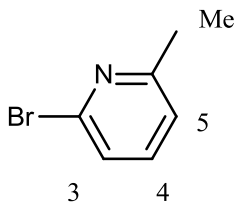

solution was stirred for another 1 h before sodium nitrite (17 g in 25 mL water, 9.88 mol L^{-1}, 247 mmol, 2.67 eq) was slowly added to the solution at -8 ℃. The temperature of the reaction mixture was raised to room temperature and the mixture stirred for 30 min and then cooled to -8 ℃ again. To destroy the remaining acid and bromine, a solution of sodium hydroxide (50 mL, 40%, 500 mmol, 5.4 eq) was added slowly. The final dark orange suspension was extracted with ethyl acetate (70 mL) three times and all organic phases were combined and dried with anhydrous sodium sulfate. After rotary vacuum evaporation of the filtrate, fractional vacuum distillation was applied to the remaining brownish oil-like liquid. Three different fractions were separated but only the first (purest)

one was selected for further applications after ^{1}H NMR analysis. Final yield: 10.7 g (68%). ^{1}H NMR ($CDCl_3$ *, 300 MHz): 7.42 (dd, ^{3}J = 7.8 Hz, 1 H, H4), 7.29 (d, ^{3}J = 7.9 Hz, 1 H, H3), 7.10 (d, ^{3}J = 7.3 Hz, 1 H, H5), 2.54 (s, 3 H, Me).

2.6.2 2-Methyl-6-((trimethylsilyl)ethynyl)pyridine. [12]

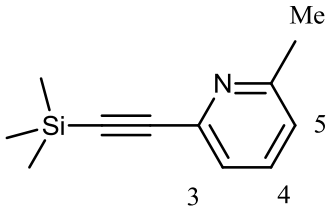

2-Bromo-6-methylpyridine (700 mg, 0.47 mL, 4.07 mmol, 1.0 eq), trimethylsilyl acetylene (440 mg, 0.58 mL, 4.48 mmol, 1.1 eq) in 10 mL degassed and dried THF and freshly distilled triethyl amine (1.65 g, 16.3 mmol, 4.0 eq) were added into a reaction flask and the solution was degassed by bubbling argon. The catalysts composed of bis(triphenylphosphine)palladium(II) dichloride (85 mg, 0.12 mmol, 0.03 eq) and copper(I) iodide (23 mg, 0.12 mmol, 0.03 eq) were then added. The mixture was degassed again as soon as the catalysts were added. The reaction mixture was stirred under argon for 15 min and then heated to 60 ℃ for 2 h and cooled to room temperature. After stirring at room temperature for 17 h, the solvent of the suspension was evaporated, the remaining solid was dissolved in dichloromethane (15 mL) and washed with water (20 mL) three times. The organic phases were combined and dried with anhydrous sodium sulphate. Dichloromethane was evaporated by rotary vacuum evaporation and column chromatography was run to isolate pure 2-methyl-6-((trimethylsilyl)ethynyl)pyridine. The eluent was a combination of 1:25 then 1:18 ethyl acetate: hexanes. Final yield: 730 mg (95%). ^{1}H NMR ($CDCl_3$ *, 300 MHz): 7.51 (dd, ^{3}J

= 8.2 Hz, 1 H, H4), 7.27 (d, ^{3}J = 8.2 Hz, 1 H, H3), 7.08 (d, ^{3}J = 7.6 Hz, 1 H, H5), 2.54 (s, 3 H, Me), 0.26 (s, 9 H, Si<u>Me</u>).

2.6.3 2-Ethynyl-6-methylpyridine. [13]

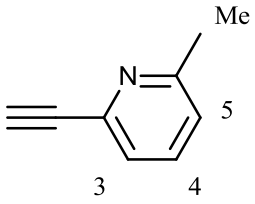

2-Methyl-6-((trimethylsilyl)ethynyl)pyridine (730 mg, 3.86 mmol, 1.0 eq) was dissolved in methanol (5 mL) and dichloromethane (10 mL). Potassium carbonate (1.3 g, 9.42 mmol, 2.4 eq) was then added and the heterogeneous mixture vigorously stirred. After 2 h, the solvent was evaporated in vacuum. Dichloromethane and water (5 mL/ 10 mL) were added and sonication was used to dissolve the salts and organic compounds. The dichloromethane layer was separated and washed with water (2 × 20 mL). The organic layer was partitioned and dried with anhydrous sodium sulfate. After removal of dichloromethane by rotary evaporation, the remaining yellow liquid was analyzed by ^{1}H NMR and confirmed as pure 2-ethynyl-6-methylpyridine. Yield: 425 mg (95%). ^{1}H NMR ($CDCl_3$ *, 500 MHz): 7.55 (dd, ^{3}J = 8.2 Hz, 1 H, H4), 7.30 (d, ^{3}J = 8.2 Hz, 1 H, H3), 7.13 (d, ^{3}J = 7.8 Hz, 1 H, H5), 3.12 (s, 1 H, ethynyl proton), 2.56 (s, 3 H, Me).

2.6.4 1,4-Bis((4-(6-methylpyridin-2-yl)-1H-1,2,3-triazol-1-yl)methyl)benzene (L1M).

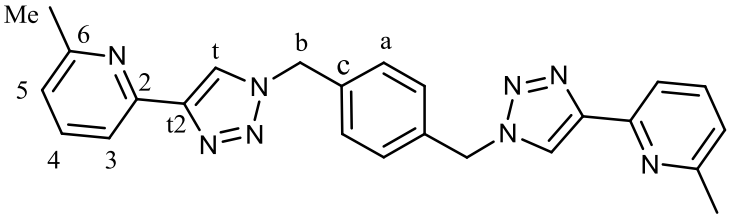

To a stirred solution of α,α'-dibromo-p-xylene (145 mg, 0.55 mmol, 1.0 eq) in DMF (10 mL), sodium azide (79 mg, 1.2 mmol, 2.15 eq) was added. The solution was stirred for 3 h. water (4.5 mL), sodium ascorbate (207 mg, 1.05 mmol, 1.9 eq), copper(II) sulfate pentahydrate (55 mg, 0.22 mmol, 0.4 eq), 2-ethynyl-6-methylpyridine (143 mg, 1.22 mmol, 2.15 eq) were then added. After degassing for 5 min, the solution was stirred under argon for two days. The solution was then exposed to air and stirred for five days to oxidize copper(I) to copper(II). The suspension was filtered and the precipitate was washed with water. Recrystallization from hot ethanol (7 mL) yielded 126 mg (54 %) of a light yellow solid. ^{1}H NMR ($CDCl_3$ *, 400 MHz): 8.07 (s, 2 H, Ht), 7.94 (d, ^{3}J = 7.6 Hz, 2 H, H3), 7.63 (dd, ^{3}J = 7.6 Hz, 2 H, H4), 7.32 (s, 4 H, Ha), 7.06 (d, ^{3}J = 7.6 Hz, 2 H, H5), 5.56 (s, 4 H, Hb), 2.51 (s, 6 H, Me). ^{13}C NMR ($CDCl_3$ *, 100 MHz): 158.2 (C6), 149.5 (C2), 149.1 (Ct2), 137.1 (C4), 135.3 (Cc), 128.9 (Ca), 122.6 (C3), 122.0 (Ct), 117.4 (C5), 53.8 (Cb), 24.5 (Me). Melting point: 194-195 ℃. EA Calc. for $C_{24}H_{22}N_8 \cdot 1.3\ H_2O$: %C 64.65, %H 5.56, %N 25.13. Found: %C 64.65, %H 5.45, %N 25.14. EI-MS: Calc. for $C_{24}H_{22}N_8$: 422.1967, found: 422.20 (M^+, 70%), 131.06 ($C_8H_7N_2^+$, 76%), 104.05 ($C_7H_6N^+$, 100%).

2.6.5 1,3-Bis(4-(6-methylpyridin-2-yl)-1H-1,2,3-triazol-1-yl)propane (L2M).

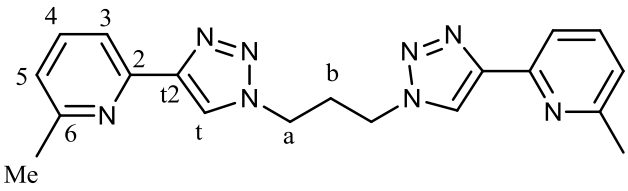

To a stirred solution of 1,3-dibromopropane (118 mg, 0.58 mmol, 1.0 eq) in DMF (12 mL) was added sodium azide (85 mg, 1.29 mmol, 2.2 eq). The mixture was stirred at room temperature for 20 h. Then were added water (3 mL), copper(II) sulfate pentahydrate (55 mg, 0.22 mmol, 0.4 eq), sodium ascorbate (214 mg, 1.08 mmol, 1.86 eq) and 2-ethynyl-6-methylpyridine (148 mg, 1.26 mmol, 2.16 eq). The resulting mixture was stirred at room temperature under argon for 70 h. To the mixture were added a saturated solution of aqueous EDTA (8 mL), ammonia (8 mL) and water (35 mL). The resulting suspension was stirred vigorously in air until the solution became dark green and the precipitate white. The solid was filtered, washed with water, air-dried and purified by column (dichloromethane: acetone, 5:1 then 1:1) to give pure **L2M** as shiny crystals with an overall yield of 78%. ^{1}H NMR ($CDCl_3$ *, 400 MHz): 8.24 (s, 2 H, Ht), 7.95 (d, ^{3}J = 7.4 Hz, 2 H, H3), 7.66 (dd, ^{3}J = 7.8 Hz, 2 H, H4), 7.10 (d, ^{3}J = 7.8 Hz, 2 H, H5), 4.49 (t, ^{3}J = 6.4 Hz, 4 H, Ha), 2.66 (quint., ^{3}J = 6.4 Hz, 4 H, Hb), 2.57 (s, 6 H, Me).^{13}C NMR ($CDCl_3$ *, 100 MHz): 158.3 (C6), 149.4 (C2), 149.4 (Ct2), 137.0 (C4), 122.6 (C3), 122.5 (Ct), 117.2 (C5), 46.9 (Ca), 30.7 (Cb), 24.5 (Me). EA: *calc*. for $C_{19}H_{20}N_8$ %C 63.32, % H 5.59, % N 31.09, *found*, % C 63.41, % H 5.64, % N 31.18. M. P. 125.5-126.7 ℃ EI-MS: Calc. for $C_{19}H_{20}N_8$: 360.1811, found: 360.20 (M^+, 100%), 131.06 ($C_8H_7N_2^+$, 73%), 104.05 ($C_7H_6N^+$, 59%), 92.05 ($C_5H_4N^+$, 59%).

2.6.6 1,4-Bis(4-(6-methylpyridin-2-yl)-1H-1,2,3-triazol-1-yl)butane (L3M).

To a stirred solution of 1,3-dibromobutane (99 mg, 0.46 mmol) in DMF (10 mL) was added sodium azide (73 mg, 1.1 mmol, 2.4 eq). The mixture was stirred at 60 ℃ for 20 h. Then were added water (3 mL), copper(II) sulfate pentahydrate (54 mg, 0.22 mmol, 0.5eq), sodium ascorbate (210 mg, 1.06 mmol, 2.3 eq) and 2-ethynyl-6-methylpyridine (117 mg , 1.0 mmol, 2.2 eq). The resulting mixture was stirred at room temperature under argon for 48 h. To the mixture were added a saturated solution of aqueous EDTA (8 mL), ammonia (8 mL) and water (36 mL). The resulting suspension was stirred vigorously in air until the solution became dark green and the precipitate white. The solid was filtered, washed with water, air-dried and purified by column (dichloromethane: acetone, 5:1 then 1:1) to give pure **L3M** white powder with an overall yield of 73%. ^{1}H NMR ($CDCl_3$ *, 400 MHz): 8.12 (s, 2 H, Ht), 7.94 (d, ^{3}J = 7.7 Hz, 2 H, H3), 7.64 (dd, ^{3}J = 7.8 Hz, 2 H, H4), 7.07 (d, ^{3}J = 7.7 Hz, 2 H, H5), 4.45 (br s, 4 H, Ha), 2.55 (s, 6 H, Me), 2.02 (br s, 4 H, Hb). ^{13}C NMR ($CDCl_3$ *, 100 MHz): 158.3 (C6), 149.5 (C2), 149.0 (Ct2), 137.0 (C4), 122.5 (C3), 121.9 (Ct), 117.2 (C5), 49.4 (Ca), 27.1 (Cb), 24.5 (Me). EA: *calc*. for $C_{19}H_{20}N_8$: %C 64.15, % H 5.92, % N 29.93, *found*, % C 64.06, % H 5.93, % N 29.94. M. P. 185-187 ℃. EI-MS: Calc. for $C_{20}H_{22}N_8$: 374.1967, found: 374.19 (M^+, 100%), 215.13 ($C_{12}H_{16}N_4^+$, 40%), 173.10 ($C_{10}H_{11}N_3^+$, 42%).

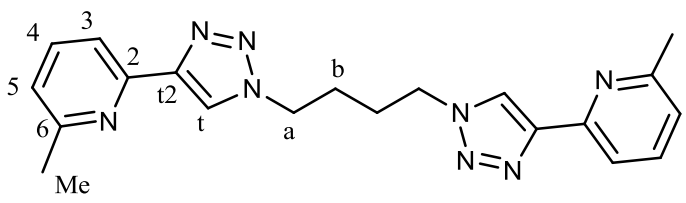

2.6.7 2-(1-Benzyl-1H-1,2,3-triazol-4-yl)-6-methylpyridine (**L4M**).

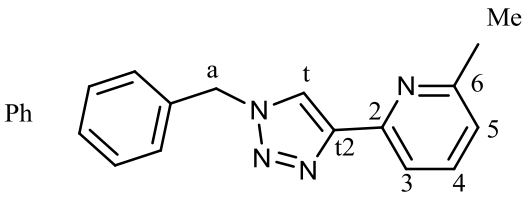

To a stirred solution of benzyl bromide (210 mg, 1.23 mmol, 1 eq) in DMF (20 mL), was added sodium azide (85 mg, 1.27 mmol, 1.05 eq) and the solution was stirred for 3 d in room temperature. The solution was directly mixed with 2-ethynyl-5-methylpyridine (145 mg, 1.24 mmol, 1 eq), copper(II) sulfate pentahydrate (122 mg, 0.49 mmol, 0.4 eq), sodium ascorbate (440 mg, 2.22 mmol, 1.8 eq) and 5 mL water. After stirring for 2 days, the mixture was transferred to a beaker containing water (70 mL), aqueous ammonia (16 mL) and EDTA tetrasodium salt solution (1.9 g in 16 mL water). The reaction mixture was filtered under vacuum and the white solid was washed with water after the solution had turned green. The solid was further purified by column chromatography (acetone: dichloromethane, 1:10). Yield: 243 mg (80%). ^{1}H NMR ($CDCl_3$ *, 400 MHz, 25 ℃): 8.05 (s, 1 H, Ht), 7.98 (d, ^{3}J = 7.8 Hz, 1 H, H3), 7.64 (dd, ^{3}J = 7.7 Hz, 1 H, H4), 7.26-7.35 (m, 5 H, Ph), 7.06 (d, ^{3}J = 7.7 Hz, 1 H, H5), 5.58 (s, 2 H, Ha), 2.53 (s, 3 H, Me). ^{13}C NMR ($CDCl_3$ *, 100 MHz, 25 ℃): 158.2 (C6), 149.7 (C2), 149.1 (Ct2), 137.0 (C4), 134.5 (Ph), 129.1 (Ph), 128.3 (Ph), 126.6 (Ph), 122.4 (C3), 121.9 (Ct), 117.3 (C5), 54.4 (Ca), 24.5 (Me). Rf (SiO_2, acetone: dichloromethane, 1:10) : 0.3. EA: *calc*. for $C_{15}H_{14}N_4$, % C 71.98, % H 5.64, % N 22.38, *found*, % C 71.91, % H 5.57, % N 22.48. Mp: 140-142 ℃**.** EI-MS: Calc. for $C_{15}H_{14}N_4$: 250.1218, found: 250.12 (M^+, 19%), 221.11($C_{15}H_{13}N_2^+$, 100%), 131.06($C_8H_7N_2^+$, 56%), 91.05 ($C_7H_7^+$, 95%).

2.7 Conclusion

In summary, we successfully prepared and characterized a series of novel 1,2,3-triazole-pyridine based bifunctional ligands **L1M, L2M, L3M** and **L4M**. We also looked into the synthesis route to increase the efficiency and further studies of complexes were needed, which are described in the next chapter.

References

1. O. Fleischel, N. Wu and A. Petitjean, *Chem. Commun.*, **2010**,*46*, 8454-8456.

2. J. Crowley and P. Bandeen, *Dalton Trans*., **2010**, 612-623.

3. C. F. C. Melan, N. Wu, K. A. Stevenson, O. Fleischel, R. Wang, F. Habib, N. J. Mosey, M. Murugesu and A. Petitjean, *Inorg. Chem.,* Submitted.

4. K. Sonogashira, Y. Tohda and N. Hagihara, *Tetrahedron Lett.*, **1975**, *16*, 4467-4470; K. Sonogashira, *J. Organomet. Chem.*, **2002**, *653*, 46-49.

5. R. Chinchilla and C. Najera, *Chem. Rev.*, **2007**, *107*, 874−922; R. Chinchilla and C. Nájera, *Chem. Soc. Rev.*, **2011**, *40*, 5084-5121.

6. A. Rieche and R. Meister, *Angew. Chem.*, **1936**, *49*, 101-103.

7. R. Huisgen, *Proc. Chem. Soc.*, **1961**, 357–369; R. Huisgen, *Angew. Chem. Int. Ed*., **1963**, *2*, 604-637; H.C. Kolb, M. G. Finn and K. B. Sharpless, *Angew. Chem. Int. Ed.*, **2001**, *40*, 2004-2021.

8. J. E. Hein and V. V. Fokin, *Chem. Soc. Rev.*, **2010**, *39*, 1302–1315.

9. K. A. Stevenson, C. F. C. Melan , O. Fleischel , R. Wang and A. Petitjean, *Cryst. Growth Des*., **2012**, *12*, 5169-5173.

10. R. E. Conrow and W. D. Dean, *Org. Process Res. Dev.*, **2008**, *12*, 1285–1286; K. Banert, Y.-H. Joo, T. Rüffer, B. Walfort, and H. Lang, *Angew Chem. Int. Ed.*, **2007**, *46*, 1168-1171.

11. U. S. Schubert, C. Eschbaumer and M. Heller, *Org. Lett.*, **2000**, *2*, 3373-3376.

12. D. Alagille, R. M. Baldwin, B. L. Roth, J. T. Wroblewski, E. Grajkowska and G. D. Tamagnan, *Bioorg. Med. Chem.*, **2005**, *13*, 197-209.

13. L. S. Kallander, Q. Lu, W. Chen, T. Tomaszek, G. Yang, D. Tew, T. D. Meek, G. A. Hofmann, C. K. Schulz-Pritchard, W. W. Smith, C. A. Janson, M. D. Ryan, G.-F. Zhang, K. O. Johanson, R. B. Kirkpatrick, T. F. Ho, P. W. Fisher, M. R. Mattern, R. K. Johnson, M. J. Hansbury, J. D. Winkler, K. W. Ward, D. F. Veber and S. K. Thompson, *J. Med. Chem.*, **2005**, *48*, 5644-5647.

Chapter 3

Novel iron(II) and nickel(II) dinuclear complexes.

3.1 Previous studies of iron(II) and nickel(II) complexes.

Iron and nickel dinuclear complexes are of particular interest in our group. The structural patterns (helicate and mesocate), metal-metal interaction, potential molecular recognition in the cavity and packing orientation were well described in previous publications.[1,2] In addition, since one of the iron complexes ($[Fe_2(\mathbf{L6})_3](BF_4)_4$) shows a spin-crossover property,[2] this encouraged us to explore SCO in modified complexes.

3.2 Design of novel iron(II) and nickel(II) complexes.

Iron(II) complexes are the most popular among SCO complexes. Some calculations about the coordination (i.e. crystal field stabilization energy (CFSE), 10Dq) also need to be considered for a better understanding of the coordination and magnetism nature.

Because many iron(II)-based SCO systems have been characterized through the ligand field of their nickel(II) complexes, we estimated the 10Dq on the basis of the analogous nickel(II) complexes rather than iron(II).[3] This is because nickel(II) has a d^8 configuration and no spin transition will happen, which allows the relatively weak d-d transition bands to be observed. Based on the wavelength of the peak, an estimate of the ligand field can be calculated.[4] The calculation is explained as follows: the

nickel(II) ion has electron configuration of [Ar] $4s^0$ $3d^8$. The spin quantum number (S) is the total sum of m_s. As there are two unpaired electrons, and all paired electrons have opposite spins values and cancel out, the equation is:

$$S = 3 \times (+1/2 + -1/2) + 2 \times 1/2 = 1$$

The orbital angular momentum quantum number (L) is 3. So the result ground term is:

$$F^{(2S+1)}=F^3$$

As Ni(II) complexes are octahedral in the context of our research, the ground state of nickel(II) complexes is A_{2g}, and the excitation energy from $^3A_{2g}(F)$ to $^3T_{2g}(F)$ equals the crystal field splitting parameter, 10Dq. Among all three spin-allowed d-d transitions from $^3A_{2g}(F)$ state, the $^3A_{2g}(F)$ to $^3T_{2g}(F)$ is the lowest for nickel(II), which means the wavelength is the longest. Former findings confirmed the band lies in the near IR,[3] thus a scanning of the UV-Vis spectrum with large range is needed. The highest scanning wavelength was set to 1100 nm.

The connection between 10Dq values of analogous iron(II) and nickel(II) complexes can be explained by the empirical equation:

$$\frac{10\mathrm{Dq(Fe)}}{10\mathrm{Dq(Ni)}} = C$$

The C value is equivalent to 1.11 ± 0.07, so determining the 10Dq(Ni) allows to have an idea about the 10Dq value of the corresponding iron(II) complex.[3]

In our group, the first investigated bifunctional ligand was **L9** (Fig. 3.1), which binds iron(II) and nickel(II) well, but only forms a low spin complex with iron(II).

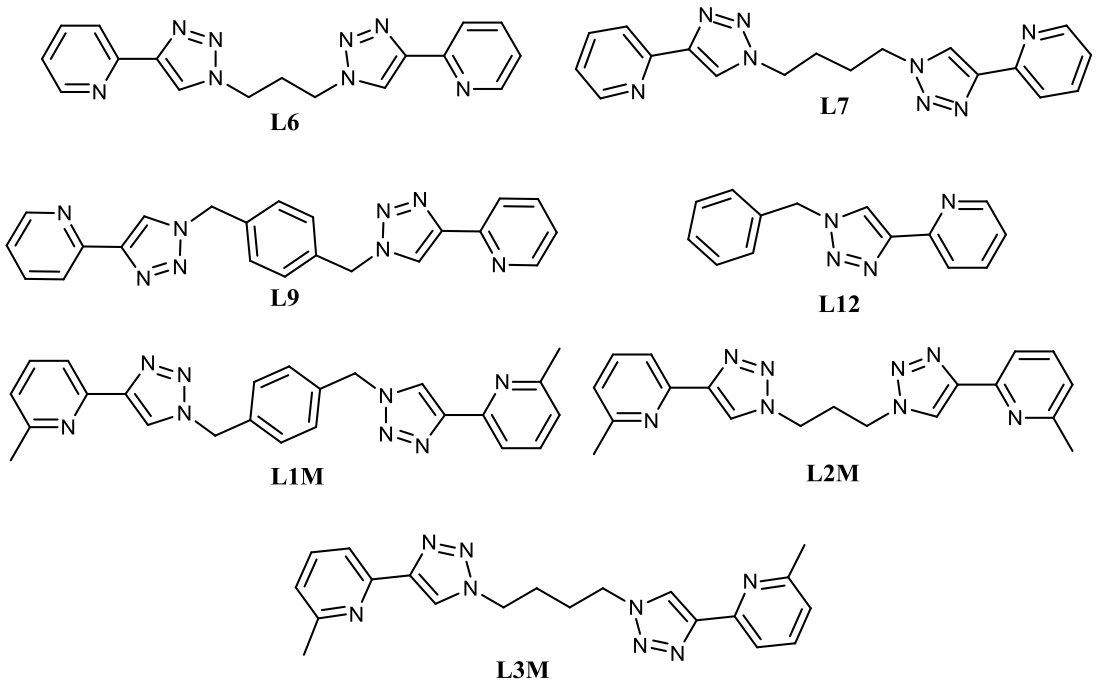

Fig. 3.1 Structure of ligands

The iron(II) **L9** complex stays at low spin, thus it is a great precursor for methyl modification. What is more, **L9** complexes crystallize easily, most likely because of the benzene ring, which provides a good backbone for packing in the crystal. The isolation of single crystals is valuable in the magnetism studies. As a result, **L9** is an ideal candidate for modification.

The $[Fe(\mathbf{L6})_3](BF_4)_4$ complex was the only one with spin crossover property in our lab's previous study. Similarly to **L9**, chemical modification on **L6** (Fig. 3.1) was expected to tune the spin transition. The original transition takes place from 40 K and does not finish even at 300 K (incomplete transition). Moreover, it lacks hysteresis as the cooling curve overlaps with the heating curve.

Ligand **L3M,** which is the methyl-bearing analog of **L7** (Fig. 3.1), was used to illustrate the effect of the length of the spacer, in comparison with **L2M**.

Ligand **L4M** was introduced to compare the mononuclear iron(II) **L4M** complex to dinuclear species, since it provides more freedom for the ligand to wrap around the metal center and may have better coordination than **L2M** and **L3M**, and may enhance the ligand field.

The aim of the research originally included the design and characterization of helicates/ mesocates, since the ligands share identical structure with previous ligands, which were reported to form helicates/ mesocates with iron(II) and nickel(II). [1]

In all experiments described below, iron(II) was introduced as $[Fe(H_2O)_6](BF_4)_2$. The tetrafluoroborate salt is considered to have low affinity to cations in coordination chemistry and will increase the solubility of salts in organic solvents, because it equally distributes its negative charge to four fluorine atoms.

3.3 Study of the coordination of L1M.

After the successful preparation and characterization of **L1M**, the ligand was mixed with $[Fe(H_2O)_6](BF_4)_2$ to test its coordination properties. It was suspended in a solution of the iron(II) salt in acetonitrile. Sadly, no coordination was observed; in the mixture of $[Fe(H_2O)_6](BF_4)_2$ and the ligand in acetonitrile, the ligand didn't go into solution even after sonication and heating were used. Trials in both large and small amounts were carried out, but only to see the precipitate at the bottom of flask. This suggests that there was no issue with the amount or conditions.

The rigid structure of **L1M** was considered as the main problem limiting coordination. First, the methyl group introduced steric hindrance at the metal center,

weakening the coordination. More importantly, the benzene ring of the xylene spacer is a rigid group with less ease to bend or even fold. If the metal center fits well in the provided binding sites, then a stable complex is formed. If not, the benzene ring will not facilitate metal ion binding, which finally prevents the metal ion to form the complex. However, ligand **L1M** successfully complexes nickel(II). A Job plot confirms the formation of a 2(metal):3(ligand) species in solution (Fig. 3.2, spectrum recorded by Dr. Petitjean).

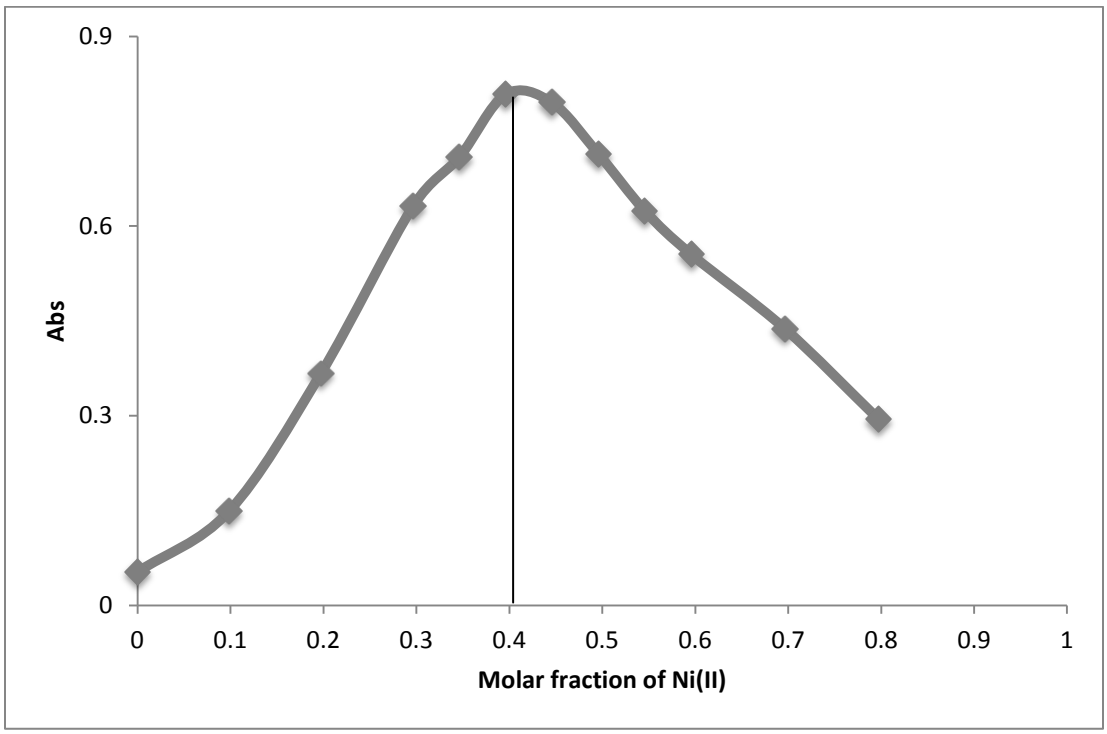

Fig. 3.2 Job plot of $[Ni_2(\mathbf{L1M})_3](BF_4)_4$ (~10^{-4} M concentration, in acetonitrile, 305 nm).

The Job plot was carried out with a constant total amount of guest and host species, thus:

x(Ni)+x(ligand)=1

The stoichiometry is determined by the point with highest absorption, and the ratio of x(Ni):x(ligand) represents the stoichiometry of the complex. Then it was used in the following calculation:

$$x(Ni):x(ligand)=x(Ni):[1-x(Ni)]=0.4:0.6=2:3$$

The major difference between the iron(II) and nickel(II) complexes are the nature of the two ions. Nickel(II) is a 'soft' metal ion comparing to iron(II), and it has better coordination to the 'soft' triazole-pyridine based ligand. This is due to the larger size of the nickel(II) ion.

Overall, incorporation of rigid spacers such as phenyl, naphthalene and other aromatic units is therefore of limited interest. The methyl group may be effective at lowering the ligand field, but the aromatic ring prevented the ligand to bind with iron(II), which is essential for SCO study. More flexible as they are, aliphatic spacers might be more successful.

3.4 Study of the coordination to L2M and L3M.

The two ligands **L2M** and **L3M** were synthesized in the same way as **L1M**. The only difference comes from the aliphatic chain. The ligands benefits from the flexible aliphatic chain and had better coordination to metal centers, as the corresponding complexes were successfully prepared (see below).

Although the aliphatic chain made the coordination possible, the drawback was that crystallization was more difficult and was never successful in my hands. As a result, no structural information from X-ray diffraction study is available. Although

those complexes were thought to be either helicates or mesocates, no supporting information is available. The crystallization procedure was the following: the acetonitrile solution of a complex was placed in a flask, and slow vapour diffusion of solvents (dichloromethane, ether, or ethyl acetate) into the solution was allowed to take place. Only powders were obtained. The reason was believed to be the flexibility of the aliphatic chain, which affected packing within the crystal.

Instead, we prepared the samples in powder form for magnetic studies. The synthesis of $[Fe_2(\mathbf{L2M})_3](BF_4)_4$ and $[Fe_2(\mathbf{L3M})_3](BF_4)_4$ powders involved mixing the ligand and iron(II) salt in acetonitrile and adding a less polar solvent (ethyl acetate) to precipitate the powder. The result was a yellow powder; with a typical recovery yield of around 60% to 80%.

The solutions of both iron(II) **L2M** and iron(II) **L3M** complexes were bright yellow (compared to low spin iron(II) **L7** complex solutions which were dark orange). This suggested the formation of high-spin species based on the color. The nickel(II) solutions were light purple. No color difference would be expected since the nickel(II) has no spin transition.

At the same time, some indirect evidence came from ^{1}H NMR spectroscopy (Fig. 3.3), which indicated that the iron(II) complexes gave broad signals suggestive of high spin species.

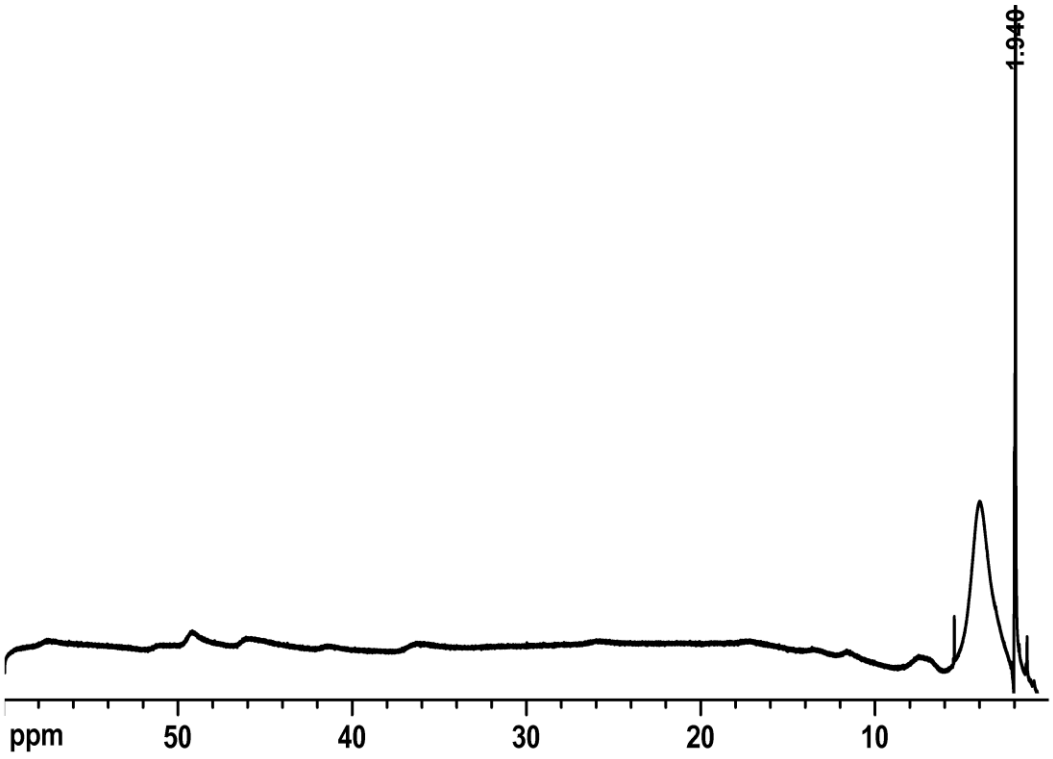

Fig. 3.3 ^{1}H NMR spectrum of $[Fe_2(\mathbf{L2M})_3](BF_4)_4$. The only sharp peak is the residual proton peak from acetonitrile-d3 (300 MHz, 298 K, 6×10^{-3} M).

To acquire a better NMR signal, species with no unpaired electrons are preferred. This is because the NMR machine detects the magnetic moment of nuclei, which is very weak. If unpaired electrons exist, the magnetic moment of unpaired electrons can't be ignored (for those which are paired, the magnetic moments cancel out as they have reverse spin quantum numbers), therefore the spectrum is not as clear. As a result, if species with unpaired electrons are in the solution, the peaks would be broad or shift to higher/lower field.

A paramagnetic species would be consistent with a high-spin iron(II) complex, as the electronic configuration models below support.

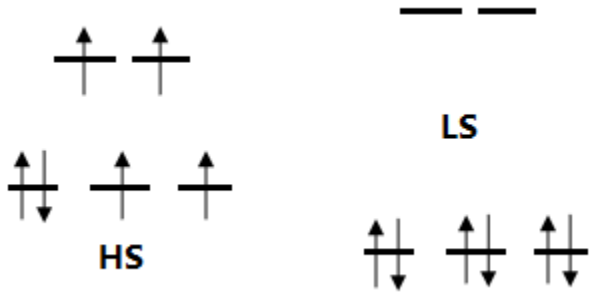

Fig. 3.4 Spin states of iron(II)

As depicted in Fig. 3.4, the LS state has no unpaired electrons and it is diamagnetic. This was a promising result, since most complexes with spin crossover property display HS properties at room temperature.

$[Fe_2(\mathbf{L2M})_3](BF_4)_4$ and $[Fe_2(\mathbf{L3M})_3](BF_4)_4$ were characterized by a UV-VIS spectral study (Fig. 3.5). The two bands of iron(II) in the UV zone correspond to absorption from ligands, due to their conjugated systems.

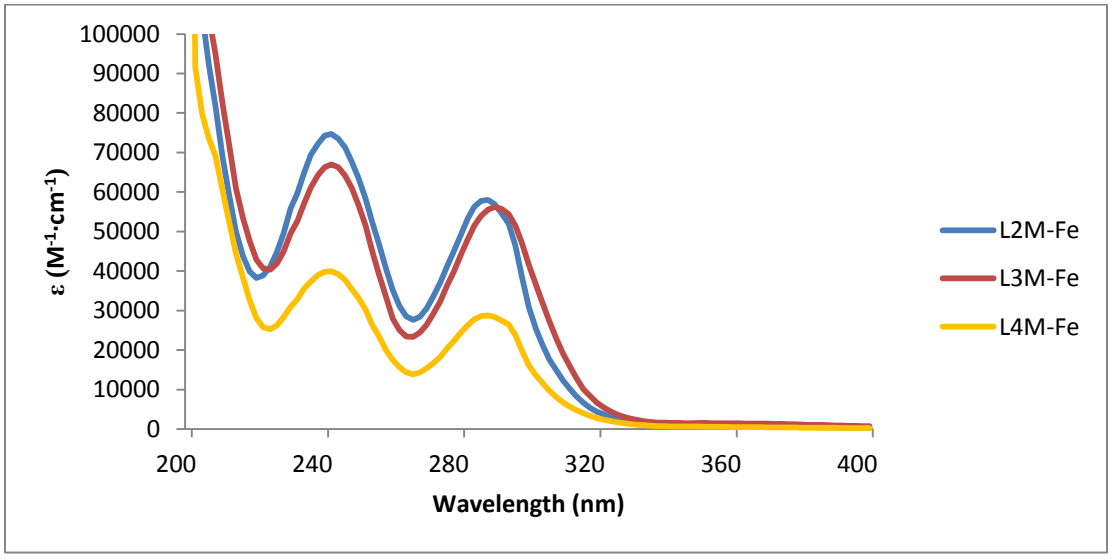

Fig. 3.5 UV-VIS Spectra of $[Fe_2(\mathbf{L2M})_3](BF_4)_4$, $[Fe_2(\mathbf{L3M})_3](BF_4)_4$ and $[Fe_2(\mathbf{L4M})_3](BF_4)_2$ (acetonitrile, 10^{-5} M).

According to the Beer-Lambert law, the molar absorption coefficient, ε, is calculated as follows:

$$\varepsilon = \frac{A}{cl}$$

The l parameter equals to 1 cm and c is based on the concentration of different solutions. Those ε values are relatively large but are of ligand absorption.

Table 3.1 Absorption values of $[Fe_2(\mathbf{L2M})_3](BF_4)_4$, $[Fe_2(\mathbf{L3M})_3](BF_4)_4$

	ε/ $M^{-1}\cdot cm^{-1}$
$[Fe_2(L2M)_3](BF_4)_4$	5.8×10^4 $M^{-1}\cdot cm^{-1}$ (288 nm) and 8.0×10^4 $M^{-1}\cdot cm^{-1}$ (242 nm)
$[Fe_2(L3M)_3](BF_4)_4$	5.6×10^4 $M^{-1}\cdot cm^{-1}$ (290 nm) and 6.7×10^4 $M^{-1}\cdot cm^{-1}$ (242 nm)

According to previous studies, iron(II) complexes may fall into two categories depending on their stoichiometry: 2(metal):2(ligand), for which each metal ion has two coordination sites available for other species to bind; the other is 2:3, where all coordination sites are bound to the provided ligand. The preferred stoichiometry was determined by different methods. The first direct method uses a Job plot which was done by Dr. Petitjean, and the results are depicted below (Fig. 3.6 and Fig. 3.7).

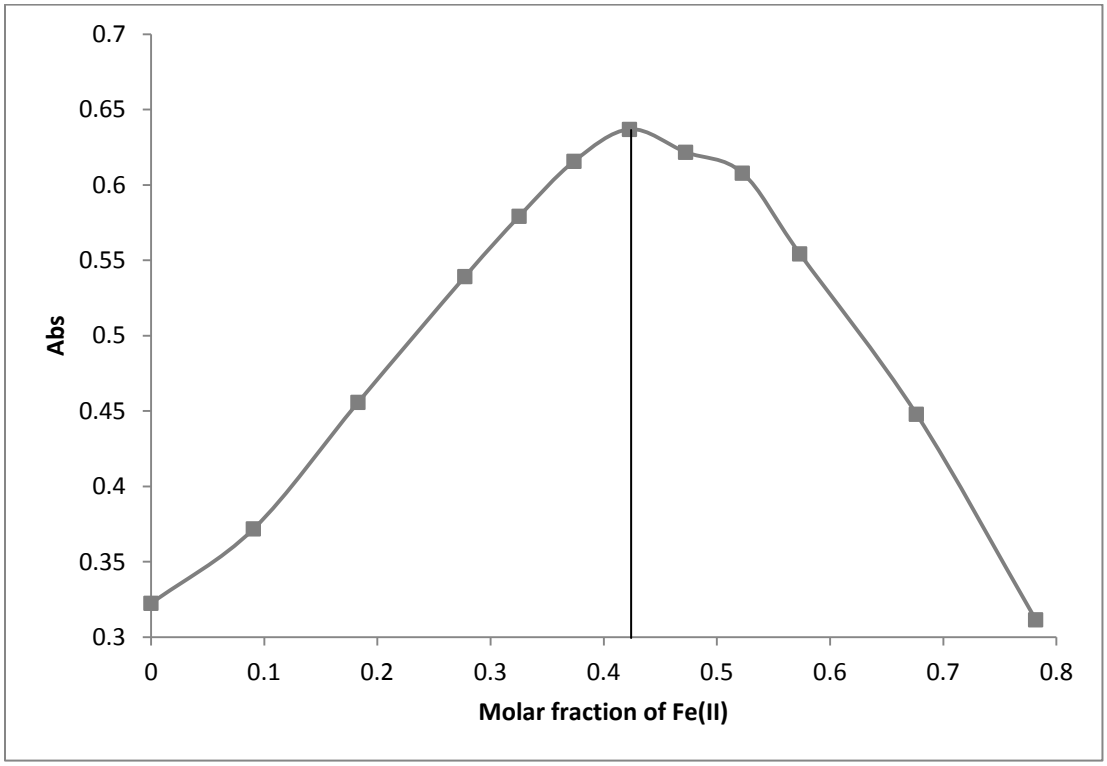

Fig. 3.6 Job plot of $[Fe_2(\mathbf{L2M})_3](BF_4)_4$ (~10^{-4} M in acetonitrile, 300 nm).

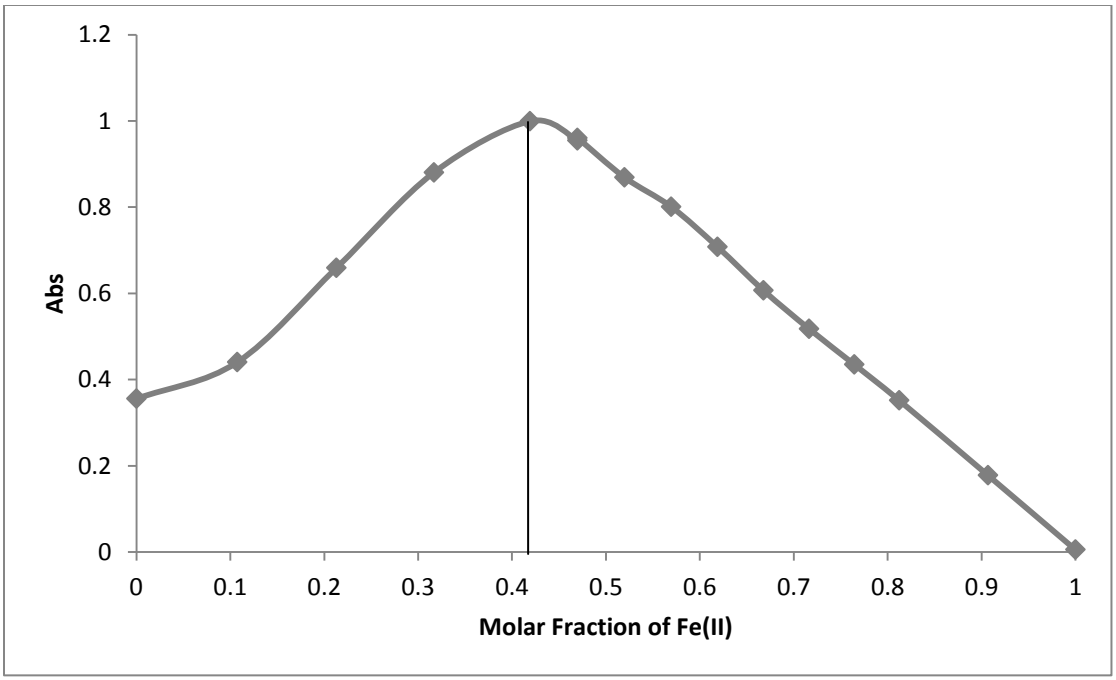

Fig. 3.7 Job plot of $[Fe_2(\mathbf{L3M})_3](BF_4)_4$ (~10^{-4} M in acetonitrile, 301nm).

The maximum values of absorption both took place at 0.4, which indicated that the complexes were both 2:3 complexes, as referring to the equation of:

iron(II) **L2M** complex: x(Fe):[1-x(Fe)]=0.43:0.57=0.75

The value is very close to 2:3 (0.67) but not 2:2 (1.0).

iron(II) **L3M** complex: x(Fe):[1-x(Fe)]=0.41:0.59≈2:3

The other method used in stoichiometry was elemental analysis. We calculated the theoretical values of both 2:2 and 2:3 ratio, which was charted below:

Table 3.2 EA prediction and findings

		$[Fe_2(L2M)_3](BF_4)_4$ (%)	$[Fe_2(L3M)_3](BF_4)_4$ (%)
Theoretical (M:L)	2:2	C 38.69, H 3.42, N 19.0	C 39.78, H 3.67, N 18.56
	2:3	C 44.45, H 3.93, N 21.83	C 45.55, H 4.2, N 21.55
Found		C 43.02, H 4.16, N 21.12 (thought to contain water)	C 44.51, H 4.43, N 20.11 (close to 2:3)

The EA strongly proved that the solid state complexes were 2:3 complexes, which implied metal centers were all bound with ligands.

As mentioned above, one can estimate the ligand field energy based on the nickel complexes. They are therefore discussed below.

3.5 Nickel(II) complexes: 10Dq value calculation and comparison to pairing energy.

The corresponding nickel(II) complexes were also prepared and the results matched expectation. The synthesis of the nickel(II) complexes was identical to that of the iron(II) complexes, and resulted in bright purple powders.

Job plot (Fig. 3.8 and Fig. 3.9) by Dr. Petitjean and EA studies also proved the 2:3 stoichiometry of the complexes.

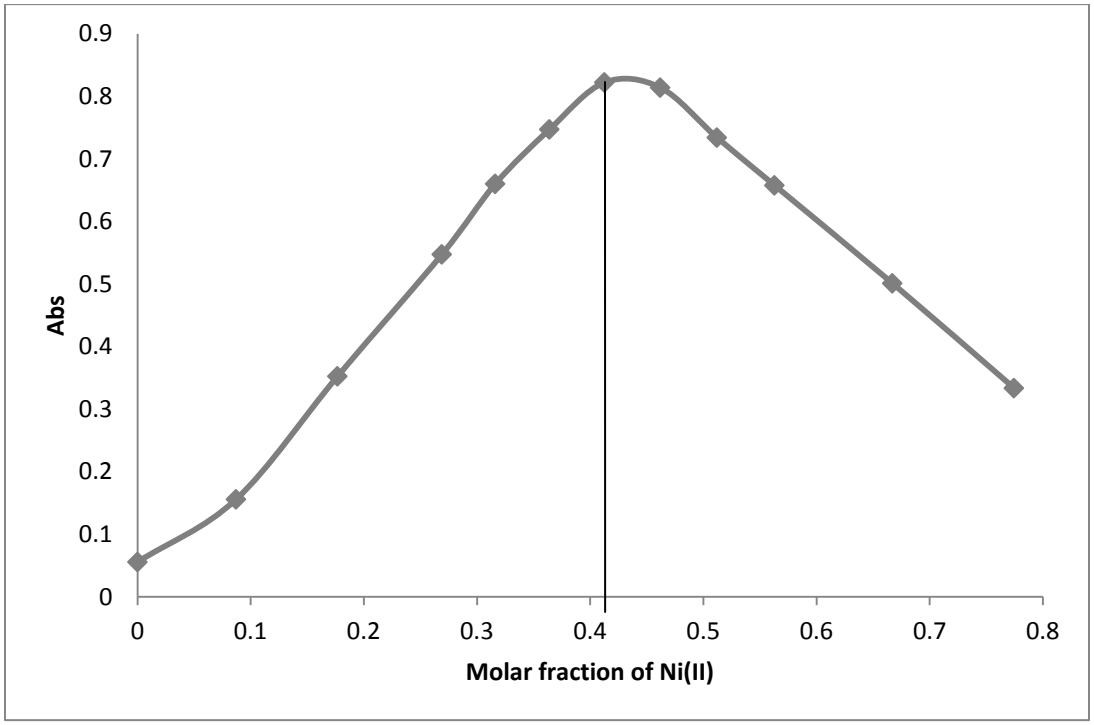

Fig. 3.8 Job plot of $[Ni_2(\mathbf{L2M})_3](BF_4)_4$ (~10^{-4} M in acetonitrile, 305 nm).

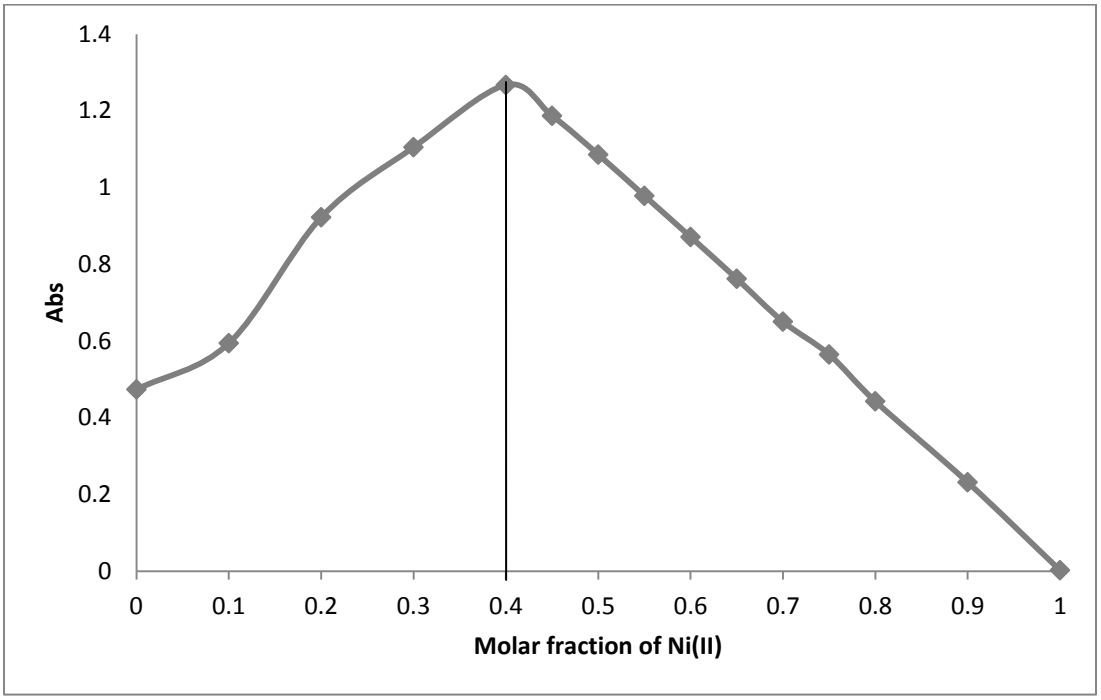

Fig. 3.9 Job plot of $[Ni_2(\mathbf{L3M})_3](BF_4)_4$ (~10^{-4} M in acetonitrile, 305nm).

EA confirmed the 2:3 stoichiometry (see experimental section).

The UV-VIS spectra of $[Ni_2(\mathbf{L1M})_3](BF_4)_4$, $[Ni_2(\mathbf{L2M})_3](BF_4)_4$, $[Ni_2(\mathbf{L3M})_3](BF_4)_4$ and $[Ni(\mathbf{L4M})_3](BF_4)_2$ in the near IR zone were recorded and plotted below (Fig. 3.10).

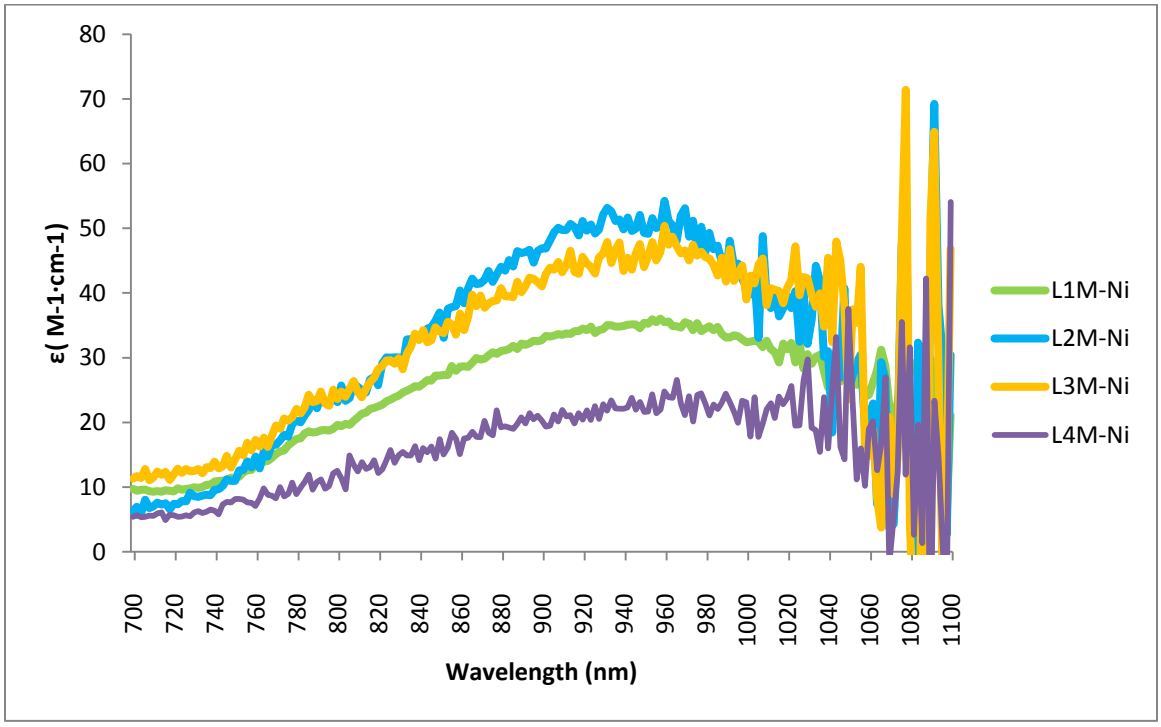

Fig. 3.10 $[Ni_2(\mathbf{L})_3](BF_4)_4$ (**L=L1M, L2M, L3M, L4M**) spectra, over 700 nm. Note the peaks above 1000 nm are unreadable because of the noise. Peaks related to d-d transition appear at 960 nm, 930 nm and 580 nm (not shown on the spectrum above). The maximum absorption wavelength, i.e. lowest energy, is 960 nm ($^3A_{2g}(F)$ to $^3T_{2g}(F)$ transition), and corresponds to 10Dq. The concentrations of complexes are around 8×10^{-3} M, in acetonitrile.

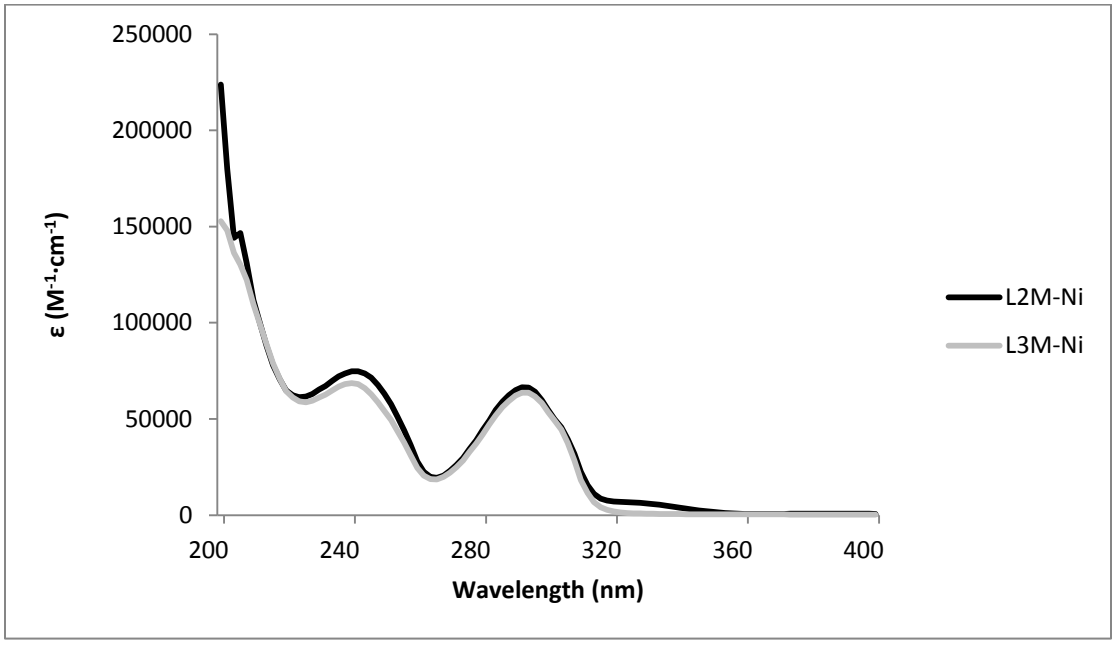

Fig. 3.11 $[Ni_2(\mathbf{L2M})_3](BF_4)_4$ and $[Ni_2(\mathbf{L3M})_3](BF_4)_4$ spectra. The concentrations are 1.5×10^{-5} M.

The ε value of $^3A_{2g}(F)$ to $^3T_{2g}(F)$ of $[Ni_2(\mathbf{L2M})_3](BF_4)_4$ and $[Ni_2(\mathbf{L3M})_3](BF_4)_4$ are 54 M^{-1} cm^{-1} and 50 M^{-1} cm^{-1}, much smaller than the absorption of ligand bands (Fig. 3.11).

As peaks of d-d transition were found, both at 960 nm, the 10 Dq value can be calculated as following:

$$\mathrm{E} = 10\mathrm{Dq} = h\nu = \frac{hc}{\lambda} = \frac{6.626 \times 10^{-34}\ \mathrm{J \cdot s} \times 3 \times 10^{8}\ \mathrm{m/s}}{9.6 \times 10^{-7}\mathrm{m}} = 2.08 \times 10^{-19}\ \mathrm{J}$$

$$\mathrm{E_{mol}} = \mathrm{E} \times\ \mathrm{N_A} = 2.08 \times 10^{-19}\ \mathrm{J} \times 6.022 \times 10^{23}\ \mathrm{mol^{-1}} = 126\ \mathrm{kJ \cdot mol^{-1}}$$

Or by frequency:

$$10\mathrm{Dq} = \frac{1}{9.6 \times 10^{-5}\mathrm{cm}} = 10400\ \mathrm{cm^{-1}}$$

Based on an empirical equation, [3] the 10Dq value of iron(II) complexes is:

$$\frac{10\mathrm{Dq_{Fe}}}{10\mathrm{Dq_{Ni}}} = 1.11 \pm 0.07$$

$$10800\ \mathrm{cm^{-1}} \leq 10\mathrm{Dq_{Fe}} \leq 12300\ \mathrm{cm^{-1}}$$

Now back to the spin crossover. According to what we described above, if 10Dq>>P (pairing energy), the complex is LS; on the contrary, if 10Dq<<P, the complex is HS; if the 10Dq value and P value are close enough, the complex may have spin transition via heating/cooling, LIESST, or other approaches. The calculation of P involves the electron-electron repulsion energy, B, and the Racal parameter, C.[5]

For the free iron(II), C equals to 4040 cm^{-1} and B equals to 917 cm^{-1}. The following calculation gives the value of the mean pairing energy Π.

$$\Pi = 2.195\mathrm{B} + 3.708\mathrm{C} = 16993\ \mathrm{cm^{-1}}$$

The mean pairing energy, Π, equals to P divided by the difference of electron pairs of LS to HS. Thus:

$$\mathrm{P} = 16993\mathrm{cm^{-1}} \times (3-1) = 33986\ \mathrm{cm^{-1}}$$

The mean pairing energy doesn't change vastly in iron(II) compounds and the value is around 17000 cm^{-1}, or 200 kJ mol^{-1}.

Since the pairing energy only changes in a relatively small extent, an empirical rule was concluded that if an HS species has 10Dq value around approximately 11000~12500 cm^{-1}, the complex potentially has spin crossover possibility.[5] While if an HS species has 10Dq value below 10000 cm^{-1}, it is probably stable in HS state.

This can be compared to our result, as the 10Dq value is around 10800 to 12300 cm^{-1}.

According to the rule, the complex is quite promising in spin crossover. However, as the calculation is an approximation, the spin crossover property needs to proven through experiments.

3.6 Study of the coordination of L4M and calculations.

L4M complexes were regarded as the mononuclear counterparts of **L1M**. However, **L4M** readily bound to both iron(II) and nickel(II), and the resulting complexes were identified and characterized. This is due to the fact that **L4M** has no spacer, which also proved that it was not the steric hindrance but the rigid spacer of **L1M** that had a major influence and prevented the ligand from coordinating to the metal center.

The **L4M** complexes have 1/2 equivalent of metal ions and binding units comparing to **L2M** and **L3M**, so their extinction coefficients were roughly half of those of the dinuclear species.

The $^{3}A_{2g}(F)$ to $^{3}T_{2g}(F)$ band appears 966 nm, and the 10Dq value is:

$$10\mathrm{Dq} = \frac{1}{9.66 \times 10^{-5}\mathrm{cm}} = 10400\ \mathrm{cm}^{-1}$$

Then we can easily calculate the approximate value of 10Dq of $[Fe(\mathbf{L4M})_3](BF_4)_2$.

$$\frac{10\mathrm{Dq}_{\mathrm{Fe}}}{10\mathrm{Dq}_{\mathrm{Ni}}} = 1.11 \pm 0.07$$

$$10800\ \mathrm{cm}^{-1} \leq 10\mathrm{Dq}_{\mathrm{Fe}} \leq 12200\ \mathrm{cm}^{-1}$$

This value also suggested a promising SCO complex, according to the

empirical value.

3.7 Magnetism.

The magnetism of all three available iron(II) complexes $[Fe_2(\mathbf{L2M})_3](BF_4)_4$, $[Fe_2(\mathbf{L3M})_3](BF_4)_4$ and $[Fe(\mathbf{L4M})_3](BF_4)_2$ was analyzed in the powder form by Fatemah Habib in the Murugesu group at the University of Ottawa. Since the crystallization was not successful, large crystal analysis was not possible. The result, however, did not show SCO behaviour. All three complexes stay in HS from 300 K to very low temperatures. A sharp change of magnetic susceptibility did not happen until 50 K, and the species still had a relatively large magnetic susceptibility at very low temperature, which implied that those complexes were all HS, with no spin transition when they are heated/cooled (Fig. 3.12).

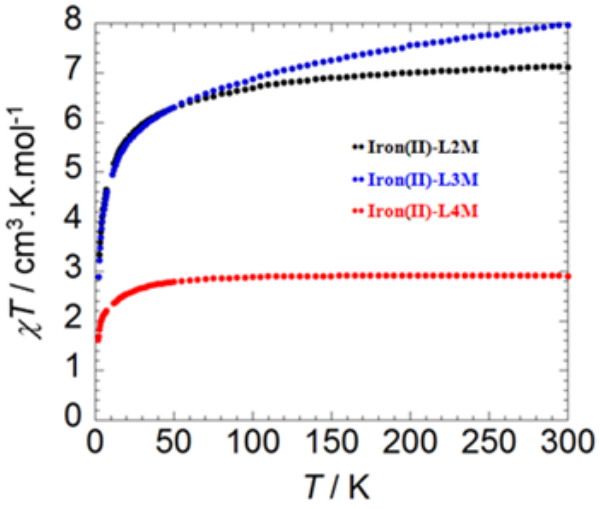

Fig. 3.12 Magnetic susceptibility versus temperature (M-T) curves of $[Fe_2(\mathbf{L2M})_3](BF_4)_4$, $[Fe_2(\mathbf{L3M})_3](BF_4)_4$ and $[Fe(\mathbf{L4M})_3](BF_4)_2$.

3.8 Helicate/mesocate determination.

As indicated above, the novel ligands have almost identical structures as previous ligands. Since those ligands are known to form helicates or mesocates with iron(II) and nickel(II), the structure of the novel complexes are of great interest. However, the complexes with aliphatic spacers are hard to recrystallize. This is partially due to the flexibility of the aliphatic chain, for a given solution of the complex may have different structure (both mesocate and helicate exist), and it is suspected to hinder the formation of large crystal. The crystal structures are not known, thus a conclusion of helicate or mesocate cannot be made.

3.9 Experimental details.

Materials and Methods: All commercially available compounds were used as received. Deuterated solvents, except for $CDCl_3$ because it may contain acid, were used as received. $CDCl_3$ was pre-treated by passing through a short column of basic alumina (such treated $CDCl_3$ will be signaled below by an asterisk, i.e., '$CDCl_3$*'). ^{1}HNMR was performed using 300 MHz Bruker instruments. Peak listings for all NMR spectra are given in ppm and referenced against the solvent residual signal. UV-vis spectra were recorded on a Cary 50 spectrometer (200-1100 nm). The variable temperature magnetic susceptibility measurements were obtained using a Quantum Design SQUID MPMS-XL7 magnetometer which operates between 1.9 and 300 K for

direct current (dc) applied fields up to 7 T. Measurements were performed on polycrystalline samples of 15.5, 21.1 and 16.8 mg for iron(II) **L2M**/**L3M**/**L4M** complexes, respectively. The data was corrected for the sample holder and any diamagnetic contributions. Magnetization data was collected at 100 K to check for ferromagnetic impurities which were absent in all samples. Alternating current (ac) susceptibility measurements were carried out under an oscillating ac field of 3 Oe and ac frequencies ranging from 10 to 1500 Hz.

General synthesis procedure of complexes:

This synthesis route is adapted from a previously reported method.[6] To a flask containing $[Fe(H_2O)_6](BF_4)_2$ (36 mg, 0.11 mmol, 1.0 eq) and **L2M** (58 mg, 0.16 mmol, 1.5 eq), was added acetonitrile dropwise until the solids fully dissolved with the help of sonication. Ethyl acetate was then added dropwise to precipitate the complex. The solvent was evaporated, ethyl acetate (10 mL) was again added and the mixture was stirred at 30 ℃ for 2 h. The mixture was filtered, the solid was washed with ethyl acetate twice, dried in air and under vacuum. The final yield was 79 mg (95%).

$[Ni_2(L1M)_3](BF_4)_4$: UV-vis (CH_3CN; λ_{max} (nm) [$\log_{10}(\varepsilon)$]): 240 [4.6], 290[4.5] 580 [1.1], 966 [1.4].

$[Fe_2(L2M)_3](BF_4)_4$: ^{1}H NMR (CD_3CN, 300 MHz, 25 °C) only has broad signals from 0

to 60 ppm. UV-vis (CH_3CN: λ_{max} (nm) [$\log_{10}(\varepsilon)$]): 242 [4.7], 290 [4.8], 362 [2.9]. EA: $C_{57}H_{60}N_{24}Fe_2B_4F_{16}\cdot 2.85\ H_2O$ *calc*.: %C 43.02, %H 4.16, %N 21.12; *found*: %C 43.21, %H 4.03, %N 20.92.

$[Ni_2(L2M)_3](BF_4)_4$: UV-vis (CH_3CN; λ_{max} (nm) [$\log_{10}(\varepsilon)$]): 240 [4.8], 252 [sh, 4.7], 294 [4.8], 304 [sh, 4.7], 365 [sh, 1.6], 580 [1.2], 930 [1.6], 960 [1.6]; EA: $C_{57}H_{60}N_{24}Ni_2B_4F_{16}\cdot 2\ H_2O$ *calc*.: %C 43.28, %H 4.08, %N 21.25; *found*: %C 42.84, %H 4.35, %N 21.49.

$[Fe_2(L3M)_3](BF_4)_4$: ^{1}H NMR (CD_3CN, 300 MHz, 25 °C) only has broad signals from 0 to 60 ppm. UV-vis (CH_3CN: λ_{max} (nm) [$\log_{10}(\varepsilon)$]): 244 [4.8], 292 [4.8], 358 [3.2]. EA: $C_{60}H_{66}B_4F_{16}Fe_2N_{24}\ 0.4\ C_4H_8O_2\cdot 2\ H_2O$ *calc*.: %C 44.75, %H 4.46, %N 20.33; *found*: %C 44.51, %H 4.43, %N 20.11.

$[Ni_2(L3M)_3](BF_4)_4$: UV-vis (CH_3CN; λ_{max} (nm) [$\log_{10}(\varepsilon)$]): 240 [4.7], 252 [sh, 4.5], 294 [4.7], 304 [sh, 4.6], 365 [sh, 1.7], 580 [1.4], 960 [1.6]; EA: $C_{60}H_{66}N_{24}Ni_2B_4F_{16}\cdot 4\ H_2O$ *calc*.: %C 43.41, %H 4.49, %N 20.25; *found*: %C 43.47, %H 4.38, %N 20.10.

$[Fe(L4M)_3[(BF_4)_2$: ^{1}H NMR (CD_3CN, 300 MHz, 25 °C): 2.5-3.4, 6.2-7.0 (broad signal). UV-vis (CH_3CN: λ_{max} (nm) [$\log_{10}(\varepsilon)$]): 242 [4.6], 288 [4.6]. EA: $C_{45}H_{42}B_2F_8N_{12}Fe\ \cdot 1.05$

H_2O *calc*.: %C 54.09, %H 4.45, %N 16.82; *found*: %C 54.23, %H 4.39, %N 16.68.

$[Ni(L4M)_3][(BF_4)_2$: UV-vis (CH_3CN; λ_{max} (nm) [$\log_{10}(\varepsilon)$]): 240 [4.6], 290 [4.5], 585 [1.1], 966 [1.4] EA: $C_{45}H_{42}B_2F_8N_{12}Ni \cdot 0.25\ C_4H_8O_2 \cdot 2\ H_2O$, *calc*.: %C 53.06, %H 4.65, %N 16.14; *found*: %C 53.02, %H 4.57, %N 16.10.

3.10 Conclusion.

In this part a number of novel iron(II) and nickel(II) dinuclear complexes are introduced, together with their synthesis, characterization and analysis. We successfully confirmed the stoichiometry of the complexes via multiple methods and the 10Dq values of nickel(II) complexes were calculated. An approximation of 10Dq value is used and compared to an empirical rule for the iron(II) complexes, which showed positive prediction of the SCO property. However, the three iron(II) complexes do not display spin crossover properties based on the results of the heating-cooling process. This indicates that further studies using alternate methods such as LIESST, or designing other ligands with modifications on position 5 of the pyridine rather than on position 6, may be worth exploring.

References

1. K. A. Stevenson, C. F. C. Melan , O. Fleischel , R. Wang and A. Petitjean, *Cryst. Growth Des.*, **2012**, *12*, 5169-5173.

2. C. F. C. Melan, N. Wu, K. A. Stevenson, O. Fleischel, R. Wang, F. Habib, N. J. Mosey, M. Murugesu and A. Petitjean, *Inorg. Chem.*, Submitted.

3. L. J. Wilson, D. Georges and M. A. Hoselton, *Inorg. Chem.*, **1975**, *14*, 2968-2975.

4. P. Gütlich, *Struct. Bonding (Berlin)*, **1981**, 83-195; J. Krzystek, J. Telser, L. A. Pardi, D. P. Goldberg, B. M. Hoffman and L-C. Brunel, *Inorg. Chem.*, **1999**, *38*, 6121-6129.

5. A.Hauser, *Top Curr. Chem.*, **2004**, 49-58; E. Konig and S. Kremer, *Theoret. Chem. Acta (Berl.)*, **1971**, 12-20.

6. M. A. Houghton, A. Bilyk, M. M. Harding, P. Turner and T. W. Hambley, *J. Chem. Soc., Dalton Trans.*, **1997**, 2725-2733.

Chapter 4

Conclusions and future work

4.1 Conclusion.

In this work a series of novel 1,2,3-triazole-pyridine based bifunctional and monofunctional ligands were successfully synthesized and characterized. Some details about the synthesis were discussed in Chapter 2. Compared to previous ligands, the introduction of a methyl group on postion 6 of the pyridyl group was explored to induce steric hindrance, which was expected to alter the magnetism of the novel complexes.

The derivative iron(II) and nickel(II) complexes were prepared in powder form. EA and Job plot confirmed the stoichiometry to be the saturated 2(metal):3(ligand) rather than 2:2 species. Broad peaks in the ^{1}H NMR spectra and the color of the complexes point to a HS spin state at room temperature. This was confirmed by the SQUID magnetism study. The UV-VIS study of the nickel(II) complexes provided promising data for the calculation of 10Dq; the data was processed and compared to an empirical rule, which predicted potential spin crossover species. However, the actual experimental findings in magnetism (by heating/cooling and monitored by SQUID instrument) unfortunately indicated that the complexes do not have spin crossover properties. Furthermore, the determination of crystal structure was not possible because no crystallization conditions were found. As the result, the identification of helicate or mesocate structures could not be determined.

4.2 Future work.

Overall, although the complexes may not be applicable to spin crossover, they do point to potential approaches in future research. The coordination of pyridine which is the better donor compared to the 1,2,3-triazole is strongly affected by the introduction of the 6-methyl group. As a result the ligand field of the methylpyridine-triazole donor unit was weakened drastically. This can be corrected by the insertion of a methyl group (or other groups) on postion 5 rather than 6 (Fig. 4.1), or by impairing the coordination of pyridine to the metal center through other method such as decreasing the electron density, or changing the pyridine group to another donor group such as imine or imidazole. According to the spin crossover prediction rule and the value of the 10Dq we have found, modifications and adjustment are worth developing on the 1,2,3-triazole-pyridine based dinuclear iron(II) complexes to finally acquire the spin crossover property.

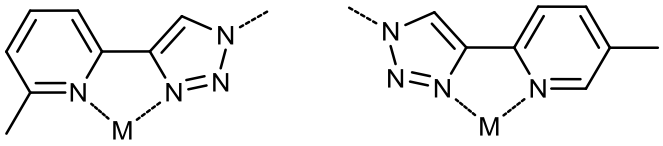

Fig. 4.1 6-Methylpyridyl group and 5-methylpyridyl group with triazole unit binding to metal center

Appendix

NMR Spectra

1) 2-Bromo-6-methylpyridine.

^{1}H NMR (300 MHz; in $CDCl_3$; 25 ℃)

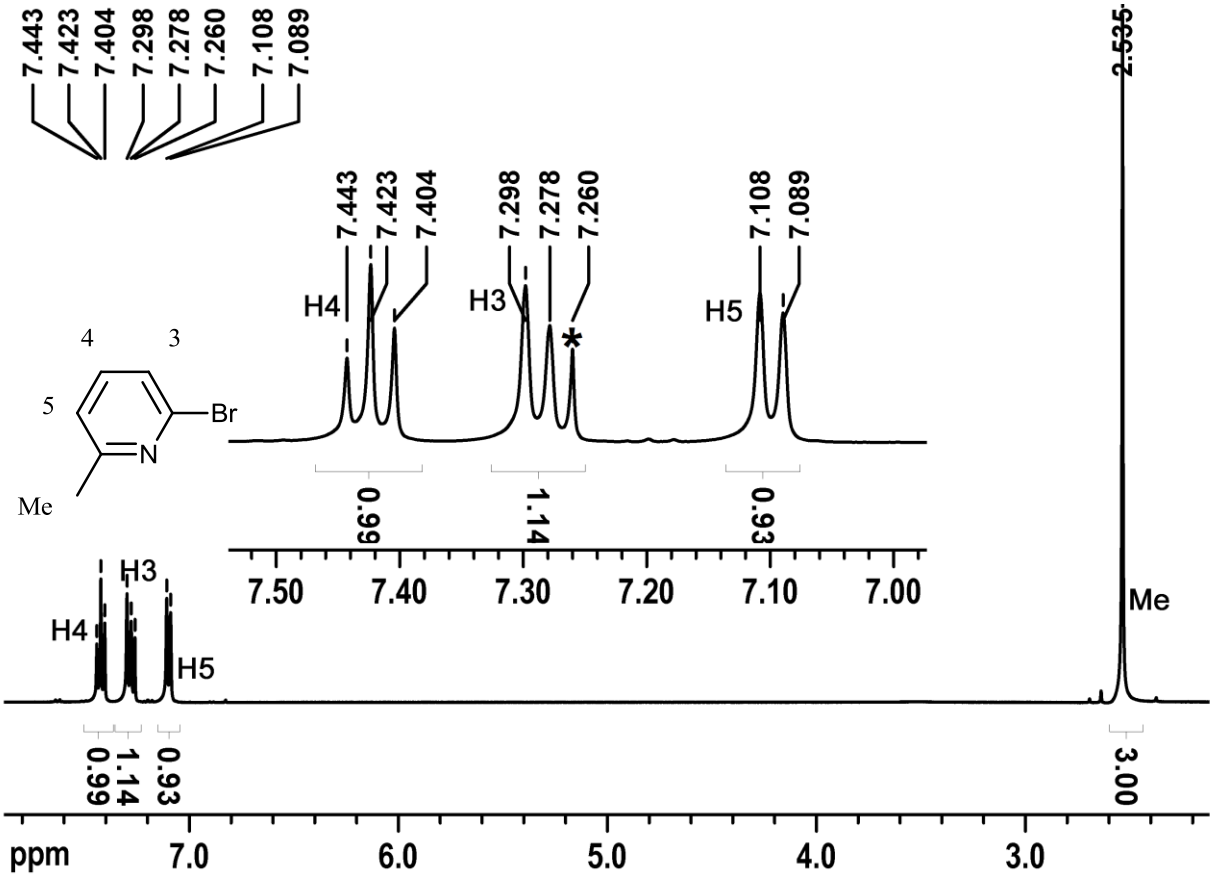

The peak marked by an asterisk is residual proton peak of $CHCl_3$.

2) 2-Methyl-6-((trimethylsilyl)ethynyl)pyridine.

^{1}H NMR (300 MHz; in $CDCl_3$; 25 ℃)

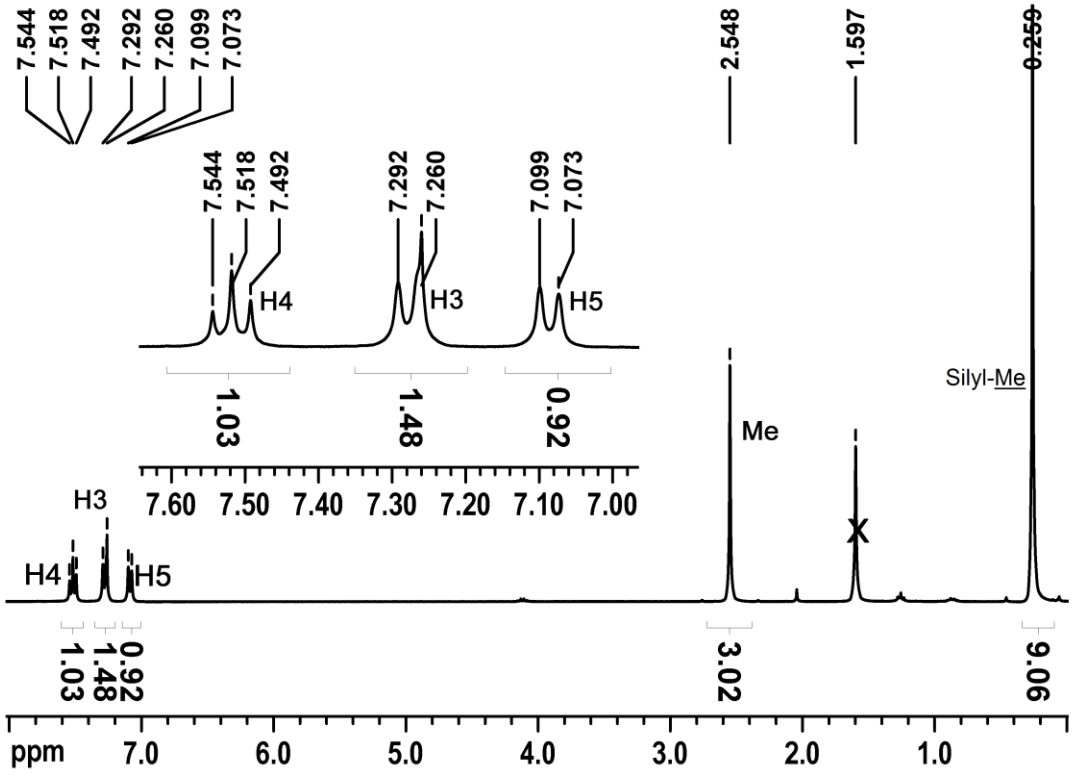

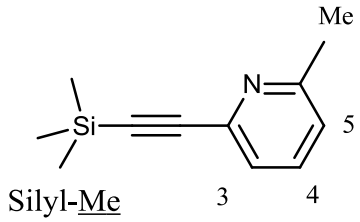

The crossed peak is water.

The doublet of H3 is overlapped with residual proton peak of $CHCl_3$.

3) 2-Ethynyl-6-methylpyridine.

^{1}H NMR (500 MHz; in $CDCl_3$; 25 ℃)

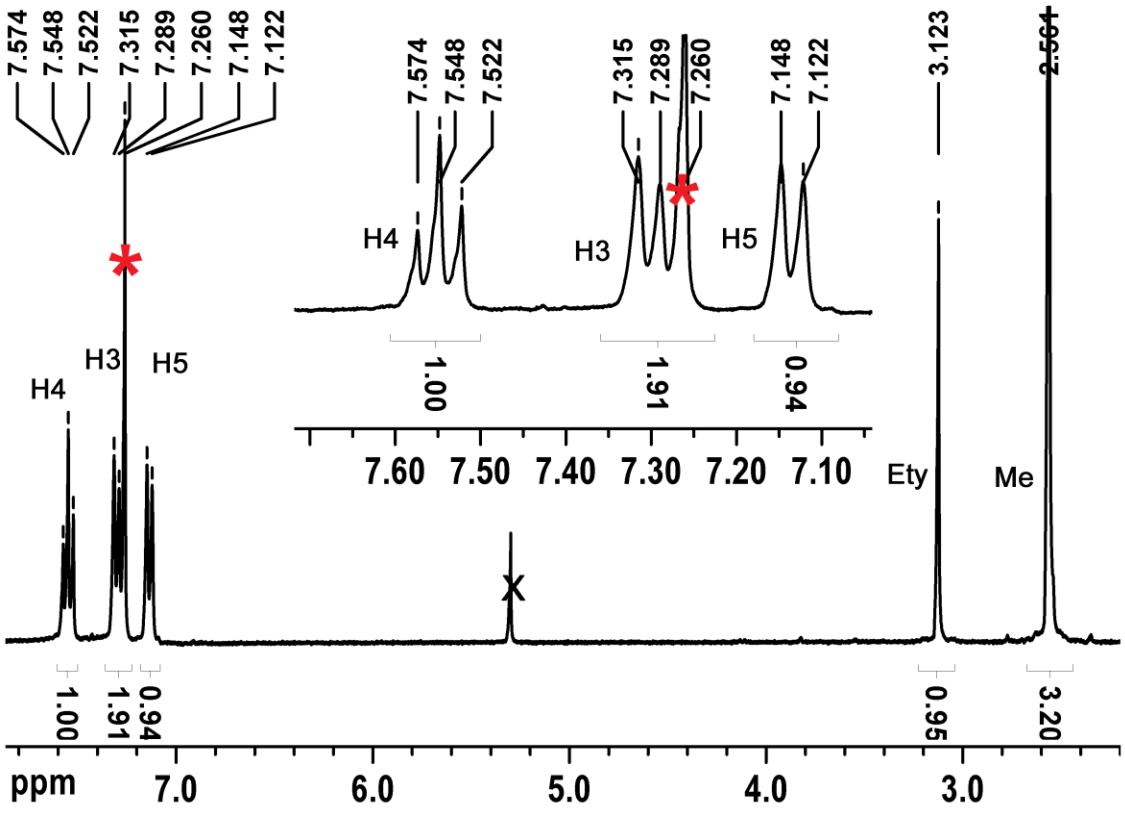

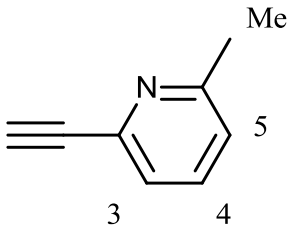

The crossed peak is dichloromethane.

The peak marked by an asterisk is residual proton peak of $CDCl_3$.

4) 1,4-Bis((4-(6-methylpyridin-2-yl)-1H-1,2,3-triazol-1-yl)methyl)benzene (L1M ligand).

^{1}H NMR (400 MHz; in $CDCl_3$; 25 ℃)

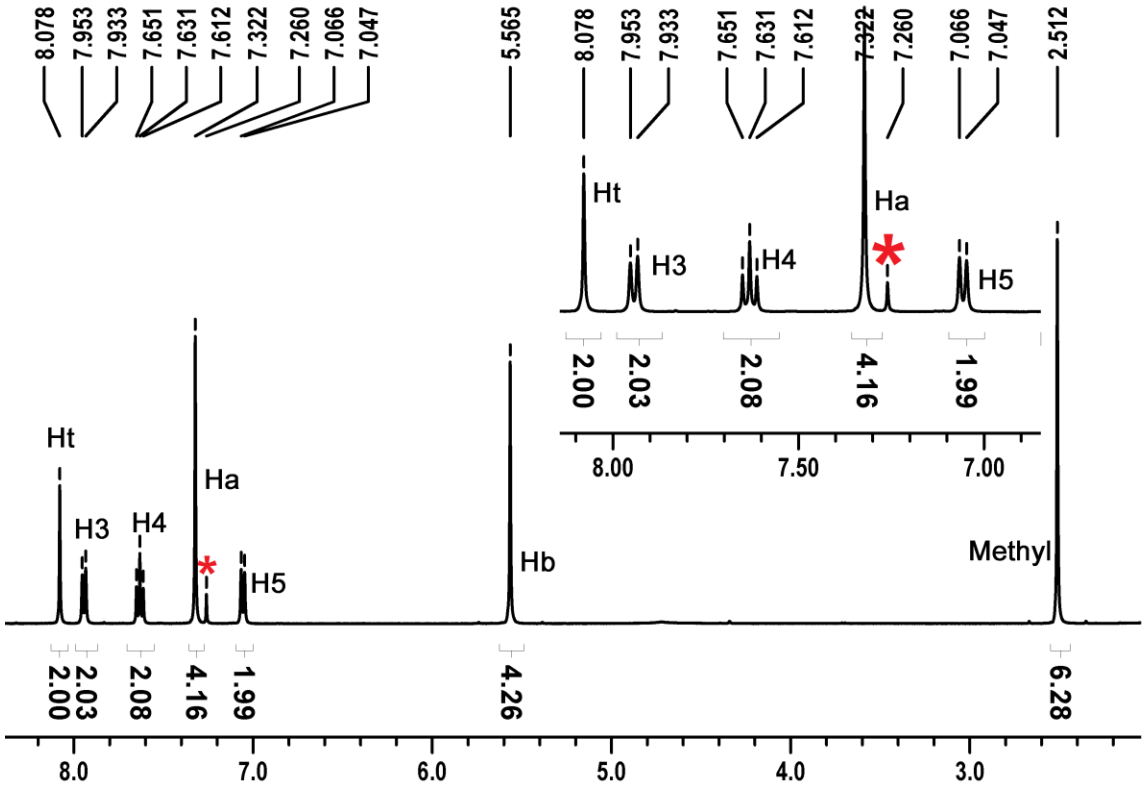

The peak marked by an asterisk is residual proton peak of $CHCl_3$.

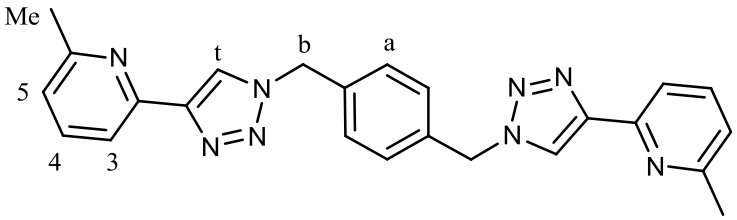

^{13}C NMR (100 MHz; in $CDCl_3$; 25℃)

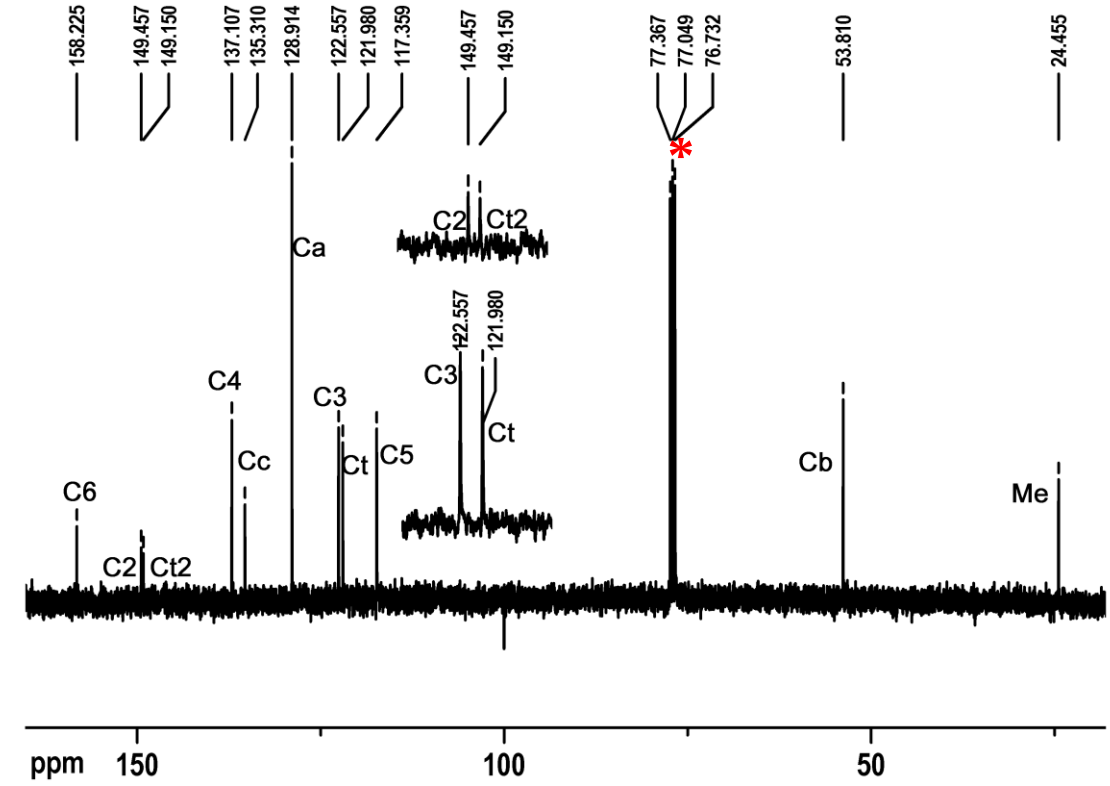

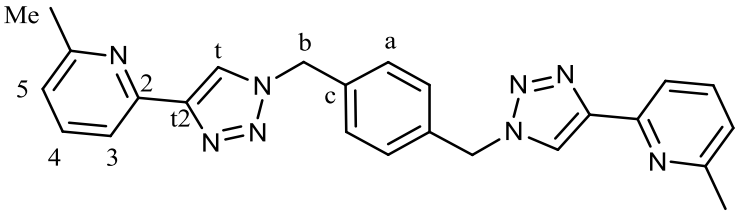

The peak marked by asterisk is $CDCl_3$.

HSQC (400 MHz; in $CDCl_3$; 25 ℃)

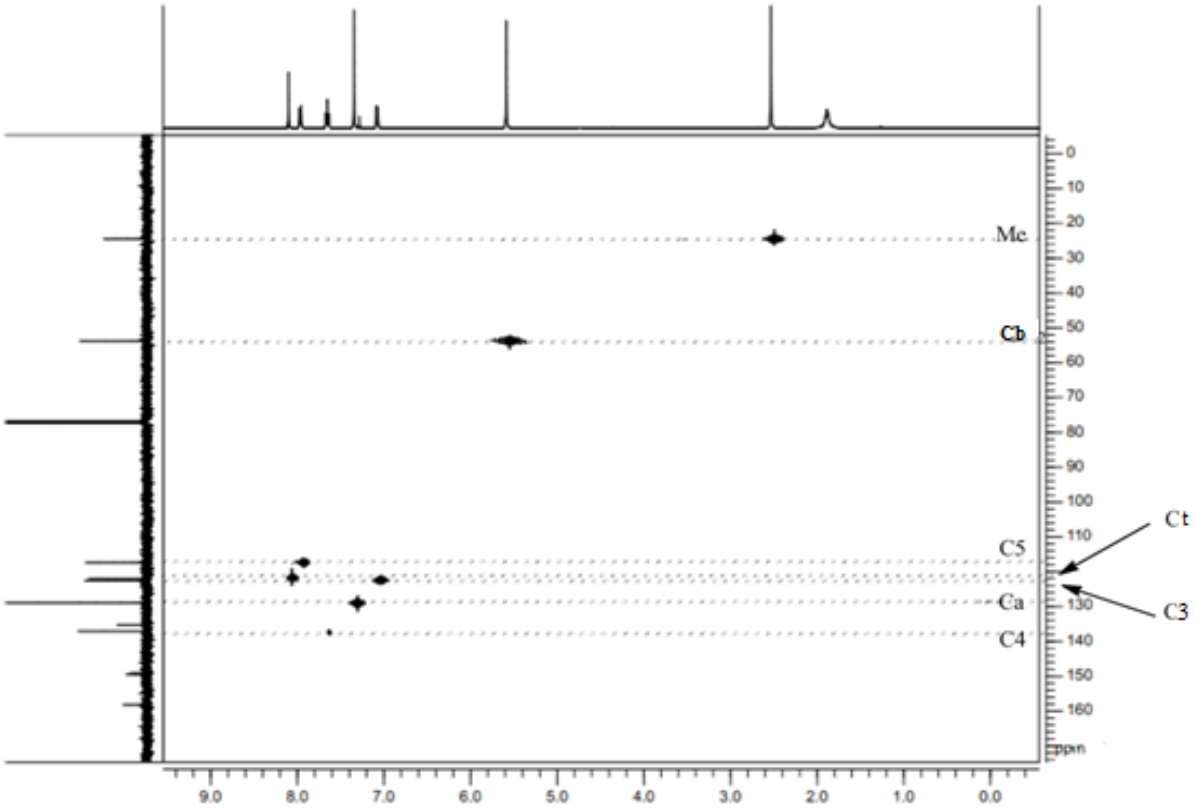

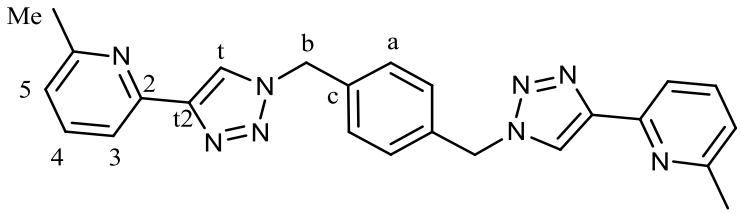

HMBC (400 MHz; in $CDCl_3$; 25 ℃)

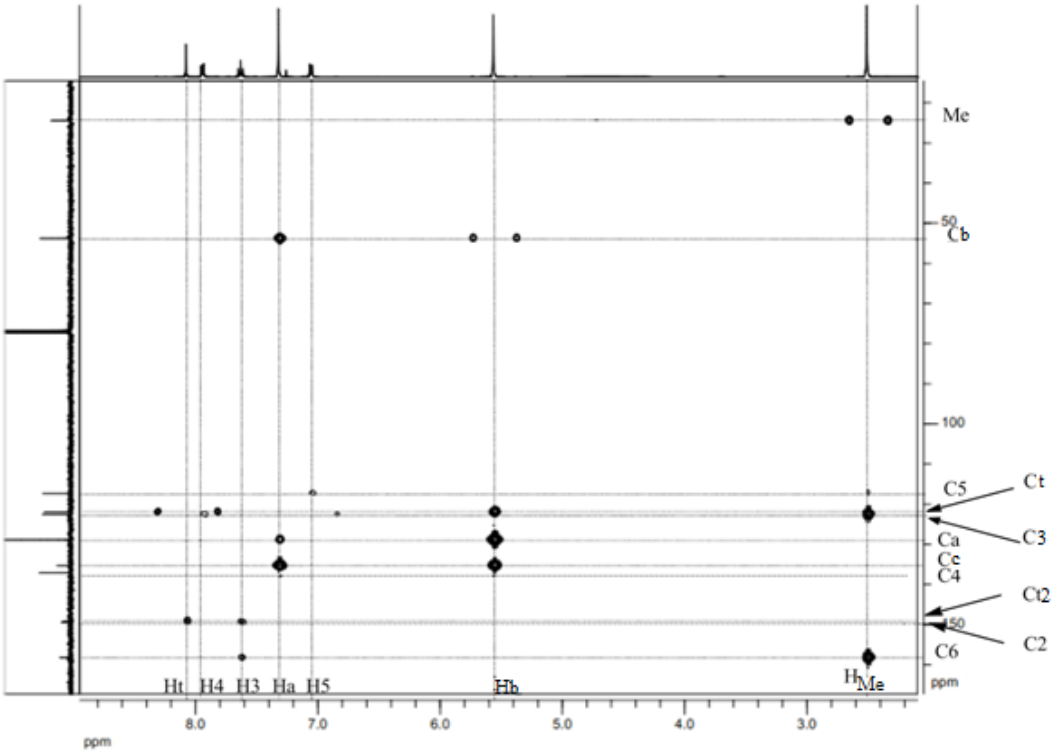

Enlarged at area of interest:

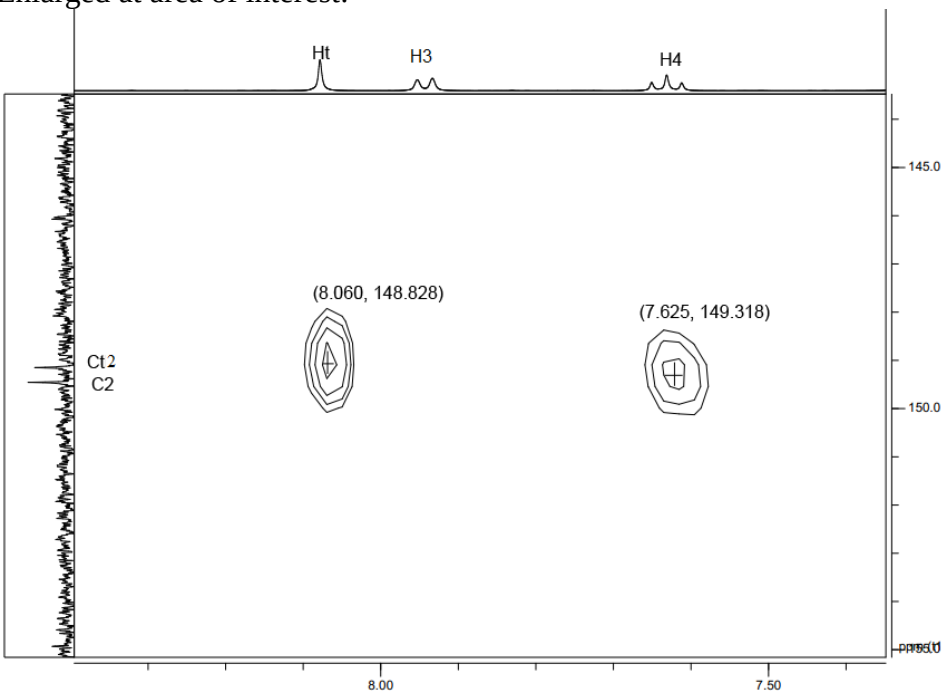

The assignment of peaks is as follows (combining with HSQC, ^{13}C NMR and ^{1}H NMR):

1. From proton NMR, the peaks of Ht, H4, Ha, Hb and Me are known: H4 peak is d-d, which is unique in the spectrum; Ht has the highest chemical shift and it is the only singlet peak with integration of 2 (for the other singlet peaks, Me has integration of 6, and Hb has integration of 4). H3 and H5 are similar; but it is reasonable to indicate the 7.94 peak as H3, since: 1. H3 has steric hindrance from the triazole group. 2. H5 is beside a methyl group which shields H5, whereas H3 gets deshielded by the triazole group beside it.

2. From HSQC, based on the knowledge from proton NMR, C3, C4, C5, Ct, Cb, Ca are known.

3. The rest of the carbon peaks (C2, C6, Ct2 and Cc) are determined by HMBC: From the enlarged figure, we can see the carbon peak of 148.8 has interaction with Ht; only Ct2 can have the interaction with Ht, thus it is Ct2. The peak of 149.3 has interaction with C4, this could be C2 or C6. But the 158.2 peak has interaction with methyl group, this confirms the 158.2 peak is C6, and 149.3 peak is C2. Cc peak should have interaction with Hb and Ha, so it is the 135.3 peak.

5) 1,3-Bis(4-(6-methylpyridin-2-yl)-1H-1,2,3-triazol-1-yl)propane (L2M).

^{1}H NMR (400 MHz; in $CDCl_3$; 25℃)

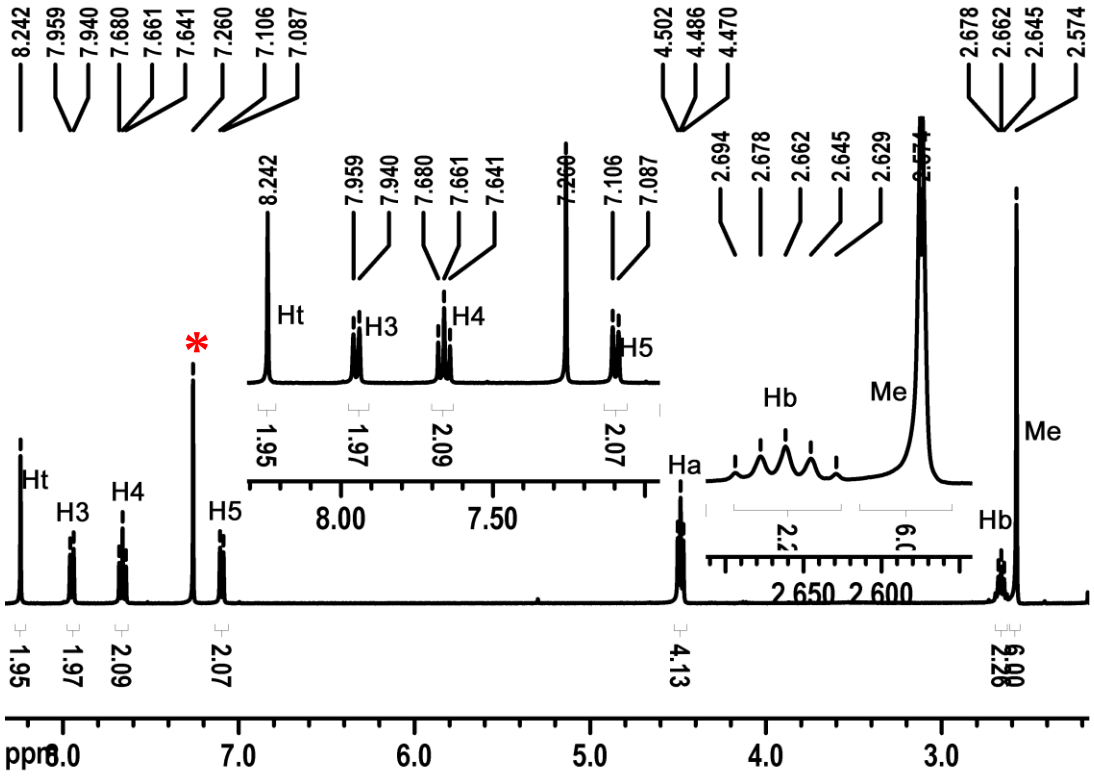

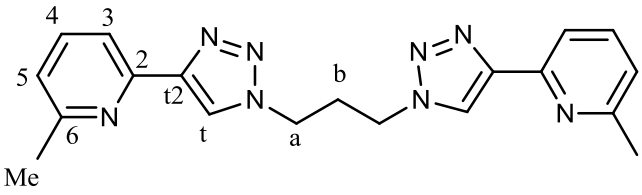

The peak marked by an asterisk is residual proton peak of $CHCl_3$.

^{13}C NMR (100 MHz; in $CDCl_3$; 25℃)

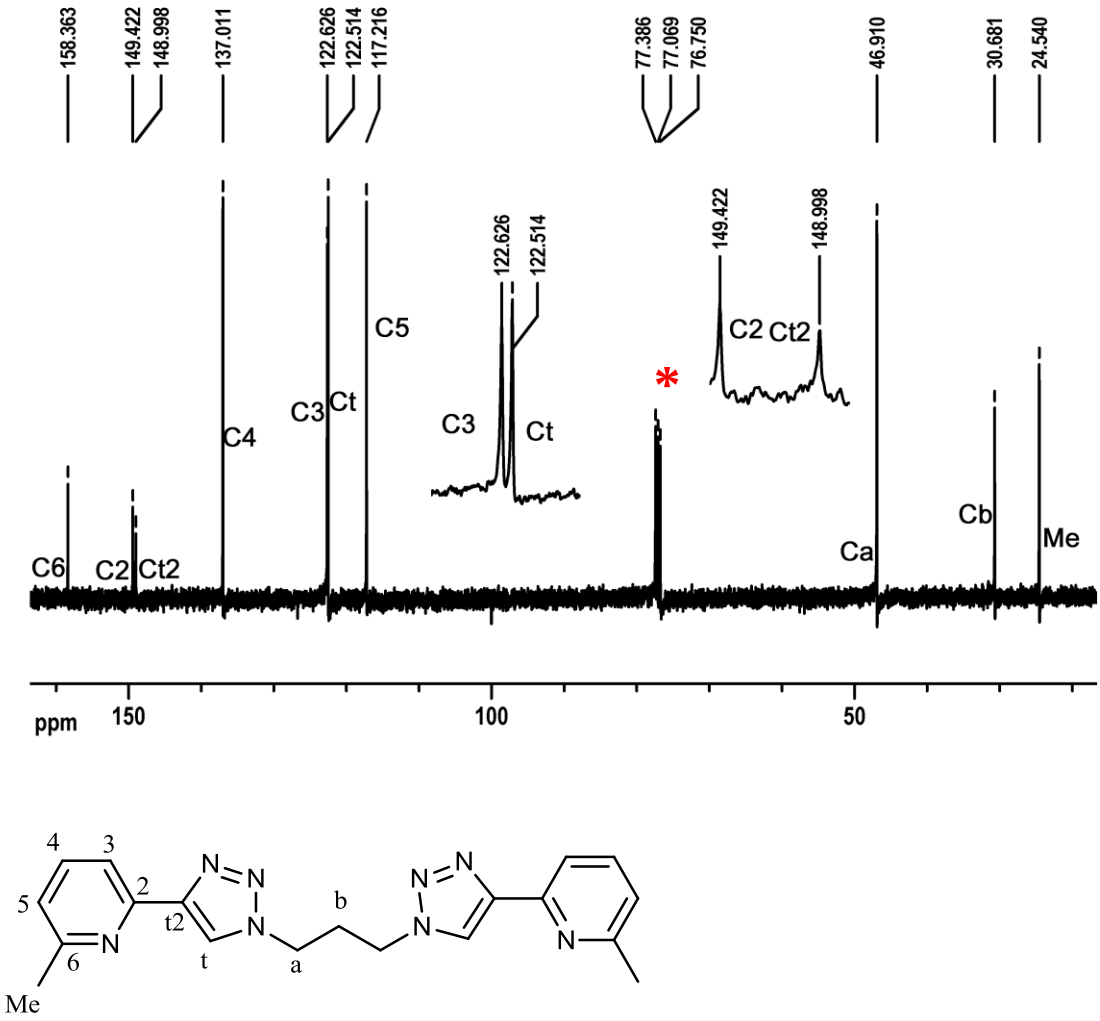

The peak marked by an asterisk is $CDCl_3$.

6) 1,4-Bis(4-(6-methylpyridin-2-yl)-1H-1,2,3-triazol-1-yl)butane (**L3M**).

^{1}H NMR (400 MHz; in $CDCl_3$; 25℃)

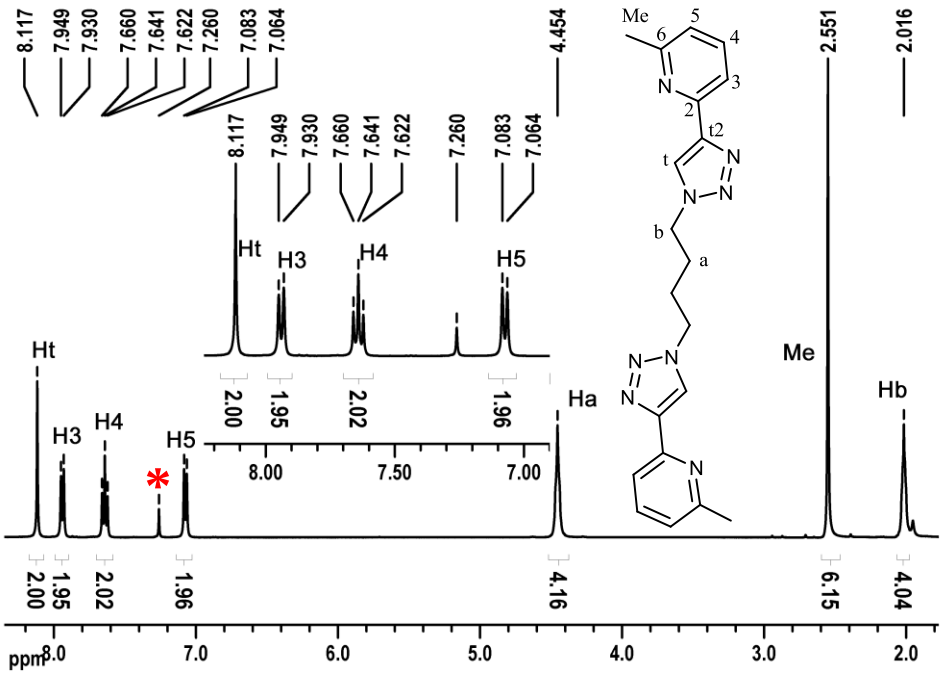

The peak marked by an asterisk is residual proton peak of $CHCl_3$.

^{13}C NMR (100 MHz; in $CDCl_3$; 25℃):

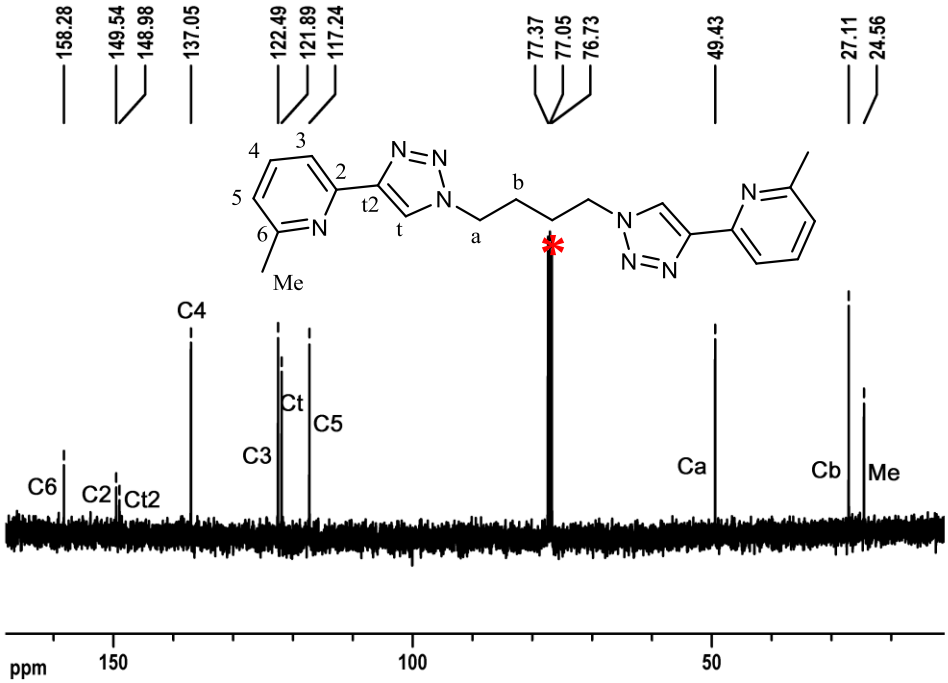

The peak marked by an asterisk is $CDCl_3$.

7) 2-(1-Benzyl-1H-1,2,3-triazol-4-yl)-6-methylpyridine (L4M).

^{1}H NMR (300 MHz; in $CDCl_3$; 25℃):

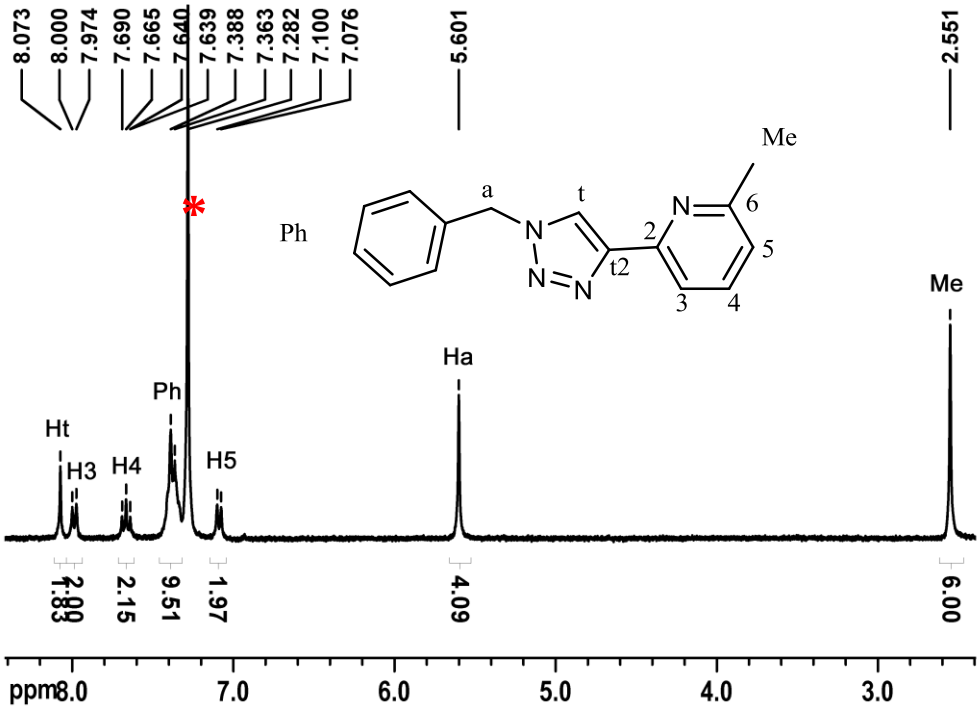

The peak marked by an asterisk is residual proton peak of $CHCl_3$.

^{13}C NMR (100 MHz; in $CDCl_3$; 25℃):

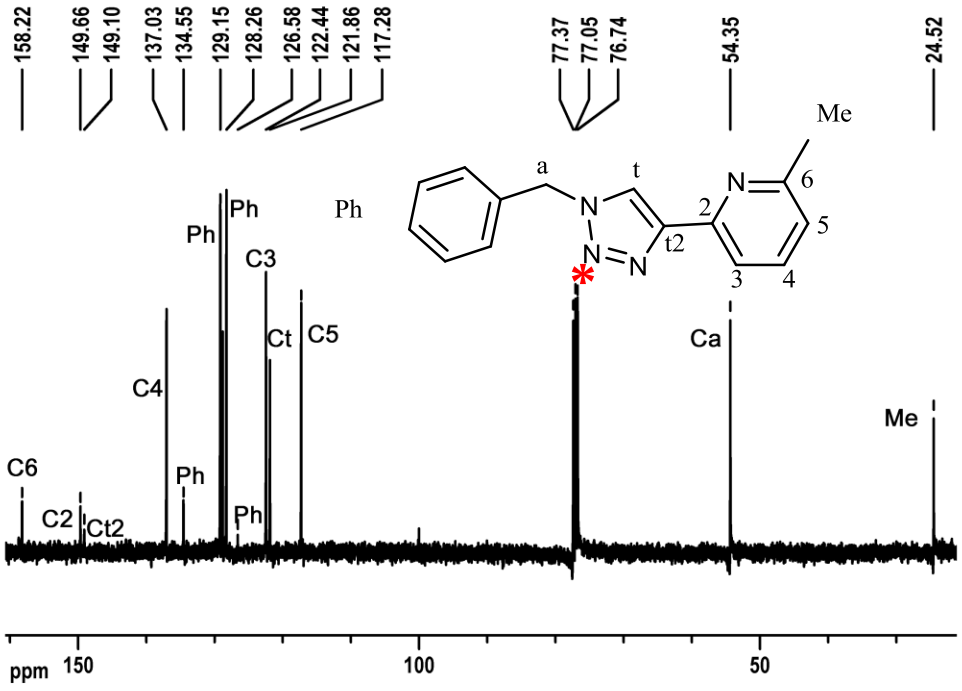

The peak marked by an asterisk is $CDCl_3$.

8) $[Fe_2(L2M)_3](BF_4)_4$.

^{1}H NMR (300 MHz; in acetonitrile-d3; 25℃):

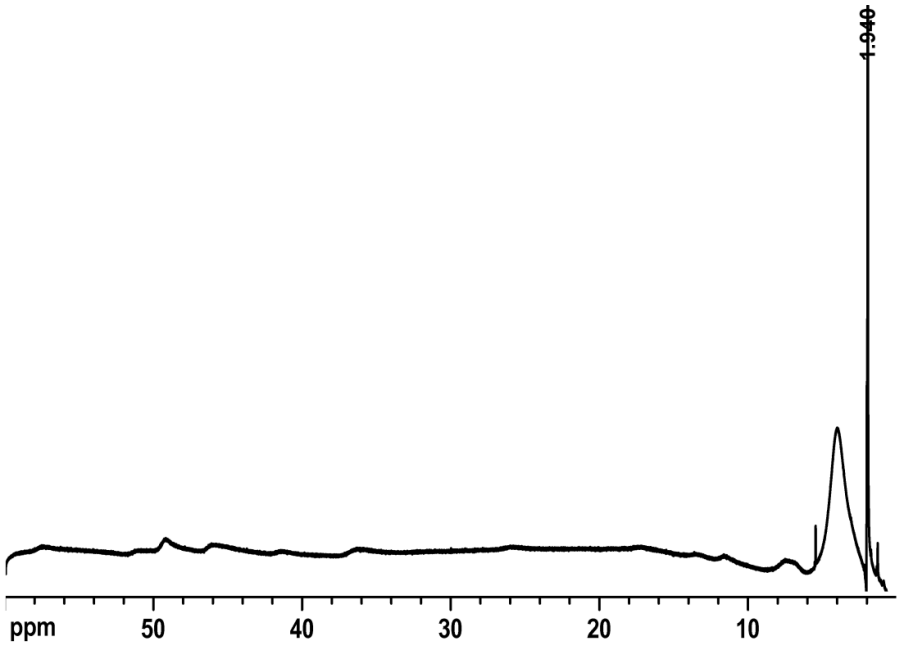

9) $[Fe_2(L3M)_3](BF_4)_4$.

^{1}H NMR (300 MHz; in acetonitrile-d3; 25℃):

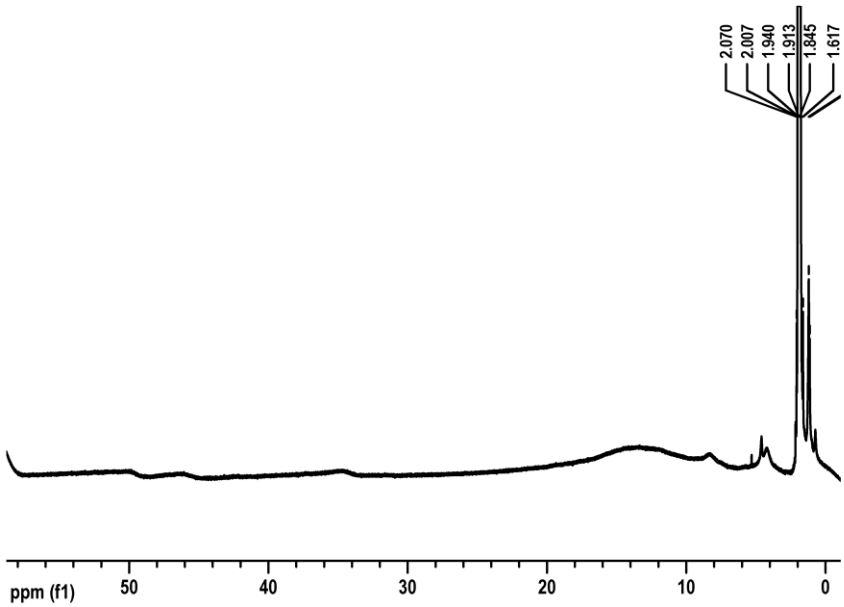

10) $[Fe(L4M)_3](BF_4)_2$.

^{1}H NMR (300 MHz; in acetonitrile; 25℃)

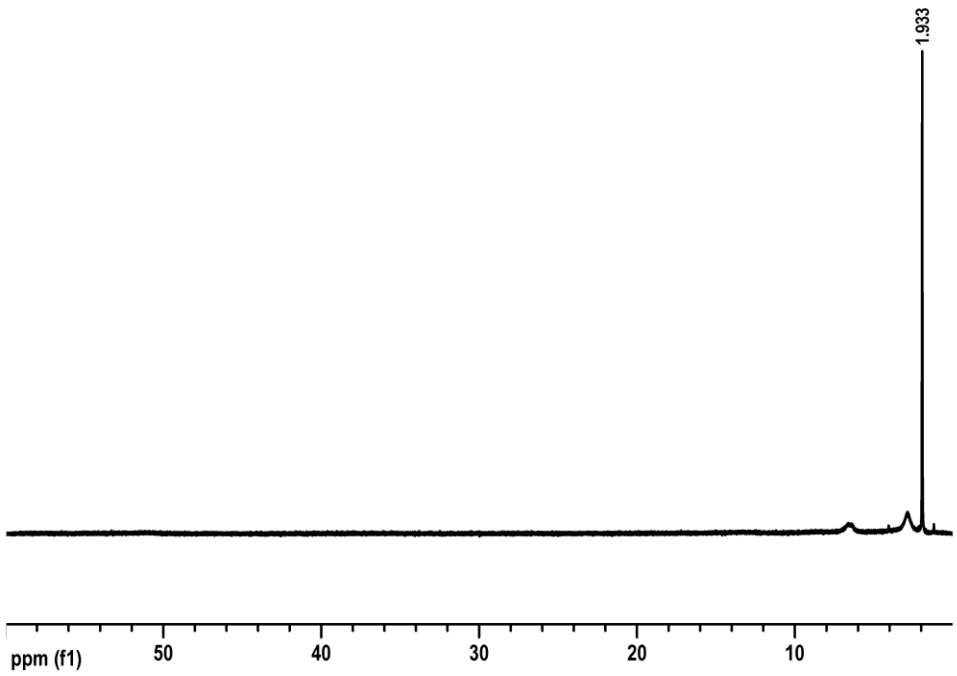

Mass spectrometry

GC-MS

1) 1,4-Bis(6-methylpyridin-2-yl)buta-1,3-diyne.

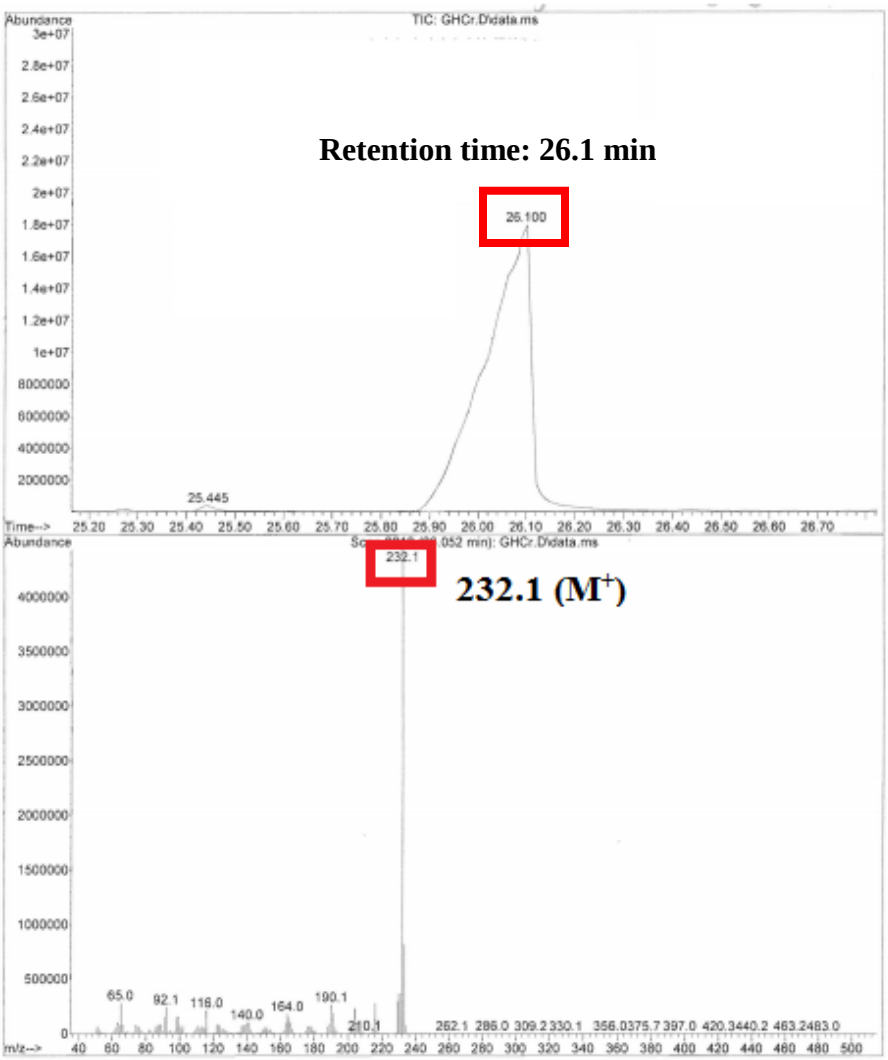

2) 1,2-Bis(6-methylpyridin-2-yl)ethyne.

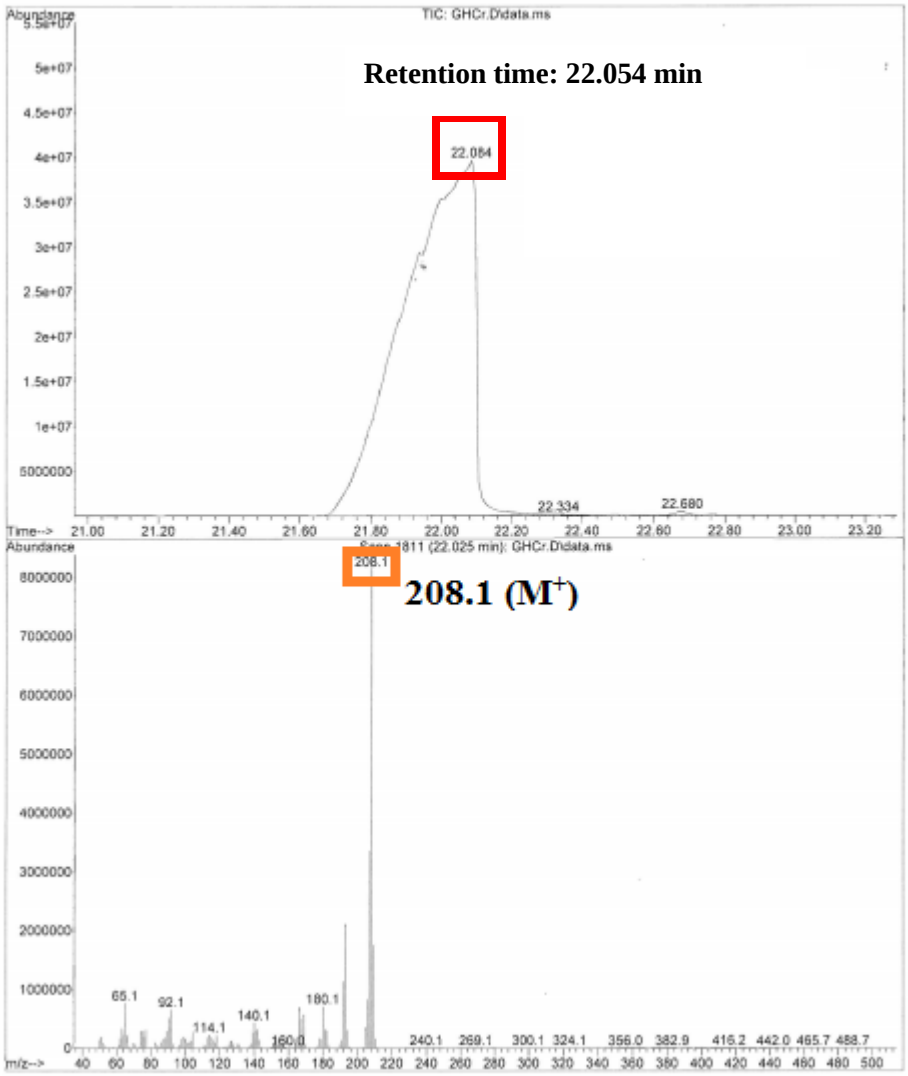

EI-MS (low resolution)

1) 1,4-Bis((4-(6-methylpyridin-2-yl)-1H-1,2,3-triazol-1-yl)methyl)benzene (L1M ligand).

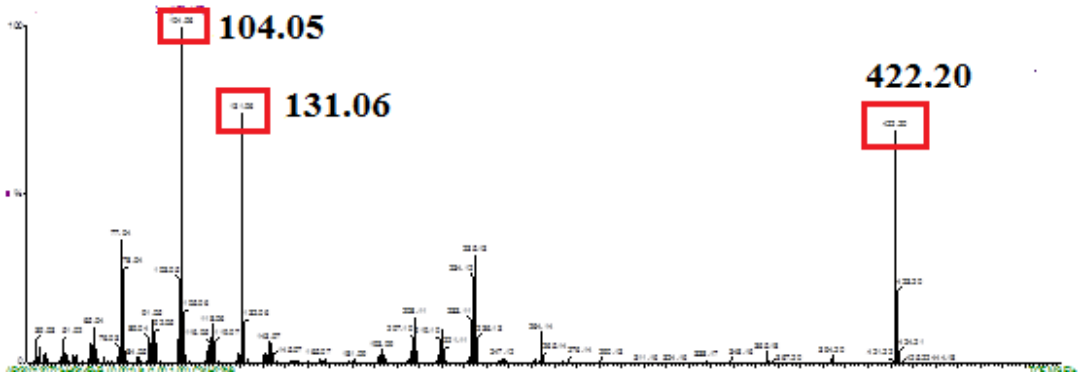

2) 1,3-Bis(4-(6-methylpyridin-2-yl)-1H-1,2,3-triazol-1-yl)propane (L2M).

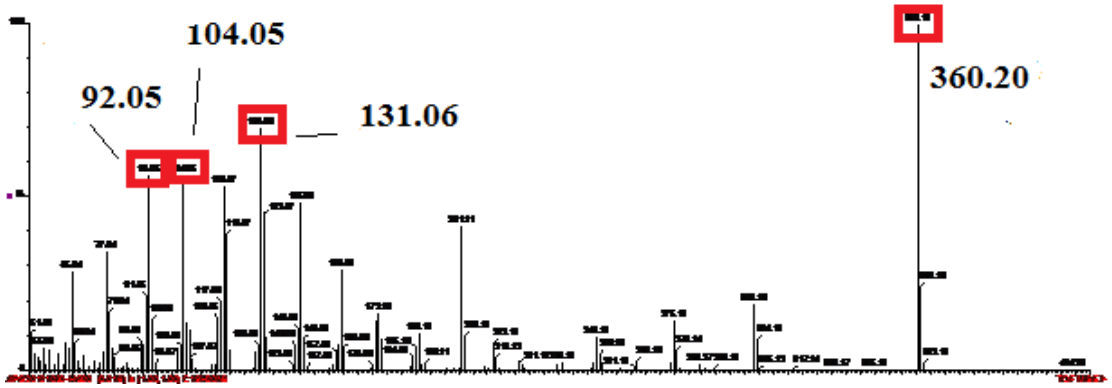

3) 1,4-Bis(4-(6-methylpyridin-2-yl)-1H-1,2,3-triazol-1-yl)butane (L3M) .

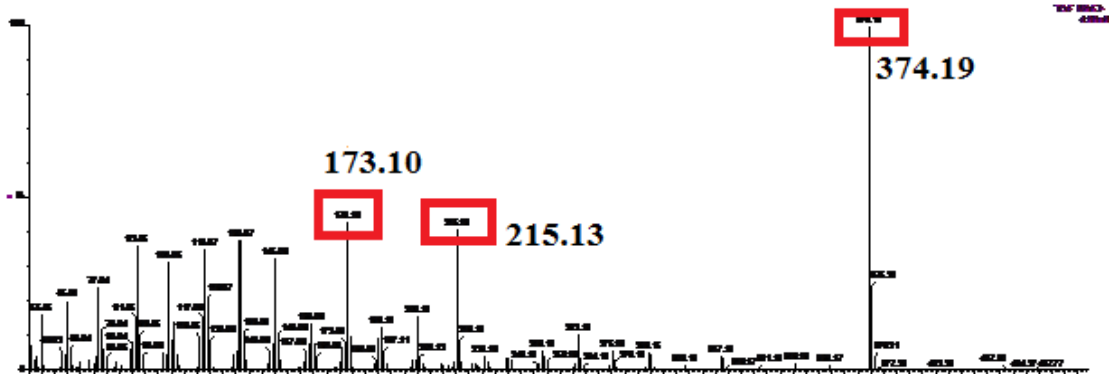

4) 2-(1-Benzyl-1H-1,2,3-triazol-4-yl)-6-methylpyridine (L4M).

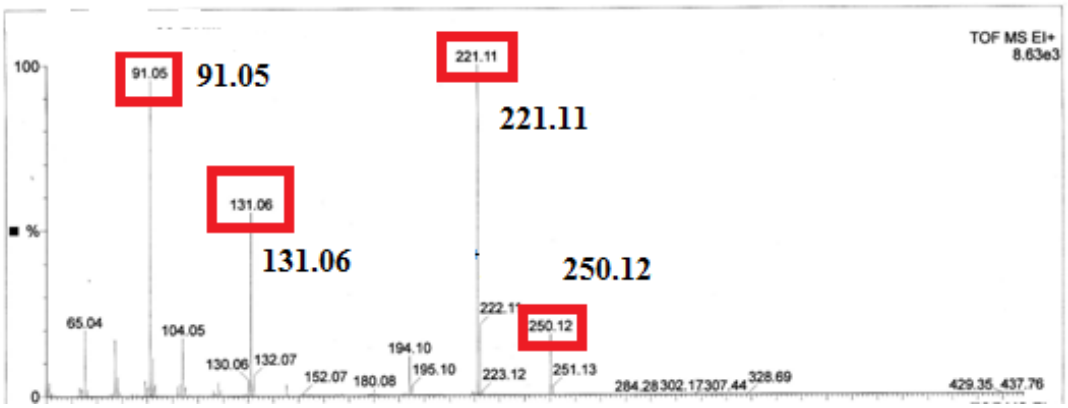

UV-Vis spectroscopy

1) UV-Vis of iron(II) complexes(~10^{-5} M, in acetonitrile, 25℃).

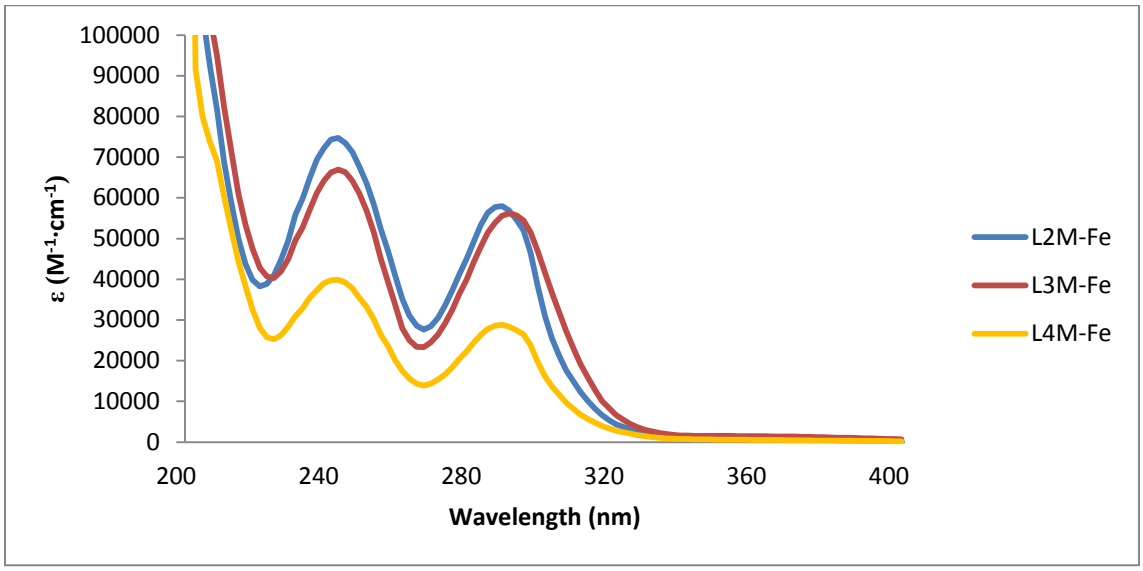

2) UV-Vis of nickel(II) complexes(~10^{-5} M, in acetonitrile, 25℃).

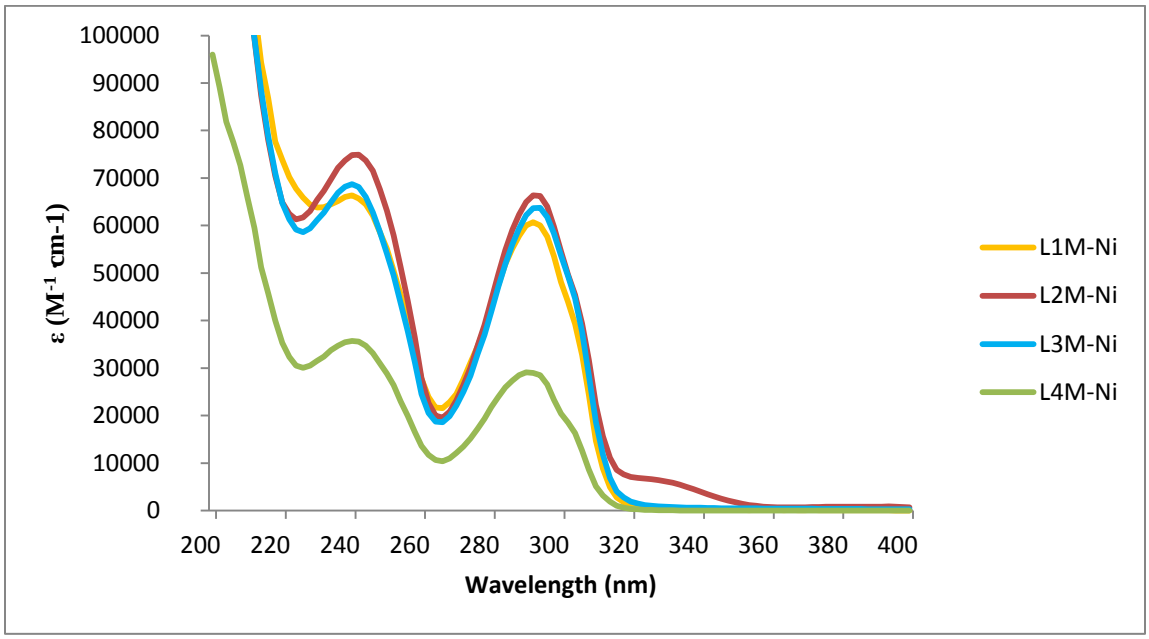

3) UV-Vis of nickel(II) complexes (~10^{-3} M, in acetonitrile, 25℃).